

CREVICE CORROSION RESISTANCES OF NEW HIGH STRENGTH
COBALT-CHROMIUM-MOLYBDENUM-CARBON ALLOYS

by

THOMAS MAURICE DEVINE, JR.

B.S. Metallurgy and Materials Science, M.I.T.
(1971)

M.S. Metallurgy and Materials Science, M.I.T.
(1971)

Submitted in partial fulfillment of the requirements

for the degree of

DOCTOR OF PHILOSOPHY IN METALLURGY

at the

Massachusetts Institute of Technology

February, 1974

Signature of Author

Department of Metallurgy and Materials Science
January 16, 1974

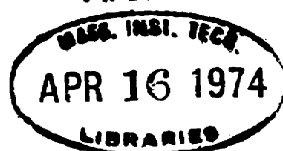
Certified by

Thesis Supervisor

Accepted by

Chairman, Departmental Committee on Graduate Students

Archives



ABSTRACT

CREVICE CORROSION RESISTANCES OF NEW HIGH STRENGTH
COBALT-CHROMIUM-MOLYBDENUM-CARBON ALLOYS

by

THOMAS MAURICE DEVINE, JR.

Submitted to the Department of Metallurgy and
Materials Science on January 16, 1974 in
partial fulfillment of the requirements for the
degree of Doctor of Philosophy
in Metallurgy

The thermomechanical processing steps required to improve the room temperature tensile strength, ductility, and fatigue resistance of cast cobalt-chromium-molybdenum-carbon alloys have been investigated. The effects of hot extrusion, press-forging, and hot and cold rolling followed by heat treatment have been studied. By a half-hour heat treatment of a hot and cold worked modified H.S. 21 alloy (26.70% Cr-5.46% Mo-.145% C-bal. Co) it was found possible to double the tensile strength and more than triple the percentage elongation of the as cast version of the same alloy which is currently used as a surgical implant material. The fatigue strength was also doubled.

The general, pit, and crevice corrosion characteristics of several commercial and experimental alloys were measured in aggressive corrodents such as 10% HCl + 1% FeCl₃ and in isotonic salt solution (0.9% NaCl) by direct immersion (loss in weight) as well as by electrochemical methods. Measurement of the corrosion current density as a function of time in deaerated solutions at 37°C of creviced samples at various applied potentials gave results which rated the various alloys studied in the same order as loss in weight measurements of similarly creviced samples immersed in the same corrodents.

Metallographic and x-ray diffraction analyses indicated that cold rolling hot rolled plate of modified H.S. 21 transformed the predominately FCC matrix to the HCP phase. Subsequent heat treatment at 800°C and 900°C for various lengths of time of slugs of the cold rolled plate resulted in a fine dispersion of a chromium carbide precipitate along the HCP-FCC interface. Heat treatment at 1000°C resulted in the formation of a coarse intergranular as well as intragranular carbide precipitate.

Little or no carbide precipitation occurred following heat treatments at 1100°C and 1200°C.

The excellent strength and ductility of tensile specimens cold rolled to 10% reduction in area and heat treated at 1065°C for 30 minutes was believed due to the particular carbide distribution and extremely fine grain size produced by this processing treatment. The superior mechanical properties and crevice corrosion resistance of the wrought cobalt-chromium-molybdenum-carbon alloys relative to their cast counterparts was attributed to the increase in chemical and structural homogeneity achieved through thermomechanical processing.

Thesis Supervisor: John Wulff, D.Sc.
Professor of Metallurgy, Emeritus

TABLE OF CONTENTS

<u>Chapter</u>		<u>Page</u>
	TITLE PAGE	1
	ABSTRACT	2
	TABLE OF CONTENTS	4
	LIST OF FIGURES	5
	LIST OF TABLES	12
	ACKNOWLEDGEMENTS	14
I	INTRODUCTION	15
II	EXPERIMENTAL	25
	2.1 Procedure	25
	2.1.1 Materials	25
	2.1.2 Mechanical Testing.	26
	2.1.3 Physical Metallurgy	27
	2.1.4 Direct Immersion Corrosion Tests.	28
	2.1.5 Electrochemistry	29
	2.2 Results	30
	2.2.1 Physical Metallurgy and Mechanical Properties	30 30
	2.2.2 Corrosion Measurements	35
III	DISCUSSION	43
IV	CONCLUSIONS	51
V	RECOMMENDATIONS FOR FUTURE WORK	53
VI	REFERENCES	56
	AUTOBIOGRAPHICAL NOTE	202

LIST OF FIGURES

<u>Figure</u>		<u>Page</u>
1	The role of a differential aeration cell in initiating crevice corrosion	60
2.	The effect of chloride ions on normal metal dissolution	62
3	The effect of chloride ions on the anodic polarization behavior of a passive metal	64
4	Rotating bending fatigue specimen and loading scheme.	66
5	Geometry of accelerated crevice corrosion specimen.	68
6	Crevice sample mounted in a Stern-Makrides electrode holder	70
7	Electrochemical cell for measuring potential variations with time of test specimens.	72
8	Anodic polarization apparatus	74
9	Microstructure of precision cast H.S. 21 after annealing at 1200°C for 4 hours. 5% HCl electrolytic etch. 158X	76
10	Cobalt, chromium, and molybdenum distributions in a precision cast H.S. 21 specimen.	77
11	Microstructure of H.S. 21 press forged from 3 inch diameter ingot to 1 inch square bar at 1150°C and hot rolled to 0.125 inch thick plate. 5% HCl electrolytic etch. 158X.	79
12	Hardness as a function of cold work in modified H.S. 21.	80
13	Weight percent HCP phase as a function of cold work in modified H.S. 21	82
14	Modified H.S. 21 hot worked at 1150°C, cold rolled to 7.1% RA. 5% electrolytic etch. 158X.	84

<u>Figure</u>		<u>Page</u>
15	Modified H.S. 21 hot worked at 1150°C, cold rolled to 15.2% RA. 5% HCl electrolytic etch. 158X.	84
16	Modified H.S. 21 hot worked at 1150°C, cold rolled to 25.0% RA. 5% HCl electrolytic etch. 158X.	85
17	Effect of 10 minute heat treatments at 800°C-1200°C on the hardness of cold rolled modified H.S. 21.	86
18	Effect of 30 minute heat treatments at 800°C-1200°C on the hardness of cold rolled modified H.S. 21	89
19	Effect of 60 minute heat treatments at 800°C-1200°C on the hardness of cold rolled modified H.S. 21	90
20	Modified H.S. 21. Hot worked at 1150°C, cold rolled to 7.1% RA, heat treated at 800°C for 10 minutes, air cooled. 5% HCl electrolytic etch. 158X	92
21	Modified H.S. 21. Hot worked at 1150°C, cold rolled to 7.1% RA, heat treated at 800°C for 60 minutes, air cooled. 5% HCl electrolytic etch. 158X.	92
22	Modified H.S. 21. Hot worked at 1150°C, cold rolled to 7.1% RA, heat treated at 800°C for 10 minutes, air cooled. 5% HCl electrolytic etch. 890X.	93
23	Modified H.S. 21. Hot worked at 1150°C, cold rolled to 7.1% RA, heat treated at 800°C for 60 minutes, air cooled. 5% HCl electrolytic etch. 890X.	93
24	Weight percent HCP phase in cold rolled modified H.S. 21 heat treated for 10 minutes at 800°C-1200°C	94
25	Weight percent HCP phase in cold rolled modified H.S. 21 heat treated for 30 minutes at 800°C-1200°C	96

<u>Figure</u>		<u>Page</u>
26	Weight percent HCP phase in cold rolled modified H.S. 21 heat treated for 60 minutes at 800°C-1200°C	98
27	Modified H.S. 21. Hot worked at 1150°C, cold rolled to 7.1% RA, heat treated at 900°C for 10 minutes, air cooled. 5% HCl electrolytic etch. 158X.	100
28	Modified H.S. 21. Hot worked at 1150°C, cold rolled to 7.1% RA, heat treated at 900°C for 60 minutes, air cooled. 5% HCl electrolytic etch. 158X.	100
29	Modified H.S. 21. Hot worked at 1150°C, cold rolled to 7.1% RA, heat treated at 900°C for 10 minutes, air cooled. 5% HCl electrolytic etch. 890X.	101
30	Modified H.S. 21. Hot worked at 1150°C, cold rolled to 7.1% RA, heat treated at 900°C for 60 minutes, air cooled. 5% HCl electrolytic etch. 890X.	101
31	Modified H.S. 21. Hot worked at 1150°C, cold rolled to 7.1% RA, heat treated at 1000°C for 10 minutes, air cooled. 5% HCl electrolytic etch. 158X.	102
32	Modified H.S. 21. Hot worked at 1150°C, cold rolled to 7.1% RA, heat treated at 1000°C for 60 minutes, air cooled. 5% HCl electrolytic etch. 158X.	102
33.	Modified H.S. 21. Hot worked at 1150°C, cold rolled to 7.1% RA, heat treated at 1000°C for 10 minutes, air cooled. 5% HCl electrolytic etch. 679X.	103
34	Modified H.S. 21. Hot worked at 1150°C, cold rolled to 7.1% RA, heat treated at 1000°C for 60 minutes, air cooled. 5% HCl electrolytic etch. 679X.	103
35	Modified H.S. 21. Hot worked at 1150°C, cold rolled to 7.1% RA, heat treated at 1100°C for 10 minutes, air cooled. 5% HCl electrolytic etch. 158X.	104

<u>Figure</u>		<u>Page</u>
35	Modified H.S. 21. Hot worked at 1150°C cold rolled to 7.1% RA, heat treated at 1100°C for 10 minutes, air cooled. 5% HCl electrolytic etch. 158X.	104
36	Modified H.S. 21. Hot worked at 1150°C, cold rolled to 7.1% RA, heat treated at 1100°C for 60 minutes, air cooled. 5% HCl electrolytic etch. 158X.	104
37	Modified H.S. 21. Hot worked at 1150°C, cold rolled to 7.1% RA heat treated at 1200°C for 10 minutes, air cooled. 5% HCl electrolytic etch. 158X.	105
38	Modified H.S. 21. Hot worked at 1150°C, cold rolled to 7.1% RA, heat treated at 1200°C for 60 minutes, air cooled. 5% HCl electrolytic etch. 158X.	105
39	Tensile properties of 10% cold worked modified H.S. 21 heat treated at 1000°C, 1065°C, and 1100°C for 30 minutes and air cooled.	107
40	Modified H.S. 21. Hot worked at 1150°C, cold rolled to 9.9% RA, heat treated at 1000°C for 30 minutes, air cooled. 5% HCl electrolytic etch. 158X.	108
41	Modified H.S. 21. Hot worked at 1150°C, cold rolled to 9.9% RA, heat treated at 1065°C for 30 minutes, air cooled. 5% HCl electrolytic etch. 158X.	108
42	Modified H.S. 21. Hot worked at 1150°C, cold rolled to 9.9% RA, heat treated at 1065°C for 30 minutes, air cooled. 5% HCl electrolytic etch. 158X.	109
43	Effect of prior cold rolling subsequent to a 12 minute anneal at 1065°C on modified H.S. 21.	110
44	Effect of prior cold rolling subsequent to a 30 minute anneal at 1065°C on modified H.S. 21.	112

FigurePage

45	Effect of prior cold rolling subsequent to a 60 minute anneal at 1065°C on modified H.S. 21.	114
46	Modified H.S. 21. Hot worked at 1150°C, cold rolled to 6% RA, heat treated at 1065°C for 12 minutes, air cooled. 5% HCl electrolytic etch. 158X.	116
47	Modified H.S. 21. Hot worked at 1150°C, cold rolled to 11.1% RA, heat treated at 1065°C for 12 minutes, air cooled. 5% HCl electrolytic etch. 158X.	116
48	Modified H.S. 21. Hot worked at 1150°C, cold rolled to 27.0% RA, heat treated at 1065°C for 12 minutes, air cooled. 5% HCl electrolytic etch. 158X.	117
49	Rotating bending fatigue tests of alloys listed in Table 3	118
50	Potential variation with time of creviced samples of several alloys immersed in oxygenated 10% HCl + 1% FeCl ₃ at 37°C	120
51	Potential variation with time of creviced samples of several alloys immersed in oxygenated 0.9% NaCl at 37°C.	122
52	Creviced sample of 316L stainless steel following 9 days of immersion in 0.9% NaCl.	124
53	Anodic polarization curves of several alloys in deaerated 10% HCl + 1% FeCl ₃ at 37°C	126
54	Cyclic anodic polarization of Elgilloy in deaerated 10% HCl + 1% FeCl ₃ at 37°C	128
55	Cyclic anodic polarization of Hastalloy C in deaerated 10% HCl + 1% FeCl ₃ at 37°C	130
56	Cyclic anodic polarization of MP35N in deaerated 10% HCl + 1% FeCl ₃ at 37°C.	132
57	Cyclic anodic polarization of H.S. 25 in deaerated 10% HCl + 1% FeCl ₃ at 37°C.	134

<u>Figure</u>	<u>Page</u>
58	Cyclic anodic polarization of precision cast H.S. 21 in deaerated 10% HCl + 1% FeCl ₃ at 37°C 136
59	Cyclic anodic polarization of wrought H.S. 21 in deaerated 10% HCl + 1% FeCl ₃ at 37°C 138
60	Cyclic anodic polarization of 316L stainless steel in deaerated 0.9% NaCl at 37°C. 140
61	Cyclic anodic polarization of Elgilloy in deaerated 0.9% NaCl at 37°C 142
62	Cyclic anodic polarization of Hastalloy C in deaerated 0.9% NaCl at 37°C. 144
63	Cyclic anodic polarization of MP35 in deaerated 0.9% NaCl at 37°C 146
64	Cyclic anodic polarization of H.S. 25 in deaerated 0.9% NaCl at 37°C. 148
65	Cyclic anodic polarization of precision cast H.S. 21 in deaerated 0.9% NaCl at 37°C . . . 150
66	Cyclic anodic polarization of wrought H.S. 21 in deaerated 0.9% NaCl at 37°C. 152
67	Corrosion current density variation with time of creviced samples of Elgilloy at various applied potentials in deaerated 10% HCl + 1% FeCl ₃ at 37°C. 154
68	Corrosion current density variation with time of creviced samples of Hastalloy C at various applied potentials in deaerated 10% HCl + 1% FeCl ₃ at 37°C. 156
69	Corrosion current density variation with time of creviced samples of MP35 at various applied potentials in deaerated 10% HCl + 1% FeCl ₃ at 37°C. 158
70	Corrosion current density variation with time of creviced samples of H.S. 25 at various applied potentials in deaerated 10% HCl + 1% FeCl ₃ at 37°C. 160

FigurePage

71	Corrosion current density variation with time of creviced samples of wrought H.S. 21 at various potentials in deaerated 10% HCl + 1% FeCl ₃ at 37°C.	162
72	Corrosion current density variation with time of creviced samples of cast H.S. 21 at various applied potentials in deaerated 10% HCl + 1% FeCl ₃ at 37°C.	164
73	Corrosion current density variation with time of creviced samples of 316L stainless steel at various applied potentials in deaerated 0.9% NaCl at 37°C	166
74	Corrosion current density variation with time of creviced samples of Elgilloy at various applied potentials in deaerated 0.9% NaCl at 37°C	168
75	Corrosion current density variation with time of creviced samples of Hastalloy C at various applied potentials in deaerated' 0.9% NaCl at 37°C	170
76	Corrosion current density variation with time of creviced samples of MP35 at various applied potentials in deaerated 0.9% NaCl at 37°C	172
77	Corrosion current density variation with time of creviced samples of H.S. 25 at various applied potentials in deaerated 0.9% NaCl at 37°C	174
78	Corrosion current density variation with time of creviced samples of precision cast H.S. 21 at various applied potentials in deaerated 0.9% NaCl at 37°C.	176
79	Corrosion current density variation with time of creviced samples of wrought H.S. 21 at various applied potentials in deaerated 0.9% NaCl at 37°C.	178

LIST OF TABLES

<u>Table</u>		<u>Page</u>
1	Summary of Statistics Compiled by J. T. Scales.	179
2	The Effect of Thermomechanical Processing and Heat Treatment on the Tensile Properties of a 20 Wt. % Chromium-10 Wt. % Molybdenum Balance Cobalt Alloy.	180
3	Nominal Compositions of Some Commercially Available Corrosion Resistant Alloys.	182
4	The Effect of Thermomechanical Processing and Heat Treatment on the Mechanical Properties of H.S. 21.	183
5	Mechanical Properties of As-Hot Worked Modified H.S. 21	186
6	The Effect of 30 Minute Heat Treatments on the Mechanical Properties of Hot and Cold Worked, Modified H.S. 21	187
7	The Effect of Prior Cold Working Subsequent to a 12 Minute Anneal at 1065°C on the Mechanical Properties of Modified H.S. 21	188
8	The Effect of Prior Cold Working Subsequent to a 30 Minute Anneal at 1065°C on the Mechanical Properties of Modified H.S. 21.	189
9	The Effect of Prior Cold Working Subsequent to a 60 Minute Anneal at 1065°C on the Mechanical Properties of Modified H.S. 21	191
10	Corrosivity of Some Corrosion Resistant Alloys in 10% HCl + 1% FeCl ₃ Solution at 37°C	192

<u>Table</u>		<u>Page</u>
11	Times to Initiate Marked Serrations in Potential vs Time plot of Creviced Samples Immersed in Oxygenated 10% HCl + 1% FeCl ₃	194
12	Times to Initiate Marked Serrations in Potential vs Time Plot of Creviced Samples Immersed in Oxygenated 0.9% NaCl.	195
13	Crevice Corrosion Behavior of Some Corrosion Resistant Alloys in 0.9% NaCl Solution at 37°C	196
14	Pitting Potentials of Alloys in Deaerated 10% HCl + 1% FeCl ₃	197
15	Protective Potential in 10% HCl + 1% FeCl ₃	198
16	Protective Potential in 0.9% NaCl	199
17	Lowest Applied Potential at Which Crevice Corrosion Occurs in Deaerated 10% HCl + 1% FeCl ₃	200
18	Lowest Applied Potential at Which Crevice Corrosion Occurs in Deaerated 0.9% NaCl	201

ACKNOWLEDGEMENTS

I am deeply indebted to Professor John Wulff for his guidance in this work, to the National Science Foundation for financial support of the research reported in this thesis, and to Mr. Guenter Arndt, project technician, for his advice and help regarding the design, building and operation of the instruments, devices, and machines used in this thesis.

I am especially grateful to my wife for typing this thesis and for her constant encouragement and understanding throughout my graduate school career.

I. INTRODUCTION

The three most widely used surgical implant alloy systems are molybdenum containing wrought austenitic stainless steel, precision cast cobalt-chromium-molybdenum-carbon alloys such as H.S. 21 and Vitallium, and wrought commercial titanium and some of its alloys. Unfortunately, none of these alloys can be regarded as ideally suitable surgical implant material. Stainless steel tends to pit and crevice corrode in body fluids (1-6). While precision cast cobalt-chromium-molybdenum alloys exhibit superior corrosion resistance, they possess insufficient mechanical properties for safe use in some weight-bearing implants (7-10). Ordinary commercial titanium and some of its alloys exhibit superior long-time corrosion resistance in body fluids relative to the other two alloy systems (11). Unfortunately, however, titanium and some of its alloys undergo a high initial rate of corrosion in body fluids (12,13) and possess little wear resistance when in rubbing contact with themselves or other metallic implant materials (14). The shortcomings of these three alloy systems are further brought out in Table 1 which represents a summary of the statistics recently compiled by the British Ministry of Health on weight-bearing surgical implants inserted and removed from patients over a seven-year period (15). The first row of this table indicates the incidence of corrosion among the implants examined and illustrates the high susceptibility of stainless steel to corrosion in body fluids relative to the other two alloy systems. The second row of Table 1 indicates all of the alloys

to be highly susceptible to fretting and/or crevice corrosion in body fluids. The greater mechanical strength of wrought stainless steel relative to the cast cobalt-chromium-molybdenum and wrought titanium alloys is indicated in the third row of Table 1. The shortcomings of these alloy systems are evident in the last three rows of Table 1 which represents the corrosion and mechanical failure statistics on screws made of these alloys and used in weight-bearing prostheses.

What appears to be required is an alloy with the mechanical properties and fabricability of 316L stainless steel and the pit and crevice corrosion resistance of the cast cobalt-chromium-molybdenum alloys. Since ample industrial research and development during the past thirty-five years has led to but marginal improvements in the corrosion resistance of the stainless steels, and since the inherent conservativeness of the American surgeon precludes the immediate use of titanium alloys for at least the near future, the research effort for this thesis was concentrated on the development of a wrought, corrosion resistant, high strength, cobalt-chromium base alloy.

The first noteworthy cobalt-chromium base alloys which received considerable attention due to their high corrosion and wear resistance were the cast cobalt-chromium-tungsten-high carbon alloys patented in 1907 by Elwood Haynes (16). Erdle (17) later patented a cobalt-chromium-tungsten-carbon alloy containing higher tungsten but lower carbon contents suitable for investment casting of surgical implants and other small, intricate-shaped parts.

Molybdenum was later substituted for tungsten in this alloy by Erdle and Prange (18). During World War II, it was found that the investment casting technique lent itself to the manufacture of heat resistant parts, and Erdle and Prange's cobalt-chromium-molybdenum-low carbon alloy modified by additions of 3-5% nickel became a popular heat resistant alloy (19). This modified alloy has become known in the literature as Haynes Stellite 21.

Most of the published data regarding the processing and mechanical properties of cobalt-chromium-molybdenum-base alloys can only be gleaned from the writings of workers interested in high-temperature rather than ambient applications. Nevertheless, a significant amount of information concerning the physical metallurgy of cobalt-chromium base alloys is attainable from these works. Pure cobalt undergoes an allotropic transformation upon heating from hexagonal close-packed (HCP) to face-centered cubic (FCC) at approximately 421°C (20). Alloying additions of nickel, carbon and iron stabilize the FCC form, whereas chromium, molybdenum, tantalum, and tungsten tend to stabilize the equilibrium HCP structure (19). The refractory elements have limited solubility in both the HCP and FCC forms of cobalt and the HCP phase terminates in a high-temperature peritectoid reaction (21). The peritectoid reaction is complex and can proceed by progressing through several metastable states as discussed by Giamei et al (22). The nature and extent of the FCC to HCP matrix phase transformation which occurs upon cooling cobalt-rich alloys depends significantly on the alloy composition, cooling rate and final

temperature (22). Pure cobalt transforms martensitically on cooling from the high temperature FCC form to the low temperature HCP form starting at approximately 390°C (20). The M_s temperature of this reaction increases with the chromium content of the alloy up to approximately 10 atomic percent chromium. Higher chromium additions depress the M_s temperature. Metallographic examination of cobalt-chromium binary alloys containing less than 15 wt. % chromium which were furnace cooled from a nine-day 1050°C solutionizing temperature revealed martensitic transformation markings. Alloys containing higher amounts of chromium showed only equiaxed grains. Despite the chromium content, all alloys were 100% HCP. Evidently, the equilibrium FCC to HCP transformation proceeds sufficiently rapidly in the alloys containing more than 15 wt. % chromium, so that the reaction goes to completion before the M_s temperature is reached. In fact anything but a severe water quench cannot suppress the formation of the equilibrium HCP phase in a cobalt-20 wt. % chromium binary alloy (22).

The matrix of precision cast and annealed samples of H.S. 21 which were air cooled from their annealing temperature consists of approximately 100% FCC (23). Evidently, the small amounts of nickel, iron, and carbon found in this alloy sufficiently stabilize the FCC phase that much longer times at high temperatures are required to initiate the equilibrium allotropic transformation, and much lower temperatures must be achieved in cooling the alloy before the M_s temperature is reached.

Attempts to develop ductile, high strength cobalt-chromium base alloys have been reported in the literature. Rausch, Simcoe, and McAndrew at the Illinois Institute of Technology reported that dilute additions of aluminum and beryllium greatly enhanced the hot and cold workability of cobalt-chromium-molybdenum alloys (24). However, such additions were found to severely limit the corrosion resistance of these alloys in chloride-ion media (25). The precipitation hardening of cobalt-chromium alloys containing additions of molybdenum, tungsten, tantalum, or niobium as reported by Drapier, de Brouwer, and Coutsouradis (26) was found to impair the ductility of the alloy as well as the corrosion resistance in chloride-ion media (25). The most instructive directive found in the literature towards the development of a ductile, high-strength, corrosion resistant, cobalt-chromium base alloy is the 1967 patent of Gaylord Smith (27). In this patent, Smith reported that cobalt-nickel alloys containing 20 wt. % chromium and 10 wt. % molybdenum could be thermomechanically processed to remarkably high strength levels. Such alloys were found to have a much greater resistance to corrosion in chloride-ion media than 316L stainless steel. Smith further reported that the corrosion resistance in chloride-ion media of cobalt-nickel-20 wt. % chromium-10 wt. % molybdenum alloys increased as the nickel content of the alloy decreased. Smith examined alloys with nickel contents varying from 35 wt. % to 5 wt. %. The corrosion tests of Smith's were repeated by immersing cobalt-nickel-20 wt. % chromium-10 wt. % molybdenum alloys with nickel contents varying from 35 wt. % to 0 wt. % in

a solution of 10% HCl + 1% FeCl₃ (25). Again, it was found that the corrosion resistance increased as the nickel content of the alloy was lowered. In fact the alloy with the greatest corrosion resistance was the 20 wt. % chromium-10 wt. % molybdenum-balance cobalt alloy (25).

Through cooperative experiments with the engineers at the Stellite Division of the Cabot Corporation, it was found possible to hot and cold fabricate this alloy (25). The marked increase in mechanical properties of this alloy achieved by thermomechanical processing and subsequent heat treatment is indicated in Table 2. In the as-cast condition, the 20 wt. % chromium-10 wt. % molybdenum-0.1 wt. % carbon-balance cobalt alloy has a yield and ultimate tensile strengths of 45,000 psi and 58,300 psi, respectively, and an elongation of 20%. By hot and cold working followed by a 1065°C anneal for 1 hour, it was possible to raise the yield and ultimate tensile strengths to 125,000 psi and 206,000 psi, respectively, while maintaining an elongation of 25%. Comparative orthodox electrochemical tests conducted in 0.9% NaCl, a solution which simulates the chloride-ion activity of the human body, indicated the wrought 20 wt. % chromium-10 wt. % molybdenum-balance cobalt alloy to be as corrosion resistant as precision cast H.S. 21 (25).

The fair amount of success achieved in hot and cold working the 20 wt. % chromium-10 wt. % molybdenum-0.1 wt. % carbon-balance cobalt alloy prompted the question as to whether or not it might also be possible to hot and cold fabricate the

cast alloy H.S. 21 which contains 27 wt. % chromium-5 wt. % molybdenum-3 wt. % (nickel + iron)-0.3 wt. % carbon-balance cobalt. In the early 1950's, attempts to hot work H.S. 21 at the Stellite Division of the Cabot Corporation resulted in an uneconomical 25% yield of the starting ingot material (28). Nevertheless, the results of the hot and cold fabrication of the 20 wt. % chromium-10 wt. % molybdenum alloy appears to warrant an investigation of the possibility of hot and cold working H.S. 21.

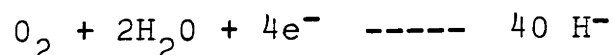
Because of the crevices inherent in the design of multi-component surgical implants as well as the relatively high susceptibility of the currently used surgical implant alloys to crevice corrosion as previously indicated in Table 1, any alloy implanted in the body should be highly resistant to crevice attack. However, the procedure for assessing an alloy's susceptibility to crevice corrosion, particularly in relatively weak corrodents, has not been clearly established. The use of chemically accelerated solutions so as to obtain results in a short time in order to predict the long time behavior of alloys in much less chemically active environments has long been questioned (29). In order to avoid the use of chemically accelerated solutions, various short time tests employing electrochemical techniques which attempt to assess the alloys long time crevice corrosive behavior in the actual solution of interest have been proposed. Jones and Greene suggested measuring the potential variation with time of creviced samples immersed in the solution of interest (30). Marked serrations in the potential versus time plot might be indicative of

the initiation of localized corrosion. The times required to initiate such serrations in the potential-time curves or the times required for a marked active trend in potential to occur might be used to compare various alloys susceptibilities to crevice corrosion. Other investigators have suggested that the pitting potential might also be indicative of an alloy's tendency to undergo crevice attack (31). Wilde has used the protective potential to rate the susceptibilities of various stainless steels to crevice corrosion in sea water (32). Lizlovs attempted to measure the relative resistances of various passive alloys to crevice corrosion in sea water by measuring the corrosion current density of creviced samples at an applied potential of 0.0 mV (33). Unfortunately, no one has yet demonstrated a one-to-one correspondence between the results of their short-time tests and results of long-time, direct immersion corrosion tests. In order to properly assess the crevice corrosion susceptibilities of surgical implant alloys or of any corrosion resistant alloy immersed in a relatively weak corrodent, a short-time test whose results concur with long-time direct-immersion test results appears to be required.

The previously cited high incidence of crevice corrosion of surgical implants in body fluids warrants a brief discussion of the mechanism of crevice corrosion.

Crevice corrosion proceeds by the operation of macro-couples between the metal inside the crevice which functions as anode and the metal outside the crevice which serves as cathode (34). Consider a cylindrical sample of a normal metal M which is

affixed with a Teflon ring and immersed in sea water. Eventually, the rate at which the cathodic reaction



proceeds on the surface of the metal within the crevice decreases due to the depletion of O_2 from the solution in the crevice (35, 36). Figure 1 indicates that because the amount of oxygen inside the crevice is less than that outside the crevice, the exchange current density for the cathodic reaction on the surface of the metal inside the crevice is less than that on the metal surface outside the crevice (34). This in effect shifts the cathodic polarization curve of the cathode surface inside the crevice to the left of that outside the crevice. Although the amount of metal dissolving per unit area inside and outside the crevice is identical, the cathodic current density inside the crevice is less than that outside the crevice (37). This results in a higher concentration of metal ions in the crevice which causes chloride ions to migrate into the crevice which, in turn, as shown in Figure 2, increases the dissolution rate of the metal in the crevice (37). The increased dissolution rate of the metal in the crevice attracts more chloride ions to that region, and the process becomes autocatalytic.

The primary action of the oxygen deficiency in the crevice is to fix the site of the localized attack by affecting the introduction of chloride ions into the crevice and thus accelerating the anodic dissolution within the crevice (38).

Thus, a differential aeration cell is not wholly essential for the initiation of crevice corrosion (39). Any other means of increasing the chloride-ion content of the solution in the crevice could serve just as well as a differential aeration cell for establishing crevice corrosion.

Where metal M is a passive metal, the increased chloride-ion and hydrogen-ion content in the crevice would alter the anodic polarization curve of the metal in the crevice by markedly increasing the critical anodic current density for passivity, slightly increasing the primary passive potential and passive dissolution rate, and lowering the breakdown potential (40,41). The extent of these changes, of course, depends on the individual metal. Figure 3 depicts the situation in which crevice corrosion proceeds with the metal surface outside the crevice passive and that inside the crevice active.

II. EXPERIMENTAL

2.1 Procedure

2.1.1 Materials

The nominal compositions of the alloys investigated are listed in Table 3. These alloys are either currently employed as surgical implant material or have been suggested as potentially usable implant alloys. The 316L stainless steel, Elgilloy, MP35N, H.S. 25, and Hastalloy C were all obtained from their fabricators as fully annealed 0.250 inch diameter rod. The cast H.S. 21 was obtained from the Stellite Division of the Cabot Corporation in the form of 0.50 inch diameter rod. Two varieties of wrought H.S. 21 were employed. The high carbon version containing 0.3 wt. % carbon was chill cast to 1 and 3 inch diameter ingots by the Stellite Division of the Cabot Corporation, Kokomo, Indiana. The 3 X 8 inch ingot was subsequently press forged to a 1-inch square cross section at 1175°C followed by a hot roll to 0.125 inch thick plate in three passes at 1175°C. The 1-inch diameter ingot was cut into three 3-inch length sections which were then extruded at the Whittaker Corporation, West Concord, Massachusetts, to 80% reduction in area at 1205°C (2200°F), 1150°C (2100°F) and 1094°C (2000°F).

The low carbon variety of H.S. 21, referred to as modified H.S. 21, contained 0.145 wt. % carbon and was vacuum melted and electroslog remelted to a 300 lb. ingot, forged and rolled at 1150°C to 0.250 inch thick plate at the Stellite Division of the Cabot Corporation. Cold Rolling and swaging experiments of

the wrought H.S. 21 and the modified H.S. 21 were performed in our laboratory at M.I.T.

2.1.2 Mechanical Testing

Mechanical Properties of the cast and wrought samples of H.S. 21 and modified H.S. 21 were tabulated in terms of hardness and tensile data. Hardness experiments utilized a Wilson-Tukon Hardness Indenter machine while tensile data was accumulated with the aid of an Instron Testing Machine using a 10,000 lb. load cell and an 0.2 inch-minute⁻¹ cross head speed. Tensile samples of cast H.S. 21 were nominally 0.250 inch in diameter with a 1.250 inch guage length. The hot extruded H.S. 21 was tested in the as hot worked condition and in the cold swaged plus heat treated state. These samples were nominally 0.200 inch in diameter with a 1.250 inch guage length. Similarly, the hot forged and hot rolled 0.3 wt. % carbon H.S. 21 was tested in both the as hot worked and cold rolled plus heat treated conditions. These tensile specimens were rectangular in cross section, nominally 0.125 inch x 0.400 inch with a gauge length of 2.000 inches. Tensile specimens of the wrought modified H.S. 21 were nominally 0.200 inch x 0.200 inch in cross section with a 1.500 inch guage length. The wrought modified H.S. 21 was also tested in both the as hot worked and cold rolled plus heat treated conditions.

Cyclic stress versus number of cycles for failure measurements were obtained for 316L stainless steel, H.S. 25, precision cast H.S. 21, wrought H.S. 21 and wrought modified H.S. 21. The fatigue specimens as illustrated in Figure 4 were

cylindrical rods 0.250 inch in diameter with a circumferential groove located 3.55 inches from the point of loading. The notch was 0.050 inch deep with a root radius of 0.020 inch. The samples were sinusoidally stressed in bending at a frequency of 1800 cycles per minute with a pre-load equal to one-half the maximum load. This resulted in a minimum stress during each cycle of zero. The testing was performed on a Sonntag SF-2-U Universal Fatigue Testing Machine.

2.1.3 Physical Metallurgy

Plates of wrought modified H.S. 21 nominally 0.250 inch x 1.0 inch x 4.0 inch were cold rolled to 7.1%, 15.2%, and 25.0% reductions in area. Sections nominally 0.20 inch x 0.10 inch x 0.10 inch were then cut from each plate metallographically polished and heat treated at 800°C, 900°C, 1000°C, 1100°C, and 1200°C for 10 minutes, 30 minutes and 60 minutes. X-ray diffraction patterns, hardness measurements and photomicrographs were obtained for each specimen. The x-ray diffraction patterns were obtained on a General Electric Diffractometer using chromium K_{α} radiation. The photomicrographs were taken on a Leitz Metallograph equipped with a bellows and camera attachment. X-ray diffraction patterns and photomicrographs were also obtained for cast H.S. 21 and cold worked plus heat treated wrought H.S. 21.

The relative amounts of HCP and FCC phases in the cobalt base alloys were obtained with the aid of equation 1 which is an expression developed by Stage and Guillaud (42) for finding the weight percent of HCP phase in pure cobalt.

$$\text{wt. \% HCP} = \frac{I_{\{10\bar{1}1\}\text{HCP}}}{I_{\{10\bar{1}1\}\text{HCP}} + 1.5 I_{\{110\}\text{FCC}}} \cdot 100\% \quad (1)$$

This equation takes into account both structural and multiplicity factors. When the HCP phase is introduced into the alloy by a strain induced martensitic transformation of the unstable FCC phase, equation (1) provides only an estimate and not an exact measurement of the amount of HCP in the alloy because this equation does not correct for the size effect of the extremely thin HCP platelets and for the effects of lattice strains produced by cold work.

2.1.4 Direct Immersion Corrosion Tests

After a mechanical polish to 4/0 grit paper, cylindrical specimens, accurately machined and finished to dimensions 0.250 inch in diameter by 1.000 inch in length were ultrasonically degreased in trichloroethylene, washed, dried, and weighed. The difficulty in reproducing crevice geometry led us to use Teflon rings force-fitted to cylindrical rod specimens. All Teflon rings were similarly accurately finished to a width of 0.125 inch and 0.015 inch smaller in diameter than the rod-shaped specimens. The Teflon rings were force-fitted to the samples with a mechanical jig to avoid scratching the prepared surfaces of the metal specimens. Figure 5 illustrates the geometry of the crevice corrosion specimens. After each corrosion test the Teflon rings were carefully cut away and specimens were scrubbed with a bristle brush, washed, dried, and weighed. Specimens were then examined

with the aid of a binocular microscope for evidence of etching, isolated pitting, and crevice corrosion. Because of the high corrosion resistance of these alloys, accelerated solutions were employed so that results could be obtained in a reasonable length of time. These tests were conducted in a 10% HCl + 1% FeCl₃ solution. Each test run involved six bare samples and six gasketed samples of each alloy. Each specimen was immersed in a 100 cc beaker of the 10% HCl + 1% FeCl₃ corrodent. These were stored in the available space of incubators whose temperature could be maintained at 37°C ± 0.5°C. Crevice corrosion was indicated by both discoloration of the test solution and the evidence of corrosion occurring in the rim of the Teflon ring.

2.1.5 Electrochemistry

Rest potential, passive film corrosion, and anodic polarization measurements were conducted on 0.250 inch diameter by 1.000 inch cylindrical samples of the alloys in both 10% HCl + 1% FeCl₃ and isotonic salt solution (0.9% NaCl). Each specimen employed in the electrochemical measurements was mechanically polished to 4/0 grit paper and then drilled and tapped to fit into a Stern-Makrides (43) electrode holder as shown in Figure 6. Each specimen was then degreased ultrasonically in trichloroethylene for about ten minutes, then rinsed with acetone and distilled water. The variation of electrode potential with time of an isolated specimen immersed in the particular solution was determined by plotting the variation of the potential difference of the electrochemical cell, depicted in Figure 7, consisting of the

oxygenated solution, the metal, and the non-polarizable silver-silver chloride electrode ($E^{\circ} = +0.244 \text{ v}$). Passive film corrosion rates were obtained by immersing the specimen in nitrogen-saturated solution and, with a potentiostat, maintaining the potential at a constant value in the passive region. The applied anodic current is equivalent to the corrosion rate in an oxygenated solution. The cell used for the passive current measurement is illustrated in Figure 8. This same experimental set-up is used to determine the anodic polarization characteristics of the alloys. In the latter experiment the specimens are potentiostatically polarized as anodes. Generally, the anode potential was smoothly varied at a constant rate of 10 mV/minute and the current was simultaneously recorded. Identical electrochemical measurements were made on cylindrical samples fitted with Teflon rings as described above in an effort to correlate the data from the accelerated crevice corrosion tests with the crevice corrosion behavior determined by electrolytic techniques.

2.2 Results

2.2.1 Physical Metallurgy and Mechanical Properties

The microstructure of precision cast H.S. 21 which has been annealed at 1200°C for 4 hours and air cooled is shown in Figure 9. It consists primarily of a coarse grained, cored matrix with coarse carbides. The degree of coring which exists in this structure is indicated in Figure 10 which represents an electron microprobe analysis of the cobalt and chromium distributions in the sample. The cobalt content ranges from a high of 69 wt. % to

a low of 37 wt. %, while the chromium content varies from 38 wt. % to 26 wt. %. The significance of this chemical inhomogeneity in the cast structure will be discussed later. X-ray diffraction studies using equation 1 indicate the matrix phase to be almost totally face centered cubic. The tensile and hardness properties of cast H.S. 21 are listed in the first row of Table 4. In the as cast condition H.S. 21 exhibits a yield stress of 80 ksi, an ultimate tensile stress of 101 ksi, an elongation of 8% and a Rockwell C hardness of 30. The second row of Table 4 indicates that by hot working H.S. 21 it is possible to raise its yield and tensile strengths to 174 ksi and 196 ksi, respectively, while maintaining or actually slightly increasing the as cast percentage elongation. The hardness is also markedly increased by the hot working to 48 R_c. Comparison of Figure 11, which illustrates the microstructure of the as-hot worked H.S. 21, with Figure 9, which indicates the microstructure of precision cast and annealed H.S. 21 illustrates the finer grain size and more uniform distribution of secondary phases achievable through hot working. By subsequent cold rolling of the hot worked material followed by a 1050°C anneal for 40 minutes and air cool, it was possible to raise the yield and ultimate tensile strengths, relative to the as cast material, to 127 and 196.5 ksi, respectively, while more than doubling the as cast percentage elongation to 19%.

In order to facilitate the hot working operations, a modified low carbon version of H.S. 21 whose chemical composition is listed in Table 3 was made. This material was vacuum melted

and electroslag remelted then hot forged and rolled at 1150°C. Table 5 lists mechanical properties of this modified H.S. 21 in the as hot worked condition. Its yield and ultimate tensile strengths are 107 ksi and 180 ksi, respectively, and its elongation is 10%; it exhibits a hardness of 37.5 R_C. X-ray analysis employing equation 1 indicates the matrix to consist of approximately 82% FCC and 18% HCP. Figure 12 illustrates the increase in hardness achieved through cold rolling and Figure 13 indicates the hardness increase to be paralleled by an increase in the amount of HCP. Figures 14-16 illustrate the changes in microstructure produced by the cold rolling. Relatively small amounts of grain deformation are evident, particularly in the more severely cold worked materials.

Figures 17-19 indicate the effect of subsequent heat treatment at various times and temperatures on the cold worked material. Despite the degree of cold working, an 800°C heat treatment, regardless of the length of time, affects little change in the hardness of the alloy. Figures 20 and 21 depict the microstructure of wrought modified H.S. 21 following a cold reduction in area of 7.1% and a 10 minute and 60 minute heat treatment, respectively, at 800°C. X-ray analysis employing equation 1 indicates the matrix to be almost totally hexagonal close-packed. Fine intragranular precipitates which appear to have formed along straight lines can be seen in the cold worked samples heat treated at 800°C when viewed at the higher magnifications depicted in Figures 22 and 23. X-ray diffraction analysis indicates the

precipitates to be a chromium carbide. Despite the degree of prior cold working, few microstructural differences could be found in samples subsequently heat treated at 800°C for varying times. Figures 17-19 indicate that between 800°C and 900°C there is a marked decrease in hardness. As shown in Figures 24-26, this decrease in hardness is accompanied by a drastic reduction in the amount of HCP found in the alloy. The microstructures of samples cold reduced to 7.1% reduction in area and heat treated for various times at 900°C as depicted in Figures 27 and 28 are quite similar to cold rolled samples heat treated at 800°C and previously referred to. In fact, as shown in Figures 29 and 30, a fine intragranular precipitate similar in morphology to that found following 800°C heat treatments is also formed during the 900°C heat treatments.

The photomicrographs of Figures 31 and 32 indicate that the decrease in hardness shown in Figures 17-19 which follows a 1000°C heat treatment is accompanied by recrystallization. In addition, as shown in Figures 33 and 34, coarse intergranular as well as intragranular precipitation has occurred.

The decreases in hardness achieved by heat treating previously cold rolled material at 1100°C and 1200°C are undoubtedly due to lack of carbide precipitation as well as the grain growth which occurred at these temperatures as shown in the photomicrographs in Figures 35-38.

In order to ascertain the temperature which would provide the best combination of strength and ductility, cold worked tensile

specimens were heat treated at 1100°C, 1065°, and 1000°C for 30 minutes and air cooled. The tensile properties resulting from these heat treatments are listed in Table 6 and graphically depicted in Figure 39. Evidently, for a 10% reduction in area by cold rolling, a subsequent heat treatment at 1065°C for 30 minutes followed by an air cool provides the maximum tensile strength and ductility. Figures 40-42 depict the microstructures of these tensile specimens which have been cold rolled to 9.9% reduction in area and heat treated for 30 minutes at 1000°C, 1065°C, and 1100°C, respectively. Evidently, carbide precipitation has occurred at all three temperatures but those treated at 1065°C and 1100°C have a finer grain size than that heat treated at 1000°C. Figures 43 and Table 7 depict the effect of prior cold rolling subsequent to a 12 minute anneal at 1065°C on the tensile properties of hot worked, modified H.S. 21. The samples cold rolled to 11% reduction in area gave the maximum tensile strength and ductility when subsequently heat treated for 12 minutes at 1065°C and then air cooled. Figure 44 and Table 8 indicate that a cold roll of 9.94% reduction in area maximizes the tensile properties of modified H.S. 21 when subsequently heat treated at 1065°C for 30 minutes. Figure 45 and Table 9 cite the effect of prior cold rolling subsequent to a 60 minute anneal at 1065°C on the tensile properties of hot worked modified H.S. 21. Again those samples cold rolled to 10% reduction in area yielded the maximum tensile properties. Figures 46-48 depict the microstructure of those samples heat treated at 1065°C for 12 minutes

subsequent to prior cold rolling of 6%, 10%, and 27% reductions in area. Those samples cold rolled to 10% and 27% reductions in area have finer grain sizes than that cold rolled 6%.

Figure 49 indicates the relative fatigue strengths of the various alloys tested. Most noticeable is the marked improvement in fatigue strength of H.S. 21 achieved by hot working. The as cast H.S. 21 did not exhibit a true endurance limit, and it failed in 10^8 cycles under a stress of 41 ksi. The wrought H.S. 21 had a fatigue endurance limit of 82 ksi. The wrought modified H.S. 21 had an endurance limit of 97.5 ksi.

2.2.2 Corrosion Measurements

Table 10 indicates the times required for the onset of visible crevice corrosion as well as weight loss measurements of the alloys listed in Table 3 in the solution of 10% HCl + 1% FeCl₃. The alloys are listed in order of their resistance to crevice corrosion. Samples of 316L stainless steel, the most widely used surgical implant alloy, were severely pitted within two hours (and did not exhibit crevice corrosion). Elgilloy which has been suggested as a possible surgical implant material (44) crevice corroded in two to three days. The corrosion resistant, high strength alloy MP35N which was developed by G. D. Smith (27) and is produced in the wrought form for surgical implants by Sulzer Brothers of Switzerland (45), crevice corroded in three to four days. The wrought alloy H.S. 25 is sometimes used as a replacement for precision cast Vitallium and H.S. 21 in thin-section implants which are difficult to cast without incurring

harmful structural defects. Four samples of H.S. 25 exhibited visible evidence of crevice corrosion in five days and the remaining two samples crevice corroded in six days. Hastalloy C, a well-known corrosion-resistant nickel-base alloy, exhibited crevice corrosion in 4-6 days. The enhanced general and crevice corrosion resistance of H.S. 21 produced by hot working is demonstrated by the fact that samples of precision cast H.S. 21 exhibited crevice corrosion in 14-21 days while no evidence of crevice corrosion was observed in samples of wrought H.S. 21 after 28 days.

For a short time test of crevice corrosion to provide an accurate assessment of the crevice corrosion susceptibility in 10% HCl + 1% FeCl₃ of the alloys listed in Table 3, it must rate these alloys in the same order as they are rated by the weight loss measurements in this solution and reported in Table 10. Jones and Greene (30) suggested measuring the rest potential of creviced samples. Marked serrations in the plot of potential versus time of a passive alloy might be indicative of localized corrosion. Figure 50 depicts the rest potential behavior of the alloys listed in Table 3 when fitted with Teflon rings to simulate a crevice and immersed in 10% HCl + 1% FeCl₃. Table 11 indicates the times required for the onset of marked serrations in the rest potential curves. Figure 50 indicates no localized corrosion in wrought H.S. 21 which agrees with the results of the weight loss measurements. The potential of H.S. 25, however, is seen to drop to an active value in only about 10 hours. Severe

crevice corrosion was observed under the Teflon ring when the test was terminated 8 days after immersion. The potentials of creviced samples of Elgilloy and Hastalloy C dropped to active values in less than an hour after immersion. Both samples exhibited extensive crevice corrosion. The potential behavior of MP35 was quite different from that of the other alloys examined. While the extent of crevice attack in the creviced sample of MP35 was similar to that of H.S. 25, a significant active drop in potential was not observed. The results of the weight-loss measurements of creviced samples immersed in the 10% HCl + 1% FeCl₃ corrodent as reported in Table 10 agree quite well with the rating of the alloys based on the initiation time for the active trend in potential. This would seem to indicate that in this 10% HCl + 1% FeCl₃ solution, the rest potential variation is a good short time test for crevice corrosion. However, as shown in Figure 51 and Table 12, in less corrosive solutions, such as isotonic salt solution, the times required for marked serrations to appear in the rest potential curves of creviced samples were of the same order of magnitude as the times required to obtain a measurable weight loss. Isotonic salt solution is used to simulate the corrosive action of body fluids. Obtaining weight loss measurements of highly corrosion resistant alloys in this solution requires extremely long times. Since the Teflon rings fitted on our samples to simulate a crevice relax in approximately 4 weeks, it was not possible to obtain highly meaningful comparative weight losses due to crevice corrosion

in this solution. Nevertheless, Table 13 lists the alloys in order of their resistance to corrosive attack as determined by visual inspection of four samples of each alloy affixed with Teflon rings and immersed in 0.9% NaCl solution for 60 days. The relative positions of several of the alloys listed in Table 13 were also based on their resistance to in vivo corrosive attack as determined from a survey of the literature on metallic surgical implants. The relative resistance of the alloys to corrosive attack in the body and in 0.9% NaCl is approximately the same as their relative corrosion resistance in 10% HCl + 1% FeCl₃, as reported in Table 10. Figure 51 depicts the potential variation with time of creviced samples immersed in 0.9% NaCl. All tests were terminated after 8 to 9 days. In this time span only 316L stainless steel exhibited any indication of localized attack. Figure 52 depicts the appearance of the sample of 316L stainless steel after the 9 days of immersion and after the Teflon ring was cut away. All other samples maintained their passivity as indicated by both the stable appearance of their rest potential curves and the absence of pits on their surface when observed under a microscope. Table 12 lists the times required to initiate marked serrations in the rest potential curves and indicates that the potential variation with time of creviced samples cannot serve as a short time test of the susceptibility of an alloy to crevice corrosion.

Some investigators have suggested that the pitting potential of an alloy might be indicative of its tendency to

crevice corrode (31). Table 14 lists the pitting potentials as obtained from the anodic polarization curves of the alloys in 10% HCl + 1% FeCl₃. The latter curves are depicted in Figure 53. The pitting potentials listed in Table 14 are somewhat arbitrary in that no abrupt changes in slope were observed on any of the anodic polarization curves which would aid in identifying the pitting potentials. Comparison of Table 14 with Table 10 which lists the weight loss measurements of creviced samples in 10% HCl + 1% FeCl₃ indicates that in this solution no correlation exists between pitting potential and the tendency to crevice corrode as measured by direct immersion corrosion.

Other investigators have suggested that the "protective potential" of an alloy might be indicative of its tendency to crevice corrode (32). Subsequent work, however, showed that the protective potential was not a material property and was primarily dependent upon experimental technique. Nevertheless, Wilde obtained a correlation between the pitting tendency of various stainless steels and a difference potential defined as the difference between the protective potential and the pitting potential (47). The protective potential in Wilde's test was obtained by tracing the anodic polarization curve up to a certain current density in the transpassive region and then returning by the same potential route until the anodic curve closed back on itself. When the same experiment was performed on the alloys listed in Table 3 when immersed in 10% HCl + 1% FeCl₃ as well as in 0.9% NaCl, Tables 15 and 16 which list the protective potentials

taken from Figures 54-66 indicate that it was not always possible to obtain any type of protective potential.

Lizlovs attempted to measure the crevice corrosion susceptibilities of several passive alloys by measuring the passive film corrosion rate of creviced samples at an applied potential of 0.0 volts (33). In Figures 67-72 are plotted the passive film corrosion rates of the alloys listed in Table 3 when fitted with Teflon rings and immersed in deaerated 10% HCl + 1% FeCl₃ at various applied potentials in the passive region. Various applied potentials were used rather than just one in order to test the crevice corrosion behavior throughout the passive region. Figure 67 indicates that immediately following immersion with its potential fixed at -25 mV, the creviced sample of 316L stainless steel was cathodic. Approximately 30 minutes after immersion, the samples began to actively corrode at a very rapid rate and was visibly pitted within minutes. Figure 68 depicts the results of the passive film corrosion tests on creviced samples of Elgilloy. Initially the corrosion rate decreases with time and the alloy exhibits the usual behavior of passive alloys in the passive region of the anodic polarization curve. However, after a certain incubation period the corrosion rate discontinuously increases. When the tests were terminated approximately 2000 minutes after immersion and the Teflon gaskets removed, corrosion was observed to have occurred under the gaskets. Similarly, in all the alloys examined, whenever the corrosion current density abruptly increased, the samples were found to have suffered corrosion under the Teflon

ring. It should be noted here that once significant localized corrosion has started, the corrosion current densities listed in these figures are much lower than the actual current densities. Since there is no way of knowing the exact area of localized attack, the entire specimen surface area exposed to the solution continued to be employed in calculating the corrosion current density. As indicated in Figure 72, no sharp increases in corrosion current density were found in the measurements conducted on creviced samples of wrought H.S. 21. Despite the applied potential, the Teflon ring affixed samples continued to exhibit passive behavior and no localized corrosion was observed. At an applied potential of +900 mV, the corrosion rate was found to increase continuously after approximately 150 minutes. This simply reflects the uniform dissolution of the protective passive film on the sample which occurs at potentials more noble than the breakdown potential. When these measurements were obtained for all the alloys listed in Table 3, the lowest applied potentials at which crevice corrosion occurred were used to rate the alloys' resistances to crevice corrosion. The higher the applied potential required to initiate crevice corrosion the more resistant the alloy was considered to be to crevice attack. These potentials are listed in Table 17. Comparison of this table with Table 10 indicates that the passive film corrosion test of creviced samples rates the alloys' susceptibilities to crevice corrosion attack in the same manner as do weight loss measurements. The results of the passive film corrosion test of creviced samples immersed in 0.9%

NaCl are depicted in Figures 73-79 and are summarized in Table 18. Comparison of the latter table with the results of long time in vivo statistics and 60 day immersion tests in 0.9% NaCl presented in Table 13 again indicates that the results of the short time passive film corrosion measurements on creviced samples agree with the results of long time immersion tests.

III. DISCUSSION

Early attempts to improve the fabricability and strength of cobalt-chromium-molybdenum alloys by compositional modifications were unsuccessful because of the accompanying decrease in corrosion resistance of the alloy. While dilute additions of aluminum and beryllium (24), and nickel additions in excess of 5 wt. % (27) were found to markedly enhance the hot and cold workability of cobalt-chromium-molybdenum alloys, such additions resulted in decreased crevice corrosion resistance in chloride-ion media (25,27). Similar impairment of the crevice corrosion resistance as well as loss in ductility resulted from the precipitation hardening of cobalt-chromium alloys containing additions of tantalum, tungsten, molybdenum, and niobium (25).

The marked enhancement of the mechanical properties of 20 wt. % chromium-10 wt. % molybdenum-0.10 wt. % carbon-balance cobalt alloy achieved by thermomechanical processing indicated the feasibility as well as the advantages of hot and cold working cobalt-chromium-molybdenum-carbon alloys (25). The hot press forging and rolling experiments of H.S. 21 and modified H.S. 21 conducted in cooperation with the engineers at the Stellite Division of the Cabot Corporation as well as the hot extrusion operations of H.S. 21 performed at the Whittaker Corporation demonstrate the hot fabricability of H.S. 21. In addition, experiments conducted at our request by the Wyman-Gordon Company indicate that hot rolled stock of H.S. 21 can be economically close-die forged into intricately shaped parts.

The wrought 20 wt. % chromium-10 wt. % molybdenum-0.10 wt. % carbon-balance cobalt alloy and the wrought H.S. 21 had after hot and cold working and heat treatment equivalent tensile properties and crevice corrosion resistance as measured by the direct immersion corrosion test conducted in the 10% HCl + 1% FeCl₃ solution at 37°C. The better crevice corrosion resistance of the wrought varieties of H.S. 21, modified H.S. 21 and the 20 wt. % chromium-10 wt. % molybdenum alloy as compared to their as-cast counterparts can in large measure be attributed to their greater chemical as well as structural homogeneity. The superior tensile properties of the wrought versions of these three alloys relative to the cast varieties is undoubtedly due to the finer grain size and more uniform distribution of secondary phases found in the wrought material.

Cold rolling the as hot worked modified H.S. 21 to circa 10% reduction in area subsequent to a 30 minute anneal at 1065°C provided the best combination of strength and ductility. The latter processing treatment resulted in an ultimate tensile strength of 238,000 psi, which is more than double the ultimate tensile strength of the as cast H.S. 21, and an elongation of 26.1% which is more than triple the as cast percentage elongation.

The improvement in mechanical properties of H.S. 21 and modified H.S. 21 achieved by thermomechanical processing can be explained in the same manner as that offered by Graham and Youngblood in their study of the effects of thermomechanical processing on the mechanical properties of cobalt-20 wt. %

chromium-10 wt. % molybdenum alloys containing nickel additions of 10 to 40 wt. %. Graham and Youngblood found that cold swaging of hot worked stock of their alloys resulted in the formation of intersecting sets of fine parallel platelets of the HCP phase. These platelets were on the order of 0.01 to 0.1 μ thick and exhibited the same crystallographic relationship with the FCC matrix phase as that found in pure cobalt; namely:

$$\{111\}_{\text{FCC}} \parallel \{0001\}_{\text{HCP}} \quad \text{and} \quad \langle 110 \rangle_{\text{FCC}} \parallel \langle 11\bar{2}0 \rangle_{\text{HCP}}$$

The lower the nickel content of their alloy the more readily the HCP platelets formed during cold working operations (46).

The metallographic investigation of the structure of the cold worked modified H.S. 21 studied in the present work indicated that heat treatment at 800°C and 900°C of small slugs sectioned from cold rolled plate resulted in linear intragranular arrays of fine carbide precipitates. The linear array of precipitates probably results from the precipitates forming along the interface between the HCP platelets and the retained FCC phase and along slip lines produced during the cold rolling. Heat treating at 1000°C small slugs sectioned from cold rolled plate resulted in the formation of intergranular as well as intragranular carbide precipitates which are much coarser than those formed during the 800°C and 900°C heat treatments.

Little or no carbide precipitation occurred in those slugs sectioned from cold rolled plate and heat treated at 1100°C. Wheeton and Signorelli reported carbide precipitation in samples

of H.S. 21 containing 0.29 wt. % carbon when heat treated at 1095°C and carbide dissolution at 1230°C. This, however, does not contradict the findings reported here since the modified H.S. 21 employed in this investigation contained only 0.145 wt. % carbon.

The microstructural investigation of tensile specimens which were cold rolled to 9.9% reduction in area and heat treated for 30 minutes at 1000°C, 1065°C, and 1100°C, respectively, indicated that carbide precipitation had occurred at all three temperatures but those heat treated at 1065°C and 1100°C had a finer grain size than that heat treated at 1000°C. The greater tensile properties achieved by the 1065°C heat treatment is indicated in Figure 39. Evidently, the finer grain size of the sample heat treated at 1065°C relative to that heat treated at 1000°C is responsible for the higher tensile properties of the former. A heavy amount of intergranular and some intragranular carbide precipitation was found in the tensile specimen heat treated at 1100°C. That the smaller metallographic slugs which were heat treated at 1100°C did not show any carbide precipitation can perhaps be rationalized by assuming that the extra cold work produced by cutting the slugs from the cold rolled plate and the shorter time required for the smaller specimen to reach the heat treatment temperature resulted in redissolution of any carbides which might have precipitated during upheating. Of particular significance is the observation that 10% cold reduction prior to heat treatment at 1065°C maximizes the tensile properties of

modified H.S. 21. Metallographic studies indicate the greater mechanical properties of those samples cold rolled to 10% reduction in area prior to heat treatment at 1065°C to be due to the finer grain size of the latter material. The finer grain size of the material cold rolled to 10% reduction in area can be attributed to the fact that deformation in these alloys is primarily accommodated by the FCC → HCP martensitic transformation. As indicated in Figure 13 cold rolling hot worked modified H.S. 21 to 6% reduction in area produces a matrix of approximately 87% HCP. Recrystallization, therefore, is more extensive at 1065°C for the 10% cold rolled material than for the 5% cold rolled material. This would also explain the little difference in grain size between those samples cold rolled to 10% reduction in area and those cold rolled to greater amounts. The amount of HCP phase produced in the as hot worked material as a function of cold work levels off at about 10% reduction in area. Thus, samples cold rolled to 10% reduction in area or more all have approximately the same activation energy for recrystallization and attain approximately the same fine grain size when annealed at 1065°C. The greater tensile properties of those samples cold rolled to 10% reduction in area relative to those rolled greater amounts might possibly be due to greater amounts of carbide precipitation in the higher cold worked material.

It is interesting to note that each of the corrosion tests employed in the present work rated the wrought H.S. 21 alloy superior in crevice corrosion resistance to all the alloys

investigated. The superior crevice corrosion resistance of the wrought H.S. 21 relative to the cast H.S. 21 can in large measure be attributed to the greater chemical as well as structural homogeneity of the wrought material. Nevertheless, the various electrochemical tests employed in the present work do not all rate the alloys' resistances to crevice attack in the same order as the direct immersion corrosion tests. This illustrates the fact that not all the electrochemical tests which are sometimes used in the literature for rating an alloy's susceptibility to crevice corrosion correctly simulate a material undergoing crevice corrosion.

Rating the alloy's crevice corrosion behavior in 10% HCl + 1% FeCl₃ on the basis of rest potential measurements of creviced samples immersed in this solution concurs with the results of the direct immersion corrosion tests of creviced samples in the 10% HCl + 1% FeCl₃ solution. The crevice corrosion behavior of a creviced sample whose potential variation with time is being electrolytically monitored closely resembles the crevice corrosion behavior of isolated creviced samples immersed in the same solution. However, as indicated in the rest potential measurements of creviced samples immersed in 0.9% NaCl, the rest potential test cannot predict in a relatively short length of time the comparative long time crevice corrosion susceptibilities of corrosion resistant alloys immersed in relatively weak corrosives. A short time rest potential measurement merely indicates whether or not localized corrosion occurs during the time of

measurement. The results of a short time rest potential test of a creviced sample cannot be used to predict the susceptibility of the alloy to localized corrosion during long time immersion.

The lack of correspondence between the results of the pitting potential measurements and the results of the direct immersion crevice corrosion tests conducted in both 10% HCl + 1% FeCl₃ and 0.9% NaCl solutions indicate that although the mechanisms of pitting and crevice corrosion have been suggested as being identical, the pitting potential does not necessarily indicate the crevice corrosion behavior of an alloy. The pitting potential represents the potential at which an aggressive anion such as a chloride ion can adsorb on the metal's surface or the potential at which an aggressive anion can migrate through the oxide film, depending upon which theory of passivity one subscribes to, thereby increasing the dissolution locally. In either case, however, pitting will first occur at defects in the passive film. Hence, the initiation of pitting and the pitting potential depend upon microscopic factors. The initiation of crevice corrosion, however, depends principally upon factors related to the geometry of the crevice.

Measurements of the protective potential as conducted by Wilde to assess the crevice corrosion susceptibility of alloys may be useful in comparing alloys of closely similar polarization characteristics but not for alloys of widely differing passive behavior such as investigated in the present work. The protective potential as determined by Wilde's procedure is that potential at

which pits created during an applied potential traverse to a certain corrosion current density in the transpassive region are repassivated on returning the applied potential to lower values. The number and the geometry of pits produced by anodically polarizing an alloy specimen to some corrosion current density in the transpassive region will depend upon the magnitude of this current density in relation to the passive corrosion current density. Consequently, the potential at which these pits are repassivated will also depend upon the passive corrosion current density. When comparing alloys of widely varying passive current densities, the protective potential as determined by Wilde's procedure has little significance.

The finding in the present study that the corrosion current density measurement of anodically polarized creviced samples rate the different alloys in the same order of crevice corrosion resistance as the direct immersion crevice corrosion tests in both the 10% HCl + 1% FeCl₃ solution and 0.9% NaCl solution is not fortuitous. This electrochemical test closely simulates a material undergoing crevice corrosion. Initially, the whole of the surface of the metal including that under the gasket is devoid of pits or holes. The passive corrosion current density decreases with time as though no crevice were present. However, within the crevice metal ions dissolved during the corrosion process build up and are not swept away as they are on the metal surface outside the crevice by convection currents. Consequently, chloride ions tend to migrate to this region. Since

chloride ions enhance the dissolution rate of the metal, more metal ions dissolve attracting more chloride ions and the process becomes autocatalytic. The greater the resistance of an alloy to chloride ion attack, the higher the potential at which crevice corrosion will first occur in this test.

Before closing this section, it should be noted that while the wrought cobalt-chromium-molybdenum-carbon alloys appear well suited for use in thin section weight bearing implants which are difficult to cast without incurring harmful structural defects, precision castings of these alloys will undoubtedly continue to find use as surgical implant material. It remains to be determined whether or not the wrought cobalt-chromium-molybdenum-carbon alloys will prove more useful than the high strength wrought alloys of titanium currently being used by surgeons in the United Kingdom and, to a much lesser extent, in the USA. To date, titanium alloys have only been faulted for use as rubbing members in certain total-joint replacement prostheses. Whether or not any abrasion corrosion tendencies of titanium alloys in body fluids will lead to premature stress corrosion and corrosion fatigue failures has also yet to be redetermined.

IV. CONCLUSIONS

1. It was found possible in the present study to hot work cobalt-chromium-molybdenum-carbon alloys containing 20-28 wt. % chromium, 5-10 wt. % molybdenum, 0.10-0.32 wt. % carbon by press forging at 1150°C as well as by extrusion at temperatures above 1094°C (2000°F).
2. It was also found possible to hot roll or hot swage such pre-worked materials at 1100°C-1200°C into sheet and rod.
3. Cold rolling the as hot worked modified H.S. 21 to circa 10% reduction in area subsequent to a 30 minute anneal at 1065°C resulted in an ultimate tensile strength of 238,000 psi which is more than double the ultimate tensile strength of the as cast H.S. 21, and an elongation of 26.1% which is more than triple the as cast percentage elongation.
4. The various crevice corrosion tests employed in the present work rated the wrought H.S. 21 superior to the cast H.S. 21 and to all the alloys investigated.
5. Of the various electrochemical tests employed only the results of the corrosion current density measurements of creviced samples rated the various alloys in the same order as the results of the direct immersion corrosion tests in both the 10% HCl + 1% FeCl₃ and 0.9% NaCl solutions.
6. Metallographic investigation indicated the superior mechanical properties and corrosion resistance of the wrought cobalt-chromium-molybdenum-carbon alloys relative to their

cast counterparts to be due to the finer grain size, greater chemical and structural homogeneity, and finer distribution of secondary phases of the wrought material relative to the cast.

V. RECOMMENDATIONS FOR FUTURE WORK

1. X-ray and electron diffraction studies should be undertaken to identify the exact nature of the chromium carbide precipitate (possibly Cr_{23}C_6 or Cr_7C_3) which forms on heat treating cold rolled samples of modified H.S. 21 between 800°C and 1065°C . It would also be useful to further investigate the kinetics of this reaction to determine the optimum age-hardening time and temperature which would provide the greatest strengthening of the alloy without markedly lowering the ductility.
2. Comparative studies of the wear characteristics in air and in 0.9% NaCl of the wrought versus the cast cobalt-chromium-molybdenum-carbon alloys should be conducted to determine what effect if any the finer grain size and finer more uniform distribution of secondary phases of the wrought material has on the abrasion corrosion behavior of these alloys.
3. Fatigue crack propagation studies in various corrodents at low stress intensity levels of the wrought and cast cobalt-chromium-molybdenum-carbon alloys should be conducted to determine the effects of (a) the greater corrosion resistance and (b) the greater tensile properties of the wrought material on the corrosion fatigue crack propagation rate in these alloys.
4. A preliminary investigation based on the work of Giamei et al (22) on cobalt-tungsten and cobalt-chromium binary alloys

indicated that a 4 to 1 reduction in grain size of cast H.S. 21 could be obtained by a fairly simple heat treating schedule. The heat treatment process consisted of heating the cast sample of H.S. 21 at 1065°C for 2 hours to ensure complete carbide precipitation and then quenching into a dry ice and acetone mixture and then into liquid nitrogen. This treatment martensitically transformed a significant fraction of the FCC matrix phase into the HCP phase. On reheating the sample at 1000°C for 30 minutes the FCC phase uncleaned at the HCP platelet-retained FCC phase interface and resulted in a 4 to 1 grain size refinement. Further tests should be conducted to determine the optimum quench from the 1065°C heat treatment and the optimum temperature and time of the subsequent heat treatment. Hardenability studies should also be conducted to determine the maximum size of the casting which will undergo the martensitic transformation for various quenching mediums. An investigation should be conducted to determine the effect of this grain size refinement on the tensile, fatigue, and wear properties of the alloy.

5. Finally, corrosion current density measurements on creviced samples of the alloys investigated in this thesis as well as other alloys should be obtained in corrodents of varying chloride ion content and pH and compared to long time weight loss measurements of isolated creviced samples immersed in the same corrodents to further assess the applicability of

this electrochemical test as a short time crevice corrosion test.

VI. REFERENCES

1. J. T. Scales, G. D. Winter, and H. T. Shirley, "Corrosion of Orthopaedic Implants," Journal of Bone and Joint Surgery, 41B, p. 810, 1959.
2. J. H. Hicks and W. H. Cater, "Minor Reactions Due to Modern Metal," Journal of Bone and Joint Surgery, 44B, p. 122, 1962.
3. J. Brettle and A. N. Hughes, "A Metallurgical Examination of Surgical Implants Which Have Failed in Service," United Kingdom Atomic Energy Authority Report No. GRO/44/83/12 (Ex).
4. F. W. Bultitude and J. R. Morris, "Corrosion of Metal Implants. The Examination of Implants Corroded In Vivo," United Kingdom Atomic Energy Authority Report No. GRO/44/83/22 (Ex).
5. V. J. Colangelo and N. D. Greene, "Corrosion and Fracture of Type 316 SMO Orthopedic Implants," Report to National Institute of Health (GM-12661-01), 1968.
6. J. T. Scales, B. M. Roantree, R. Perry, and R. Eborall, "Ten Years of Fixation of Fractures," Engineering in Medicine, 2, p. 51, 1973.
7. T. P. Hoar and D. C. Mears, "Corrosion-Resistant Alloys in Chloride Solutions Materials for Surgical Implants," Proceedings of the Royal Society (London), A294, p. 486, 1966.
8. K. Asgar and F. A. Peyton, "Effect of Casting Conditions on Some Mechanical Properties of Cobalt Base Alloys," Journal of Dental Research, 40, p. 73, 1961.
9. J. Charnley, "Stainless Steel for Femoral Hip Prostheses in Combination with a High Density Polythene Socket," Journal of Bone and Joint Surgery, 53B, p. 342, 1971.
10. J. Brettle, "A Survey of the Literature on Metallic Surgical Implants," United Kingdom Atomic Energy Authority Report No. GRO/44/83/13 (Ex).
11. P. G. Laing, A. B. Ferguson, and E. S. Hodge, "Tissue Reaction in Rabbit Muscle Exposed to Metallic Implants," Journal of Biomedical Materials Research, 1, p. 135, 1967.
12. R. W. Revie and N. D. Greene, "Comparison of the In Vivo and In Vitro Corrosion of 18-8 Stainless Steel and Titanium," Journal of Biomedical Materials Research, 3, p. 465, 1969.

13. R. W. Revie and N. D. Greene, "Corrosion Behavior of Surgical Implant Materials: I. Effects of Sterilization," Corrosion Science, 9, p. 755, 1969.
14. F. J. Kummer, "Permanent Surgical Implant Alloys," M.I.T. Ph.D. Thesis, submitted June, 1973.
15. J. T. Scales, "Examination of Implants Removed from Patients," Proceedings and Reports of Councils and Associations, Journal of Bone and Joint Surgery, 53B, p. 344, 1971.
16. E. Haynes, U.S. Patent 873,755; 1907.
17. R. W. Erdle, U.S. Patent
18. R. W. Erdle and C. H. Prange, U.S. Patent 1,956,278; 1934.
19. C. P. Sullivan, M. J. Donachie, and F. R. Morral, "Cobalt-Base Superalloys - 1970," Centre D'Information du Cobalt, Brussels, 1970.
20. A. R. Troiano and J. L. Tokich, "The Transformation of Cobalt," Transactions, American Institute of Mining and Metallurgical Engineers, 175, p. 728, 1948.
21. M. Hansen, "Constitution of Binary Alloys," McGraw-Hill Book Company, London, 1958.
22. A. Giamei, J. Burma, and E. J. Freise, "The Role of the Allotropic Transformation in Cobalt-Base Alloys," Cobalt, 39, p. 88, 1968.
23. T. M. Devine, F. J. Kummer, and J. Wulff, "Wrought Cobalt-Chromium Surgical Implant Alloys," Journal of Materials Science, 7, p. 126, 1972.
24. J. J. Rausch, J. B. McAndrew, and C. R. Simcoe, "Effect of Alloying on the Properties of Wrought Cobalt," in "High Temperature Materials II," Metallurgical Society Conferences, 18, p. 259, J. Wiley and Sons, New York, 1963.
25. T. M. Devine, "A Wrought Cobalt-Chromium-Molybdenum Alloy for Surgical Implants," M.I.T. SB-SM Thesis, submitted May 14, 1971.
26. J. M. Drapier, J. L. de Brouwer, and D. Coutsouradis, "Refractory Metals and Intermetallic Precipitates in Cobalt-Chromium Alloy," Cobalt, p. 1, 1965.
27. G. D. Smith, U.S. Patent 3,356,542; 1967.

28. Personal Communication, June 1971, S. Wlodek, Cabot Corporation, Stellite Division, Kokomo, Indiana.
29. R. P. Jackson and D. van Rooyen, "Crevice Corrosion of Some Ni-Cr-Mo-Fe Alloys in Laboratory Tests," in "Localized Corrosion -- Causes of Metal Failure," ASTM Special Technical Publication 516.
30. D. A. Jones and N. D. Greene, "Electrochemical Detection of Localized Corrosion," Corrosion, 25, p. 367, 1967.
31. J. Degerbeck, "On Accelerated Pitting and Crevice Corrosion Tests," Journal of the Electrochemical Society, 120, p. 175, 1973.
32. B. E. Wilde and E. Williams, "The Relevance of Accelerated Electrochemical Pitting Tests to the Long-Term Pitting and Crevice Corrosion Behavior of Stainless Steels in Marine Environments," Journal of the Electrochemical Society, 118, p. 1057, 1971.
33. E. A. Lizlovs, "Polarization Cell for Potentiostatic Crevice Corrosion Testing," Journal of the Electrochemical Society, 117, p. 1335, 1970.
34. I. L. Rosenfeld and I. K. Marshakov, "Mechanism of Crevice Corrosion," Corrosion, 20, p. 115t, 1964.
35. U. R. Evans and D. E. Davies, "The Pitting of Zinc by Distilled Water and Dilute Solutions," Journal of the Chemical Society, p. 2607, 1951.
36. U. R. Evans, L. C. Bannister, and S. C. Britton, "The Velocity of Corrosion from the Electrochemical Standpoint," Proceedings of the Royal Society, A131, p. 355, 1931.
37. M. G. Fontana and N. D. Greene, "Corrosion Engineering," McGraw-Hill, p. 42, 1967.
38. G. J. Schafer, J. R. Gabriel, and P. K. Foster, "On the Role of the Oxygen Concentration Cell in Crevice Corrosion and Pitting," Journal of the Electrochemical Society, 107, p. 1002, 1960.
39. U. R. Evans, "The Corrosion and Oxidation of Metals: First Supplementary Volume," St. Martins Press, p. 87, 1968.
40. N. D. Greene and G. Judd, "Relation Between Anodic Dissolution and Resistance to Pitting Corrosion," Corrosion, 21, p. 15, 1965.

41. M. G. Fontana and N. D. Greene, "Corrosion Engineering," McGraw-Hill, p. 322, 1967.
42. M. Sage and Ch. Guillaud, Rev. Met., 47, p. 139, 1950, as cited in reference number 46.
43. M. Stern and A. C. Makrides, "Electrode Assembly for Electrochemical Measurements," Journal of the Electrochemical Society, 107, p. 782, 1960.
44. F. R. Morrall, "Cobalt Alloys as Implants in Humans," Journal of Materials, 1, p. 384, 1966.
45. Sulzer Catalogue of Surgical Implant Prostheses.
46. A. H. Graham and J. L. Youngblood, "Work Strengthening by a Deformation Induced Phase Transformation in 'MP Alloys'," Metallurgical Transactions, 1, p. 423, 1970.
47. B. E. Wilde, "A Critical Appraisal of Some Popular Laboratory Electrochemical Tests for Predicting the Localized Corrosion Resistance of Stainless Alloys in Sea Water," Corrosion, 28, p. 283, 1972.
48. J. Wulff and J. Cohen, "Clinical Failure Caused by Corrosion of a Vitallium Plate," Journal of Bone and Joint Surgery, 54A, p. 617, 1972.
49. R. M. Rose, A. Schiller, and E. Radin, "Corrosion-Accelerate Mechanical Failure of a Vitallium Nail-Plate," Journal of Bone and Joint Surgery, 54A, p. 854, 1972.

Figure 1. The role of a differential aeration cell in initiating crevice corrosion.

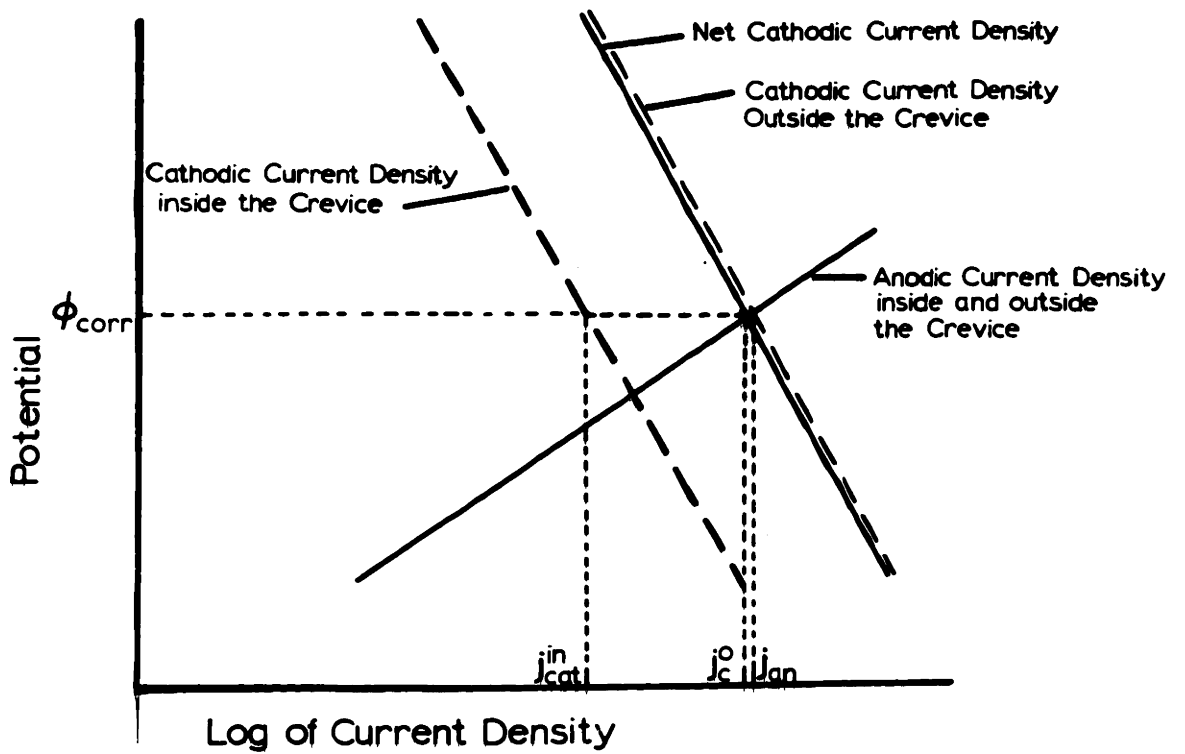
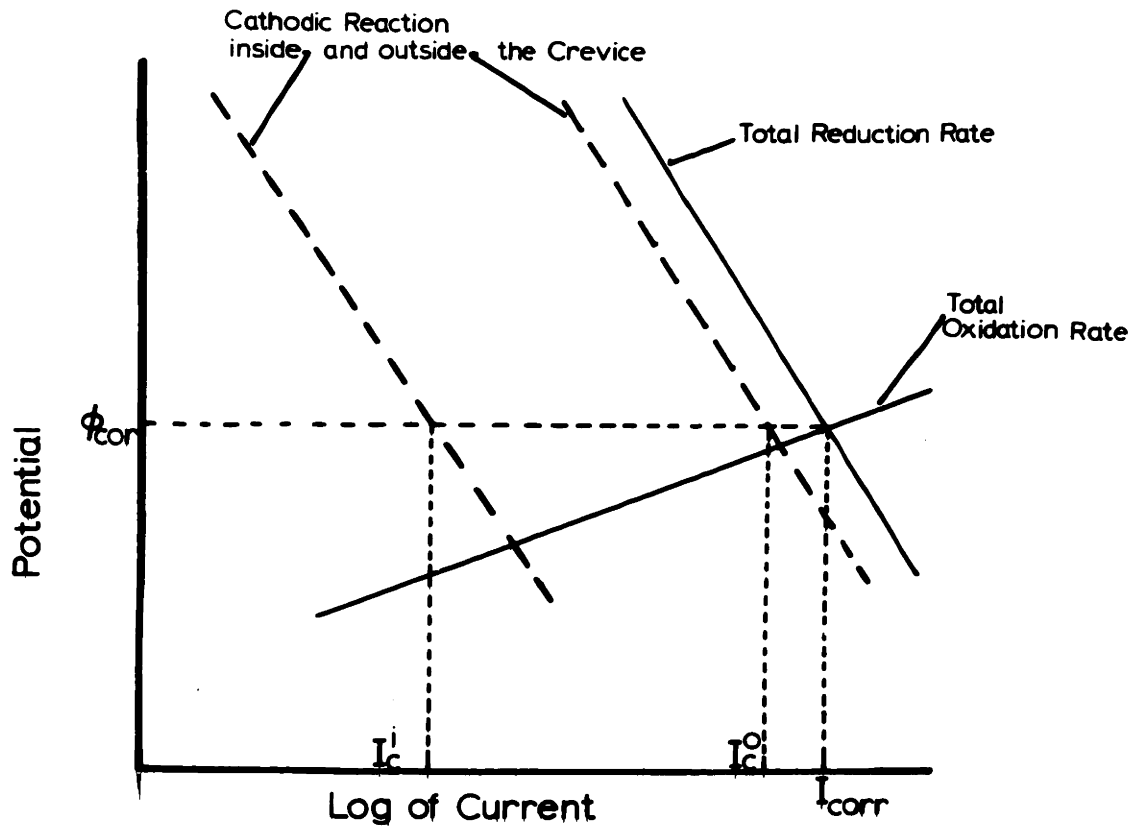


Figure 2. The effect of chloride ions on normal metal dissolution.

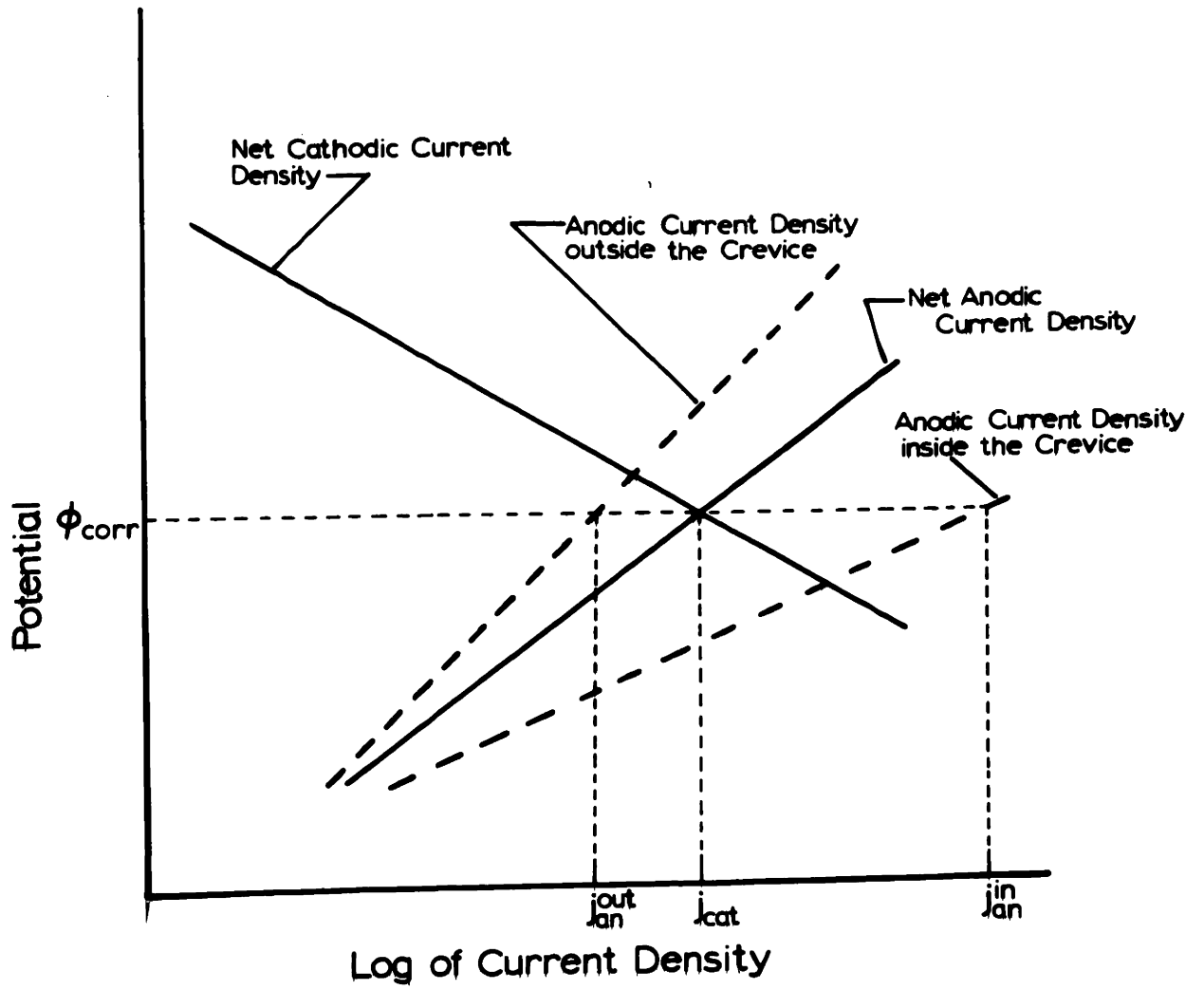


Figure 3. The effect of chloride ions on the anodic polarization behavior of a passive metal.

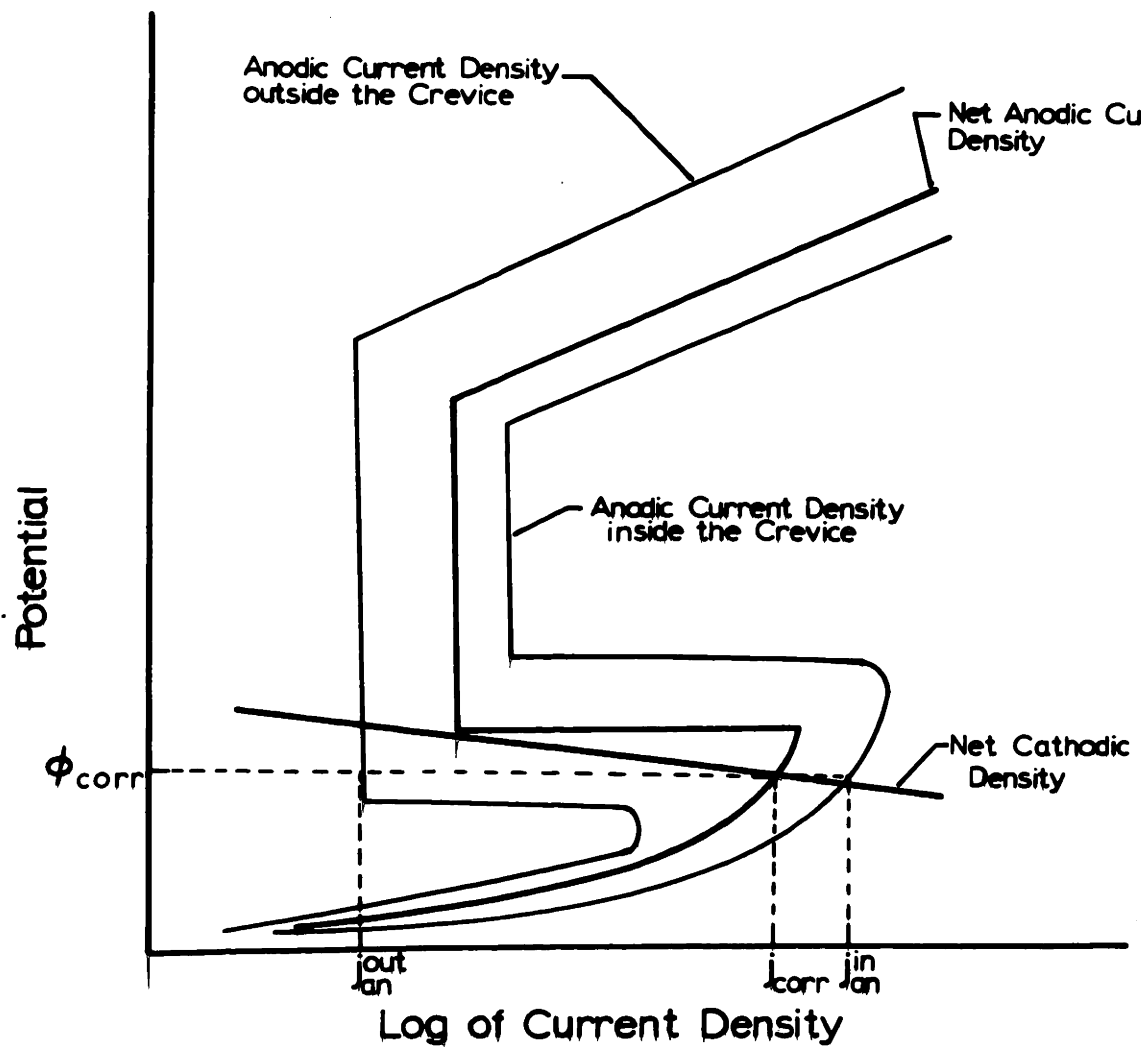


Figure 4. Rotating bending fatigue specimen and loading scheme.

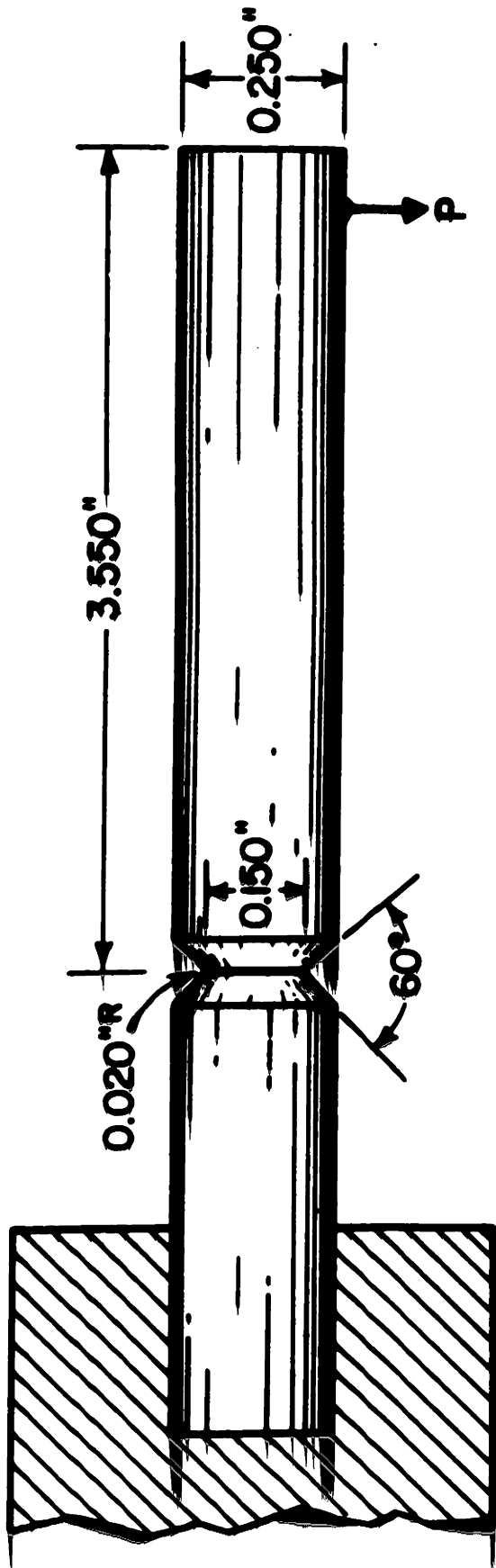
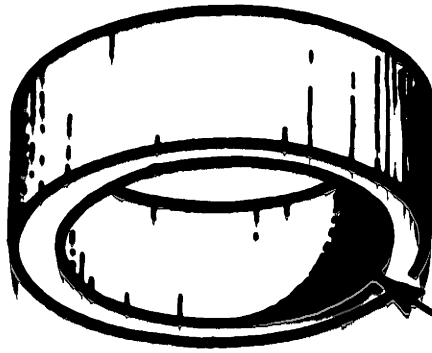


Figure 5. Geometry of accelerated crevice corrosion

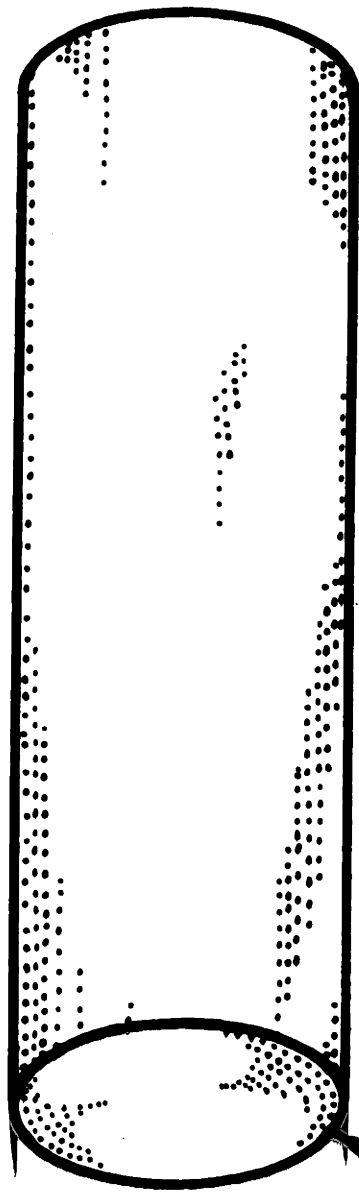
Teflon ring



0.235" D

0.125" length

Sample



0.250" D 1.000" length

Figure 6. Creviced sample mounted in a Stern-Makrides electrode holder.

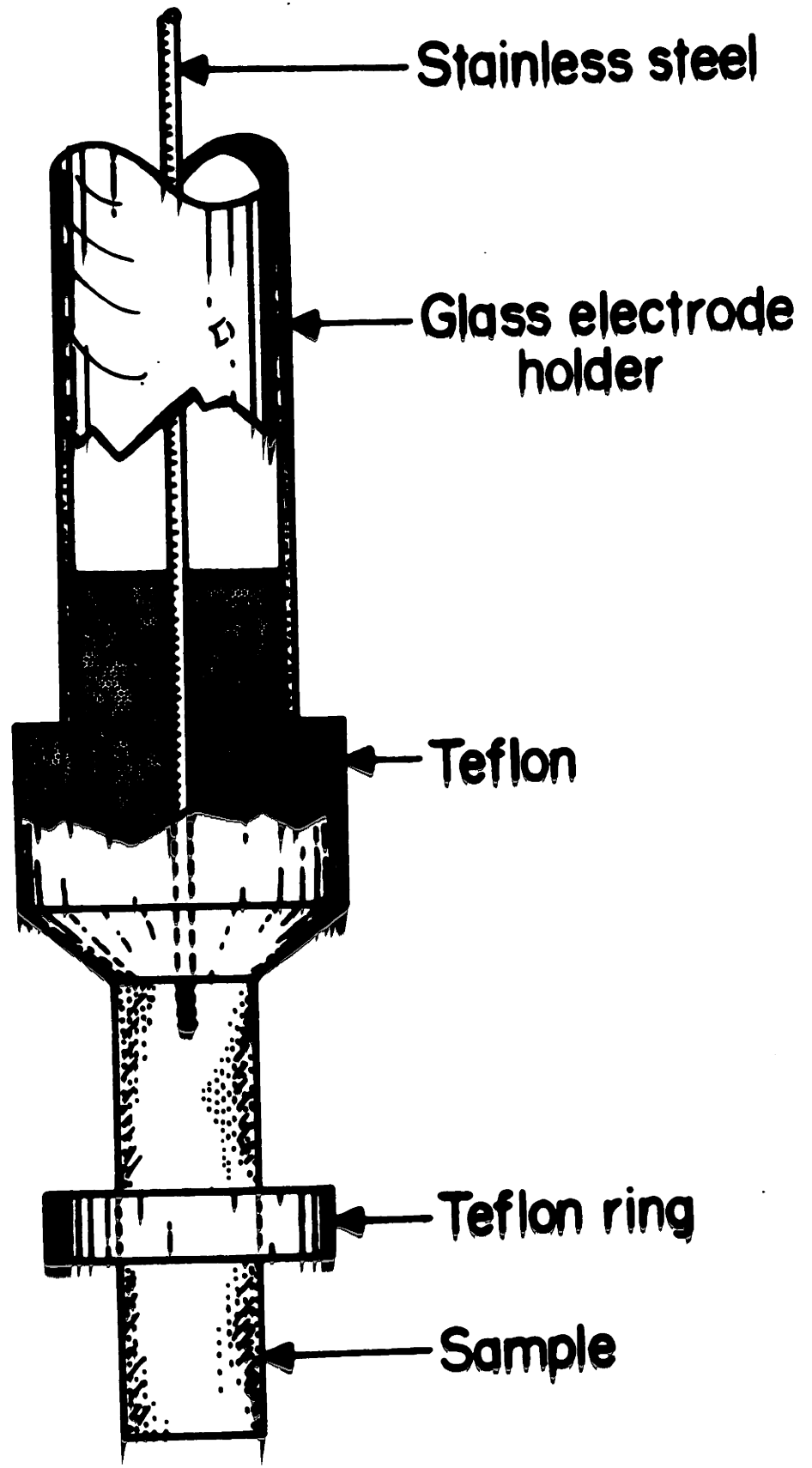


Figure 7. Electrochemical cell for measuring potential variations with time of test specimens.

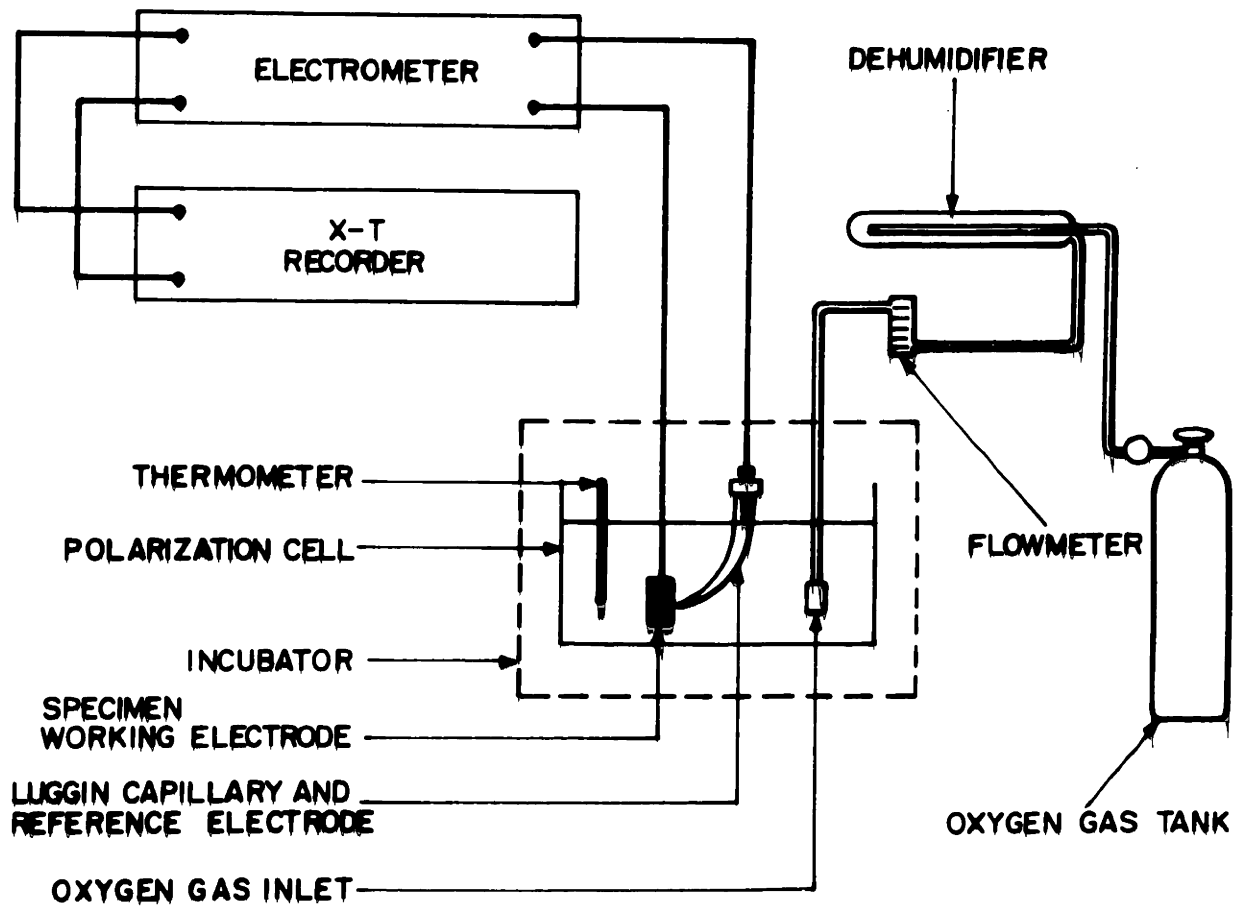
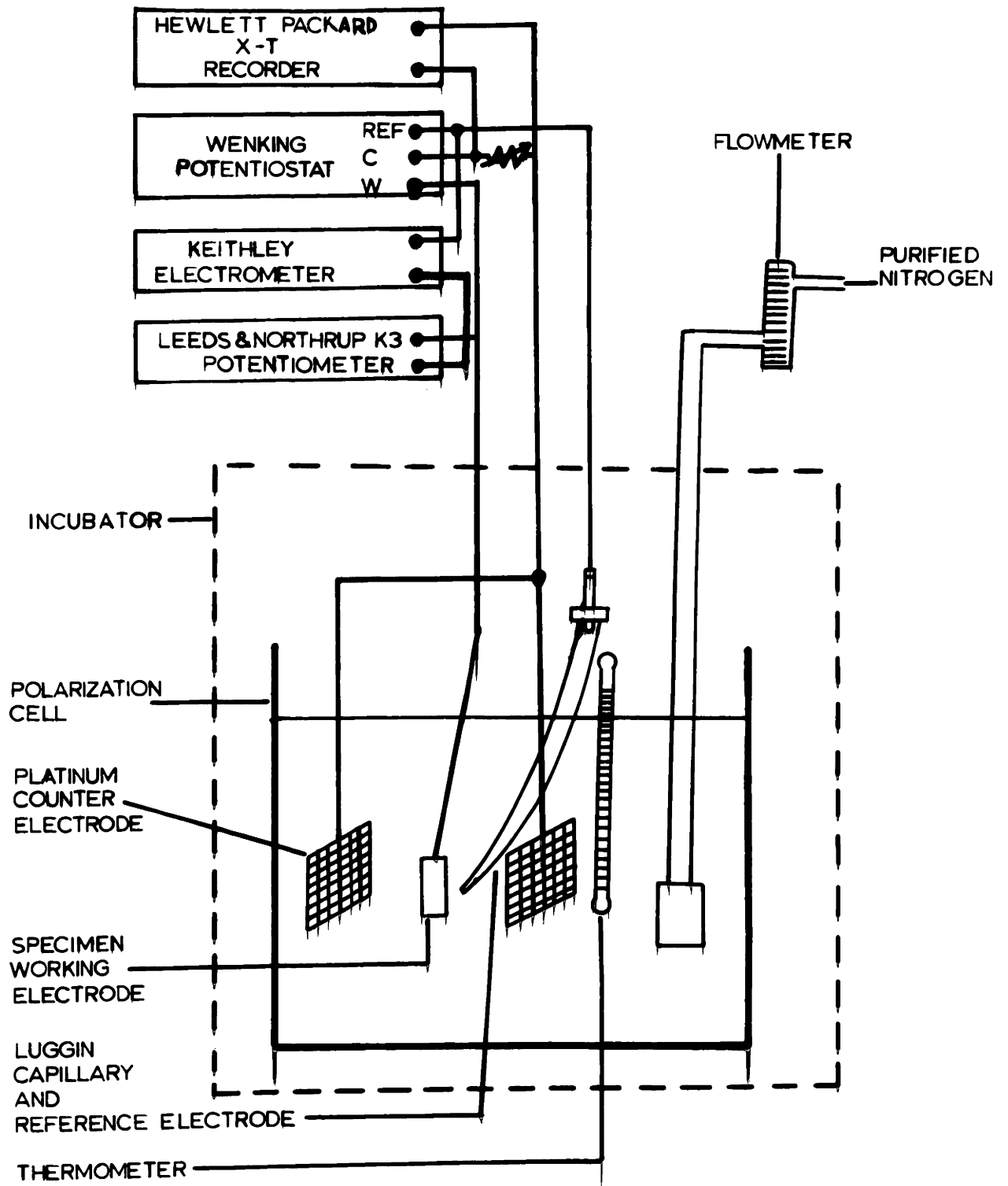


Figure 8. Anodic polarization apparatus.



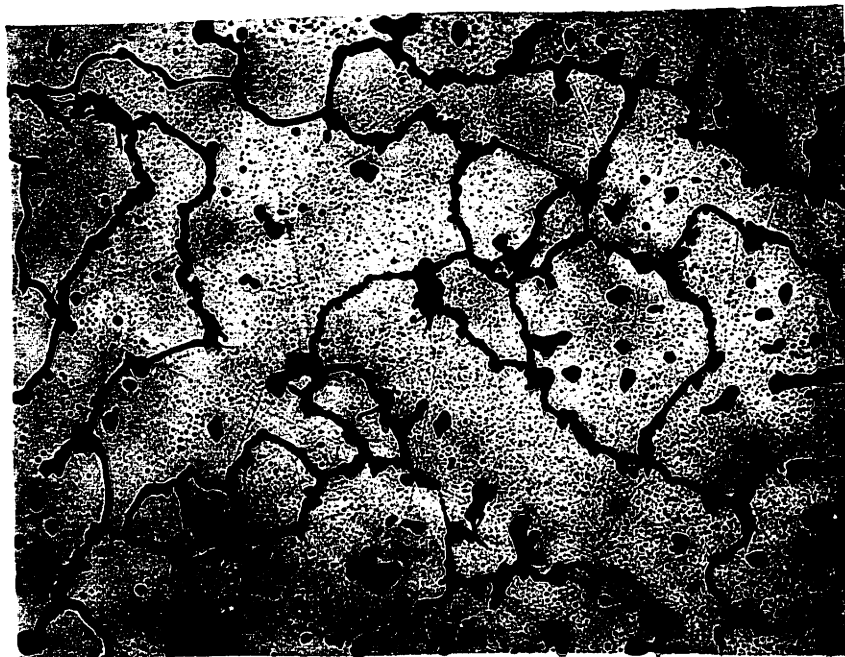
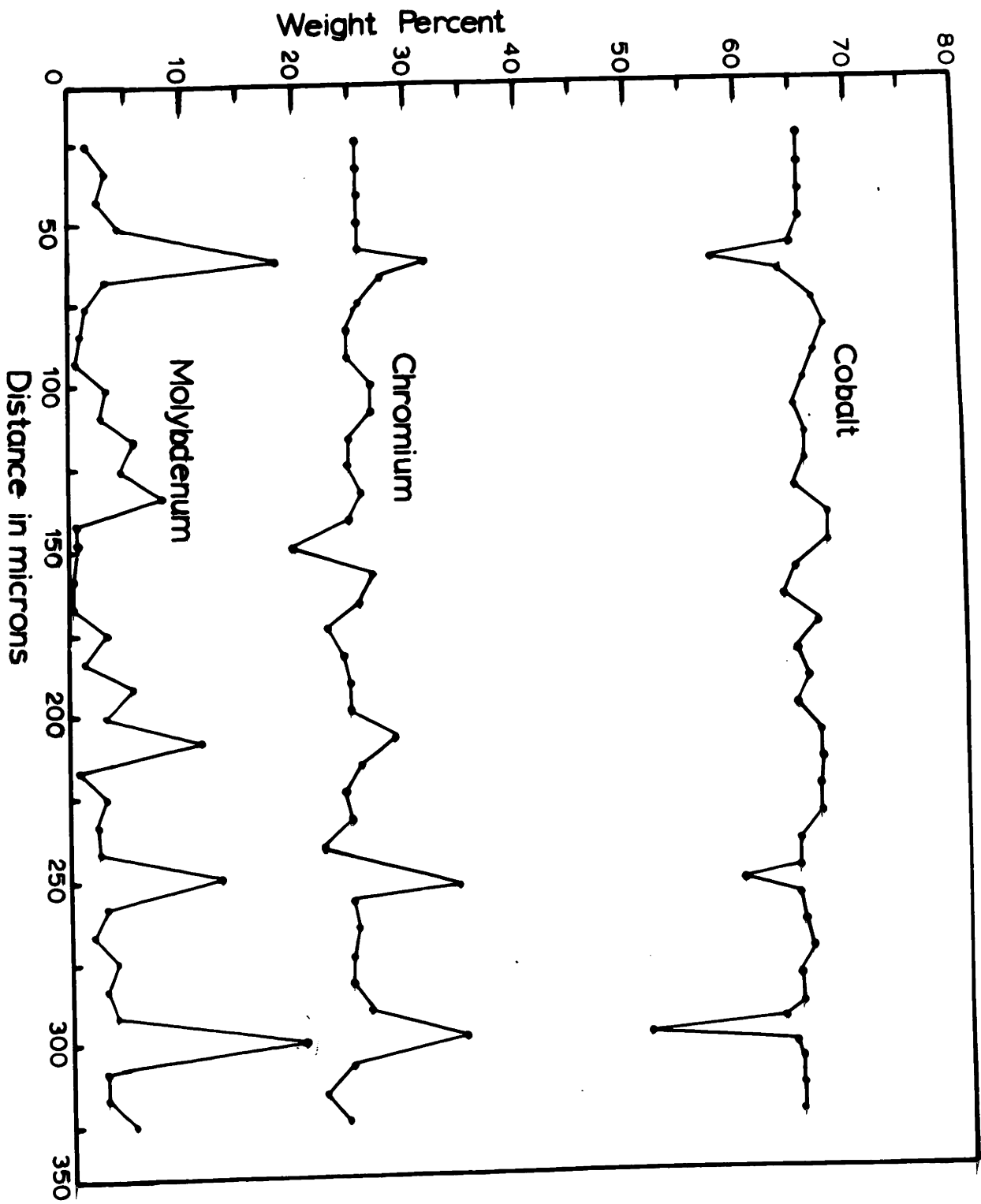


Figure 9. Microstructure of precision cast H.S. 21 after annealing at 1200°C for 4 hours. 5% HCl electrolytic etch. 158X.

Figure 10. Cobalt, chromium, and molybdenum distributions in a precision cast H.S. 21 specimen.



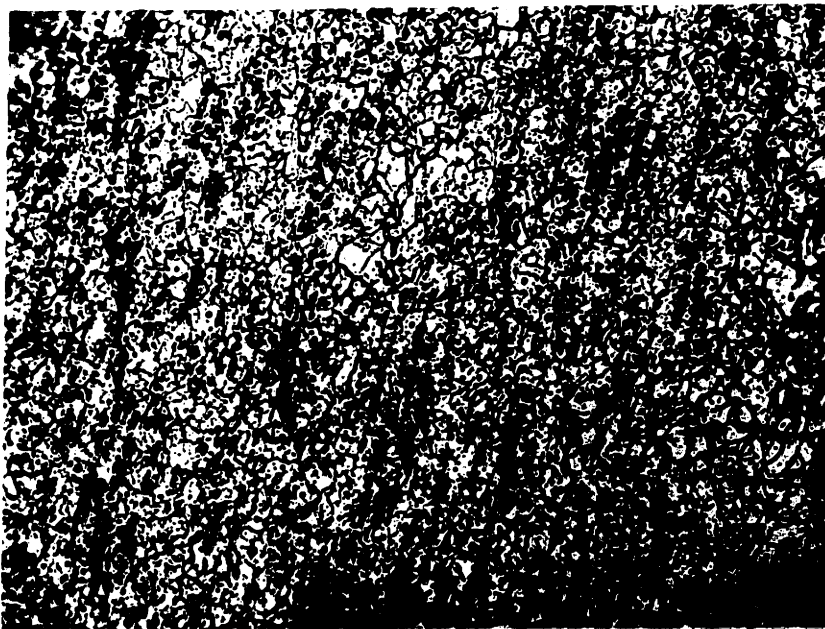


Figure 11. Microstructure of H.S. 21 press forged from 3 inch diameter ingot to 1 inch square bar at 1175°C and hot rolled to 0.125 inch thick plate. 5% HCl electrolytic etch. 158X.

Figure 12. Hardness as a function of cold work in modified H.S.
21.

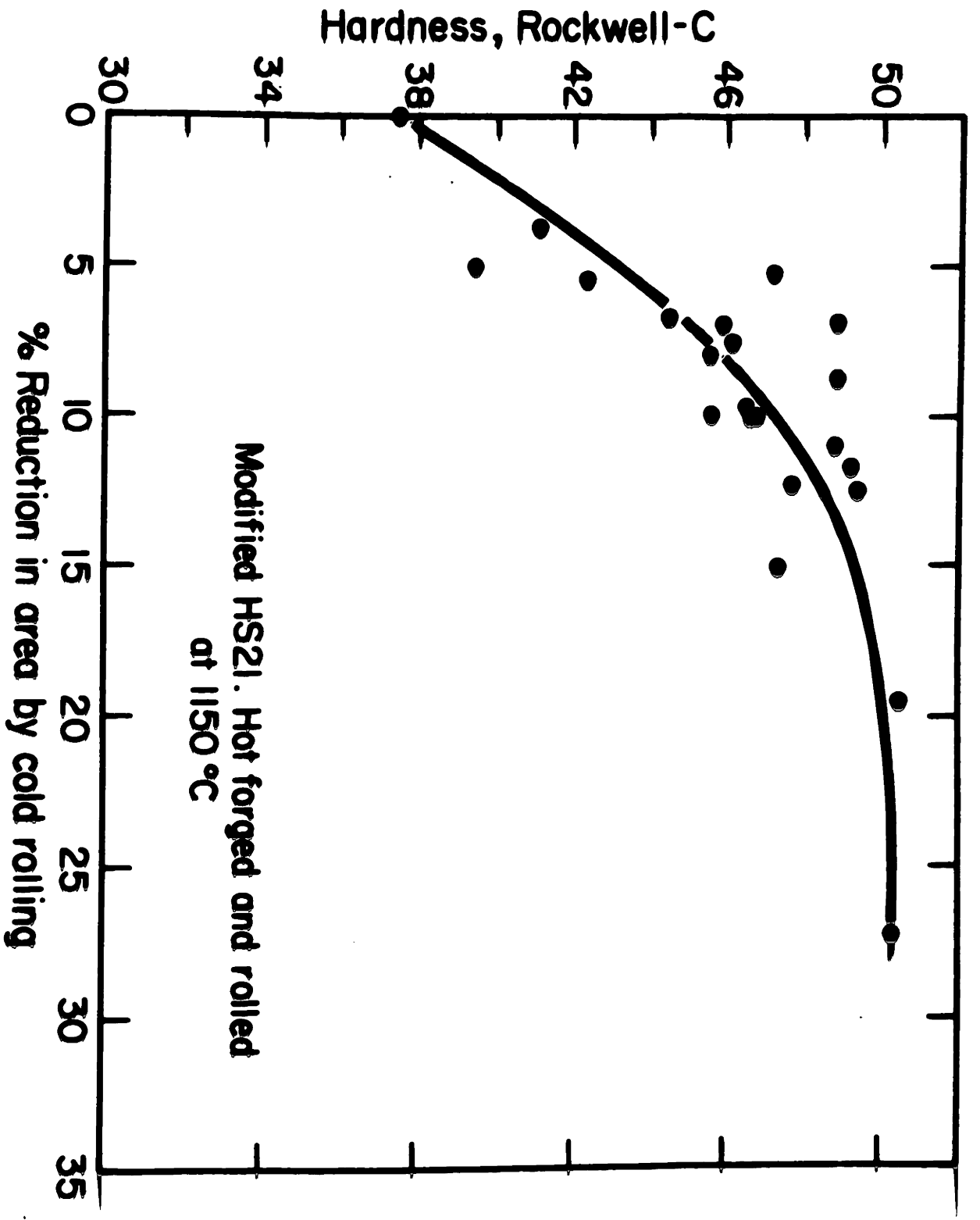


Figure 13. Weight percent HCP phase as a function of cold work in modified H.S. 21.

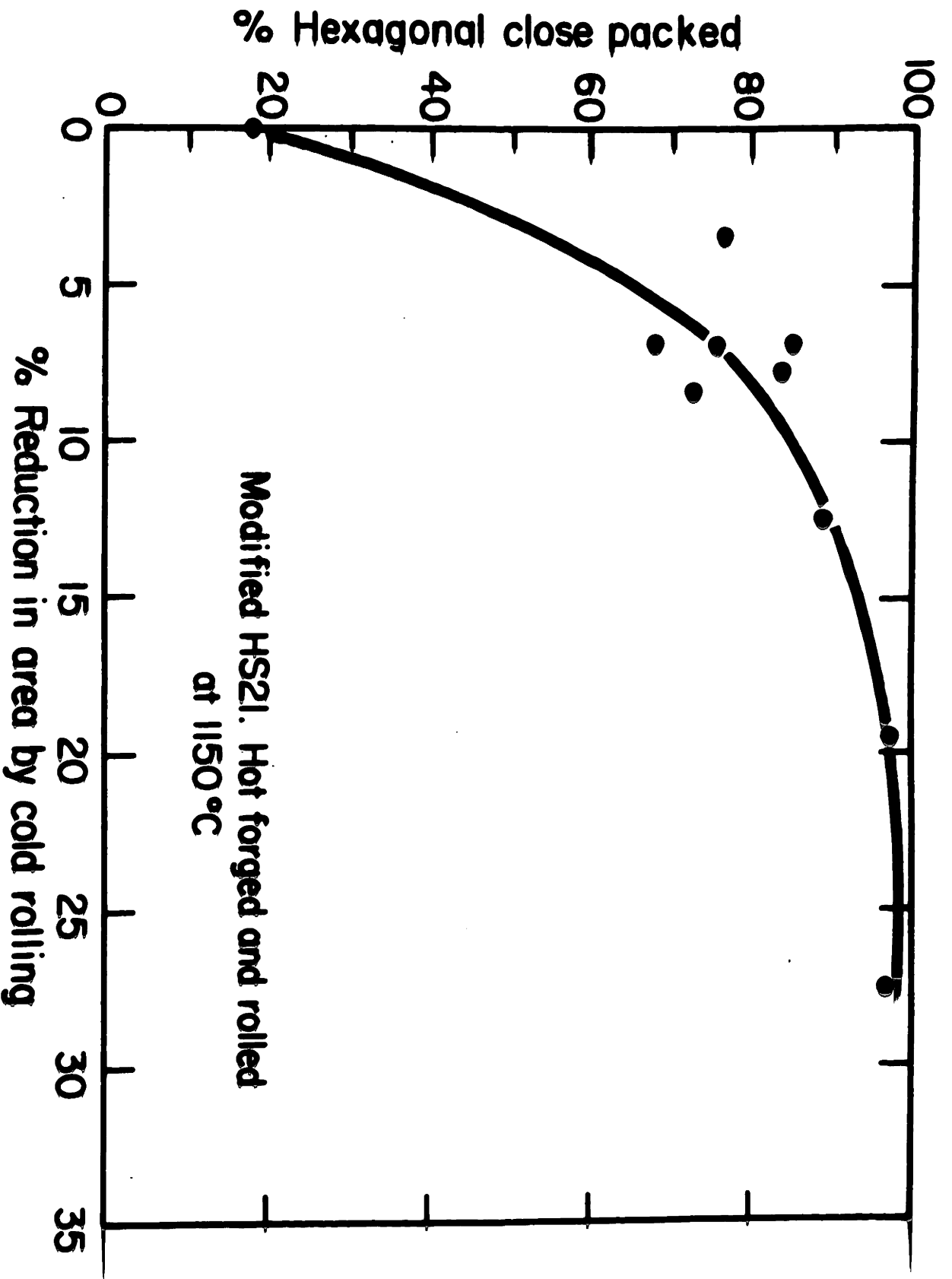




Figure 14. Modified H.S. 21 hot worked at 1150°C, cold rolled to 7.1% RA. 5% HCl electrolytic etch. 158X.



Figure 15. Modified H.S. 21 hot worked at 1150°C, cold rolled to 15.2% RA. 5% HCl electrolytic etch. 158X.

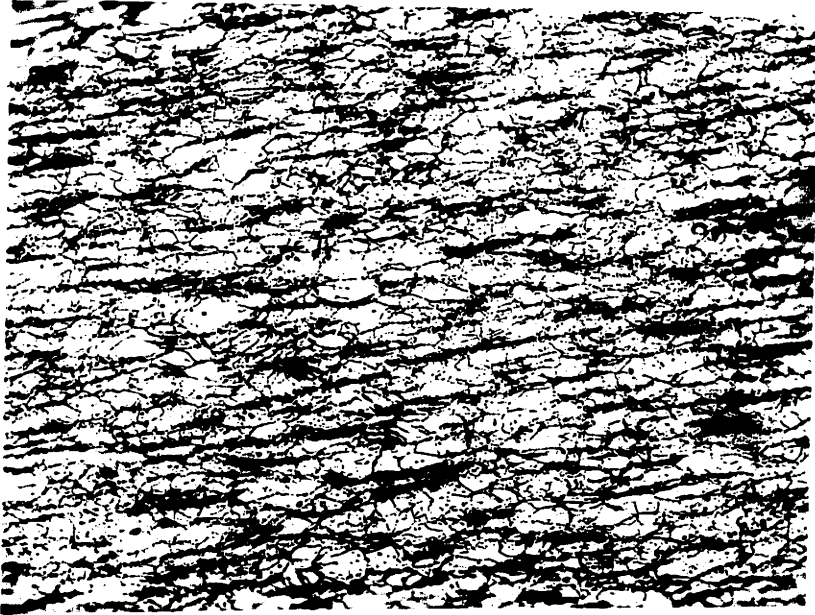


Figure 16. Modified H.S. 21 hot worked at 1150°C , cold rolled to 25.0% RA. 5% HCl electrolytic etch. 158X.

The following pages are missing from the original

#86

Figure 17. Effect of 10 minute heat treatments at 800°C-1200°C on the hardness of cold rolled modified H.S 21.

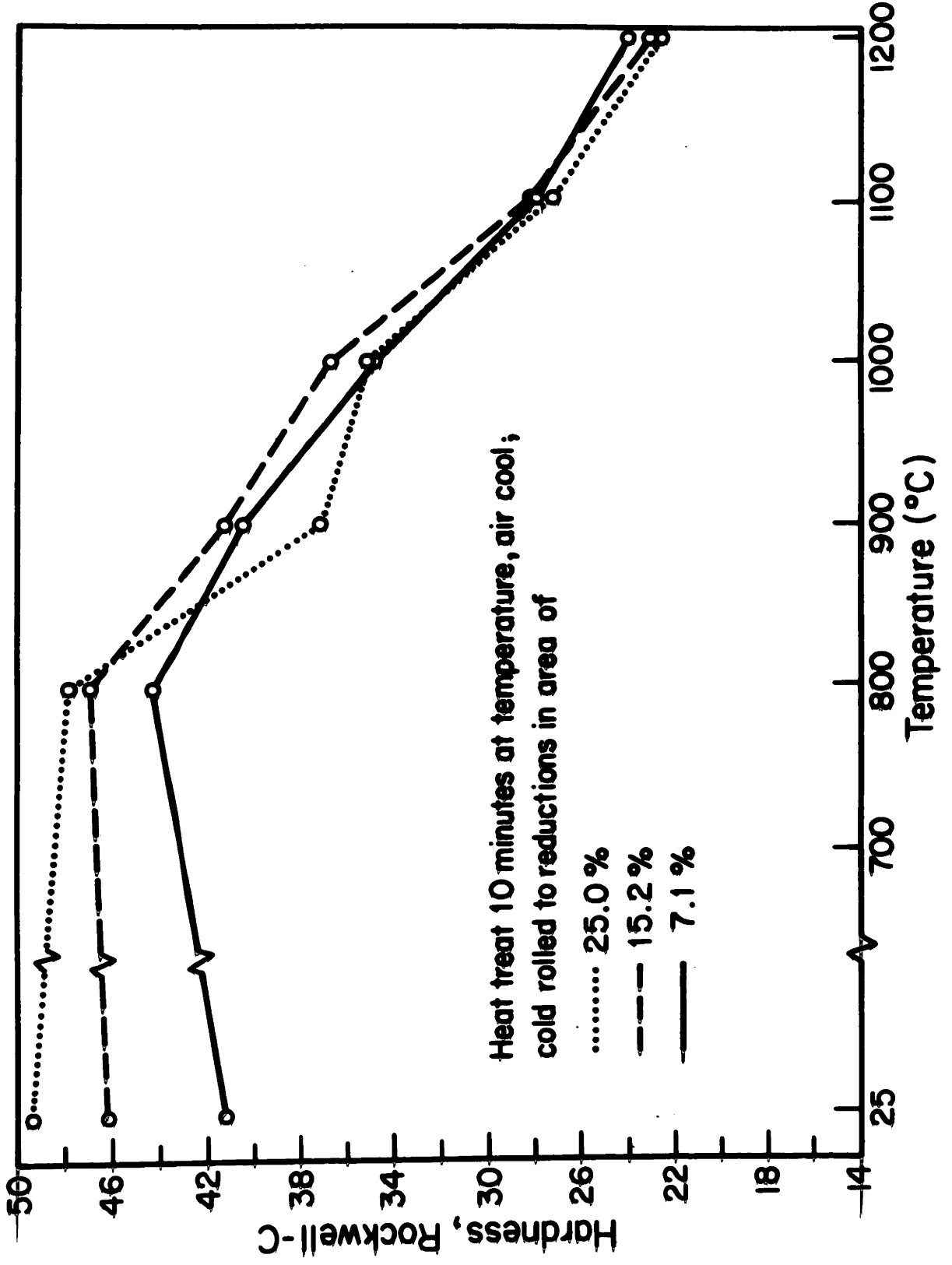


Figure 18. Effect of 30 minute heat treatments at 800°C-1200°C on the hardness of cold rolled modified H.S. 21.

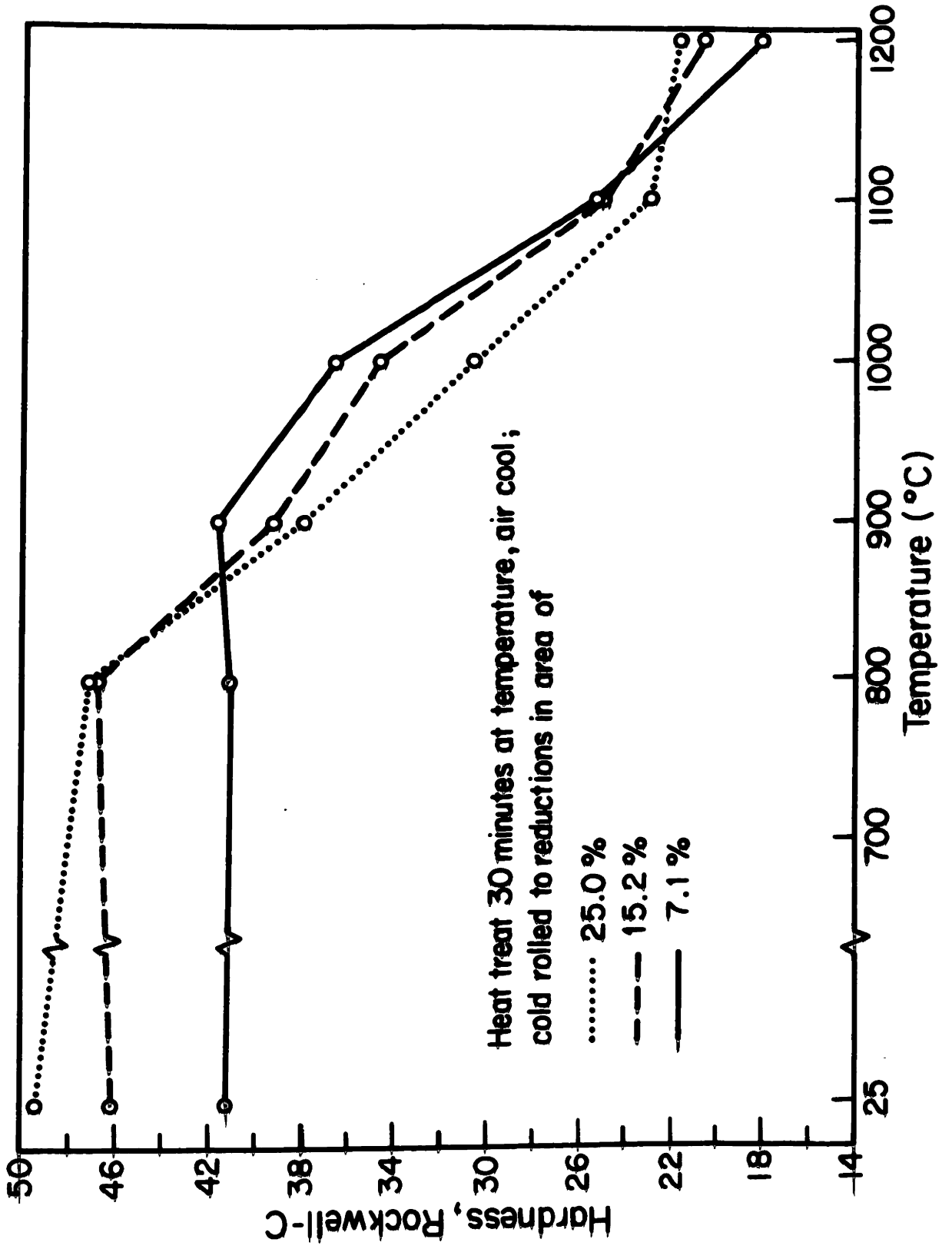


Figure 19. Effect of 60 minute heat treatments at 800°C-1200°C on the hardness of cold rolled modified H.S. 21.

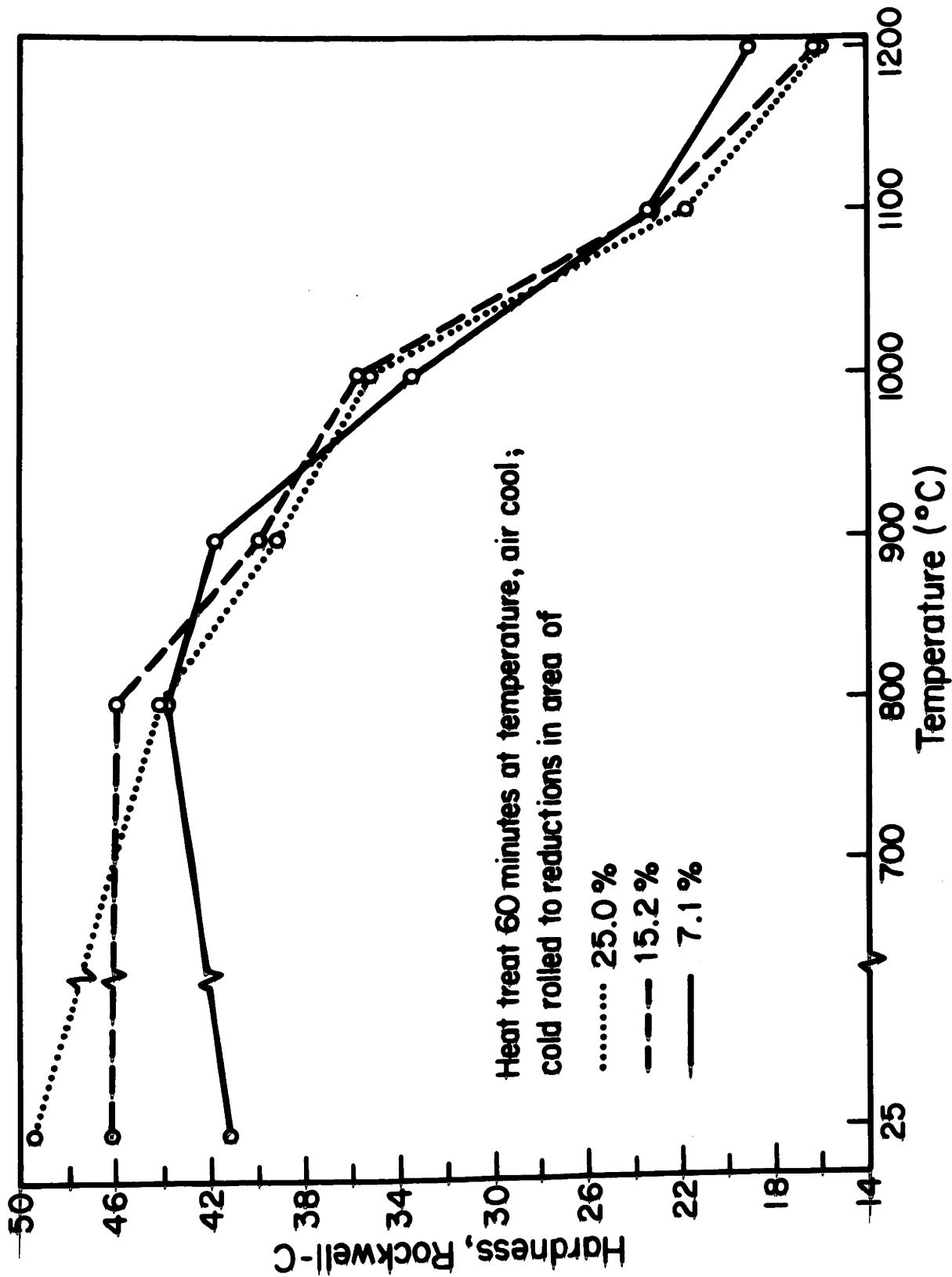




Figure 20. Modified H.S. 21. Hot worked at 1150°C, cold rolled to 7.1% RA, heat treated at 800°C for 10 minutes, air cooled. 5% HCl electrolytic etch. 158X.

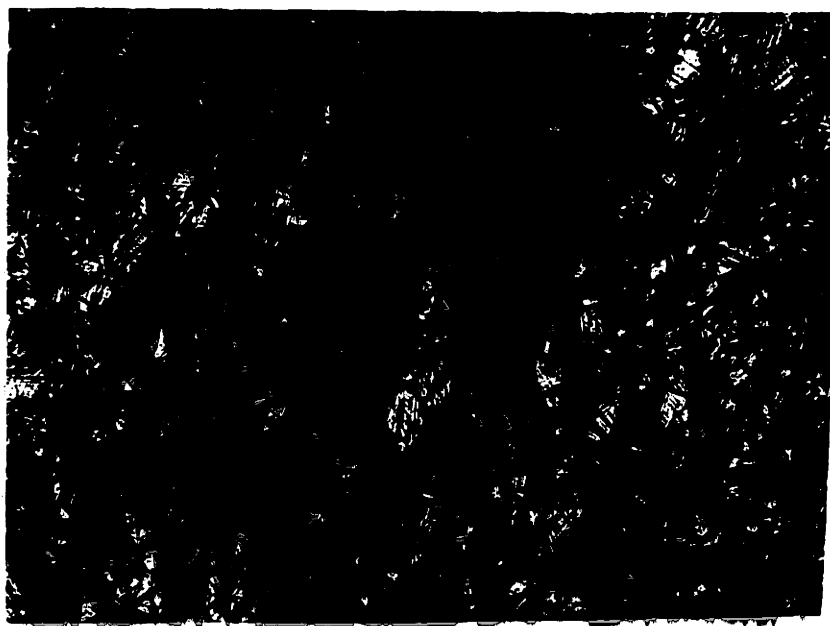


Figure 21. Modified H.S. 21. Hot worked at 1150°C, cold rolled to 7.1% RA, heat treated at 800°C for 60 minutes, air cooled. 5% HCl electrolytic etch. 158X.



Figure 22. Modified H.S. 21. Hot worked at 1150°C, cold rolled to 7.1% RA, heat treated at 800°C for 10 minutes, air cooled. 5% HCl electrolytic etch. 890X.

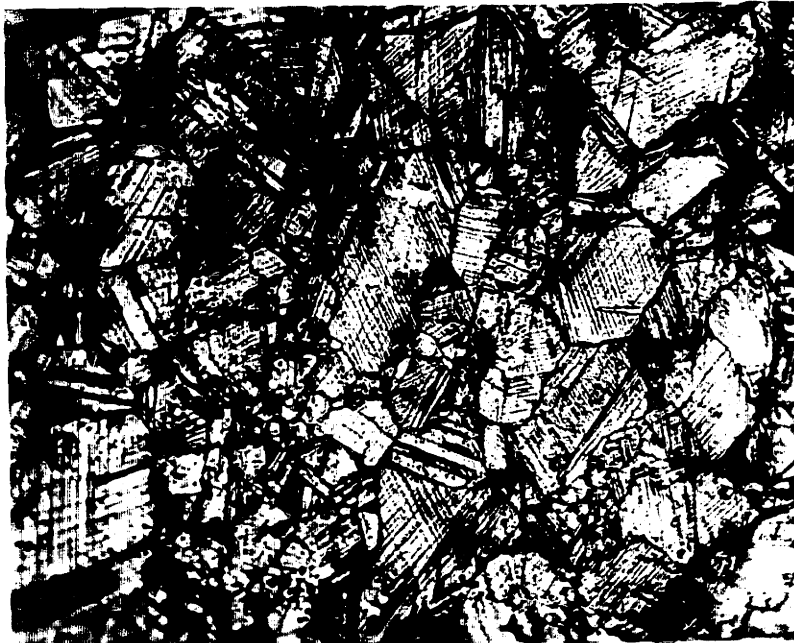


Figure 23. Modified H.S. 21. Hot worked at 1150°C, cold rolled to 7.1% RA, heat treated at 800°C for 60 minutes, air cooled. 5% HCl electrolytic etch. 890X.

Figure 24. Weight percent HCP phase in cold rolled modified H.S. 21 heat treated for 10 minutes at 800°C-1200°C.

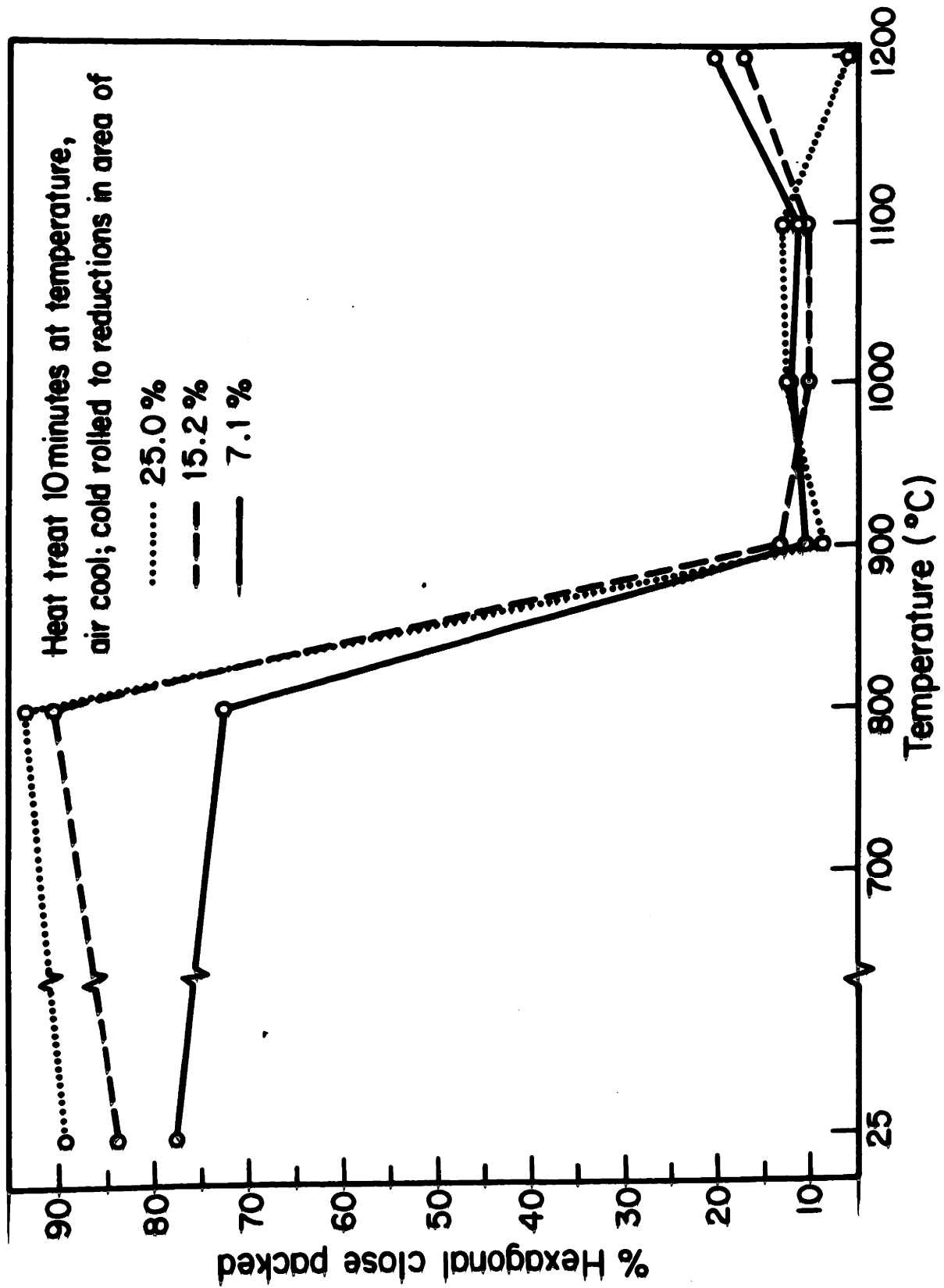


Figure 25. Weight percent HCP phase in cold rolled modified H.S. 21 heat treated for 30 minutes at 800°C-1200°C.

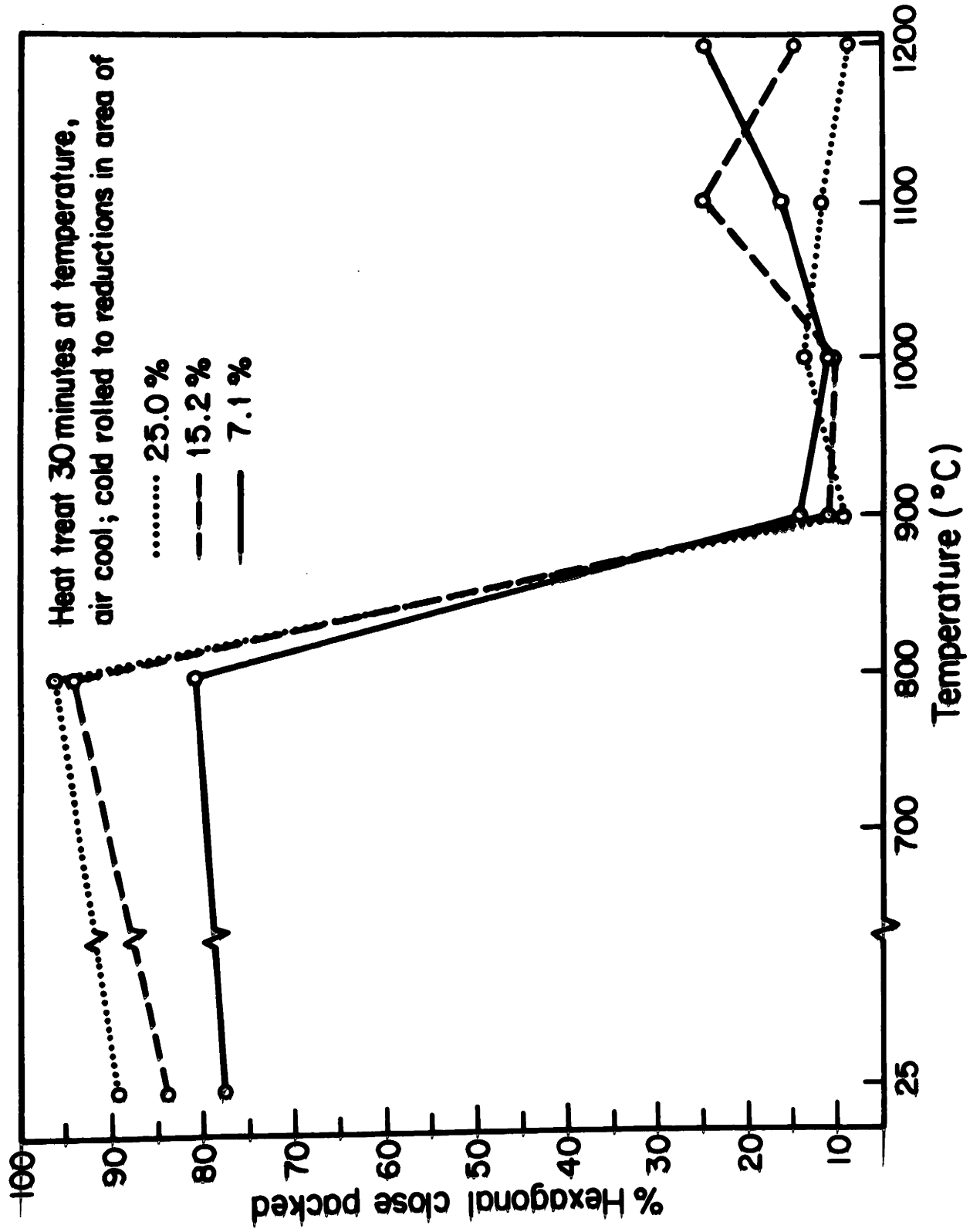


Figure 26. Weight percent HCP phase in cold rolled modified H.S. 21 heat treated for 60 minutes at 800°C-1200°C.

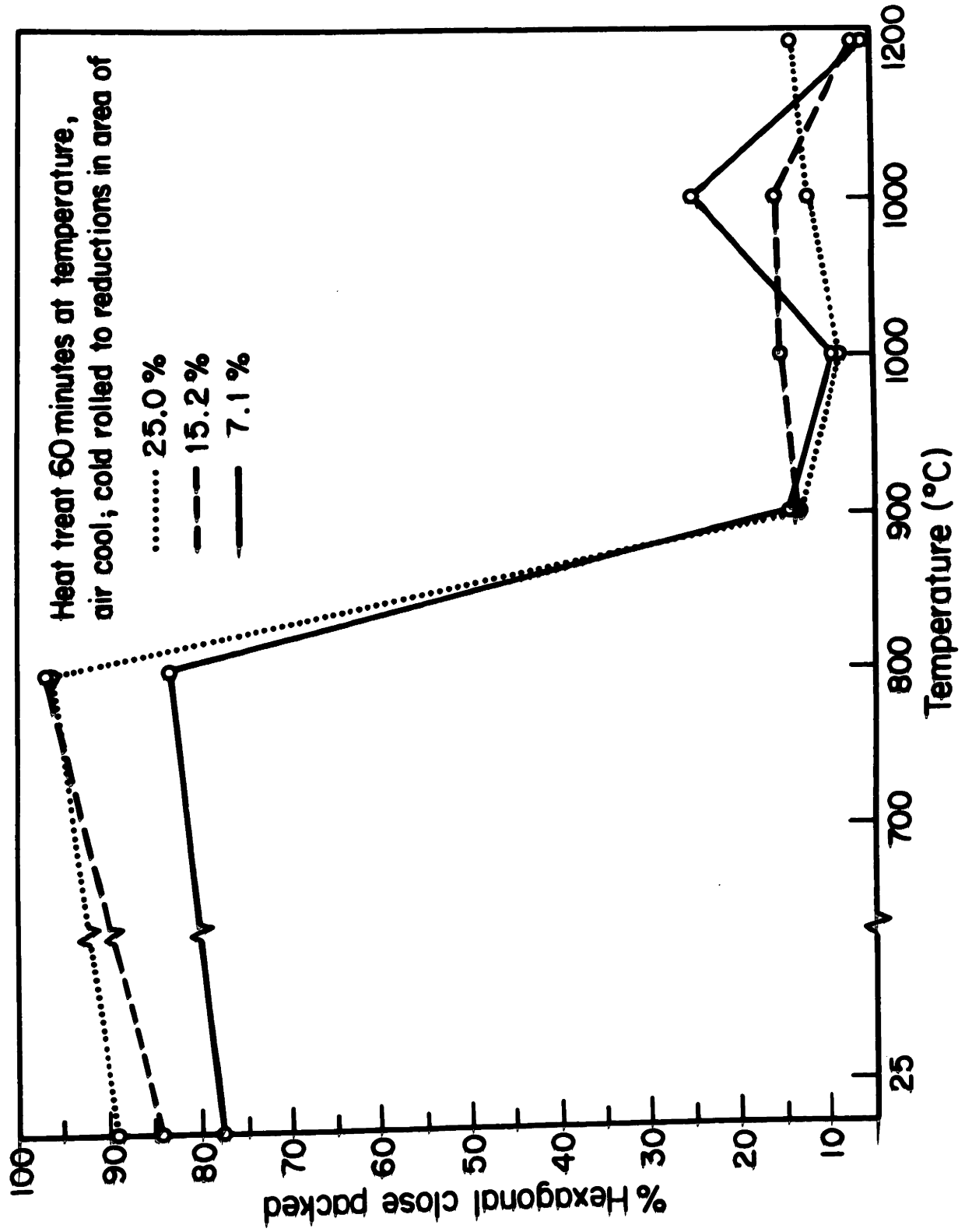




Figure 27. Modified H.S. 21. Hot worked at 1150°C , cold rolled to 7.1% RA, heat treated at 900°C for 10 minutes, air cooled. 5% HCl electrolytic etch. 158X.

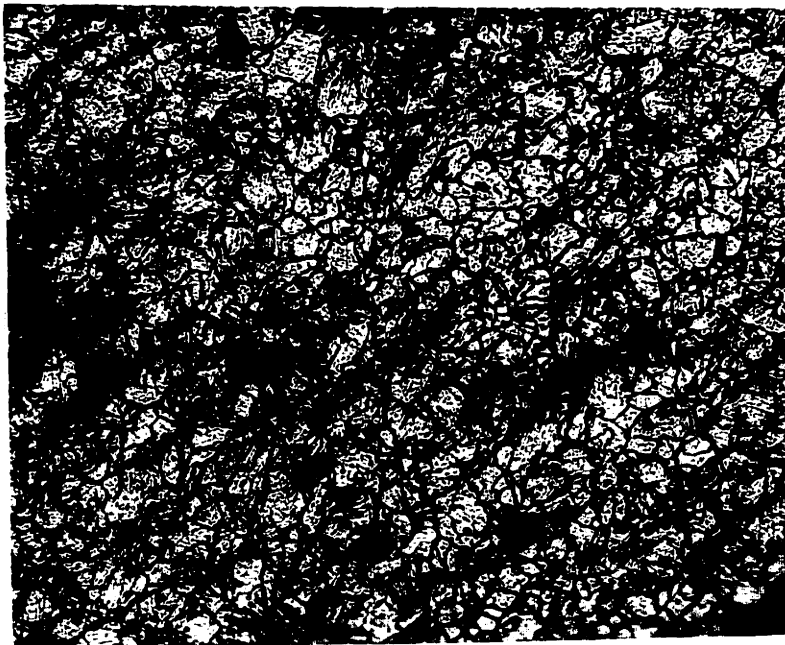


Figure 28. Modified H.S. 21. Hot worked at 1150°C , cold rolled to 7.1% RA, heat treated at 900°C for 60 minutes, air cooled. 5% HCl electrolytic etch. 158X.

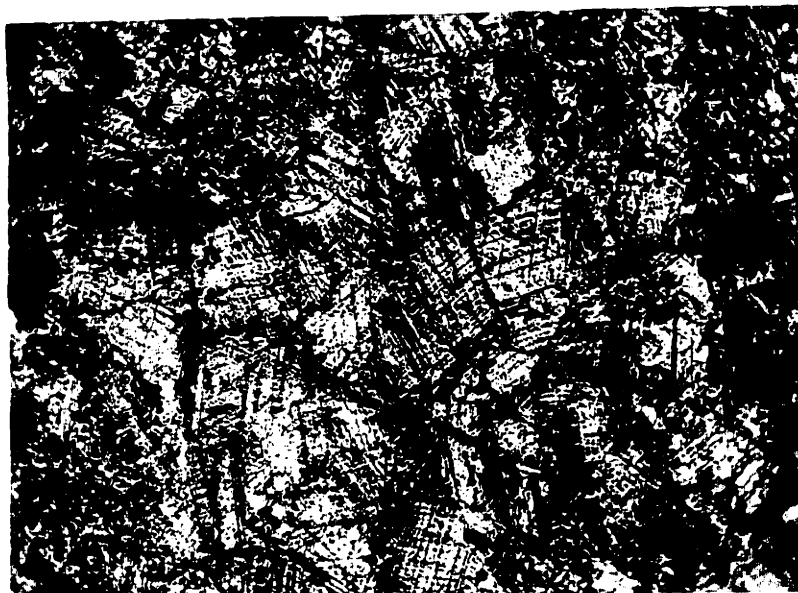


Figure 29. Modified H.S. 21. Hot worked at 1150°C, cold rolled to 7.1% RA, heat treated at 900°C for 10 minutes, air cooled. 5% HCl electrolytic etch. 890X.

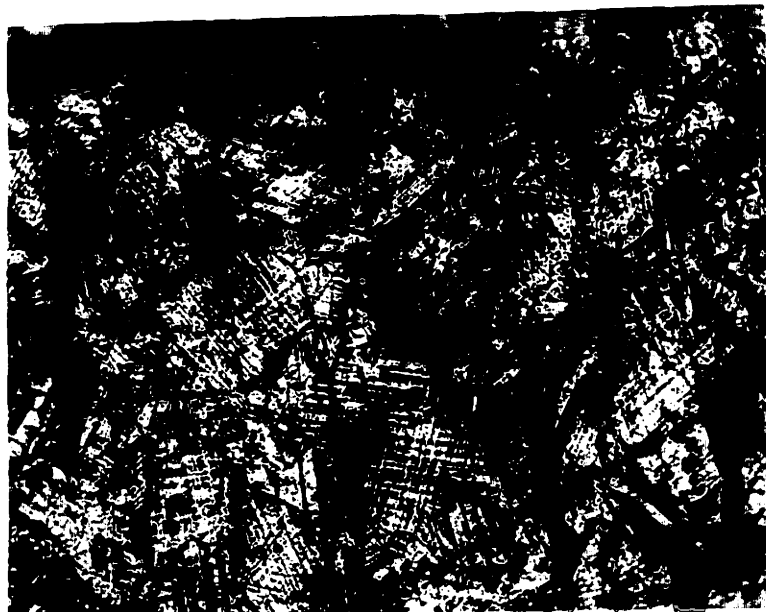


Figure 30. Modified H.S. 21. Hot worked at 1150°C, cold rolled to 7.1% RA, heat treated at 900°C for 60 minutes, air cooled. 5% HCl electrolytic etch. 890X.

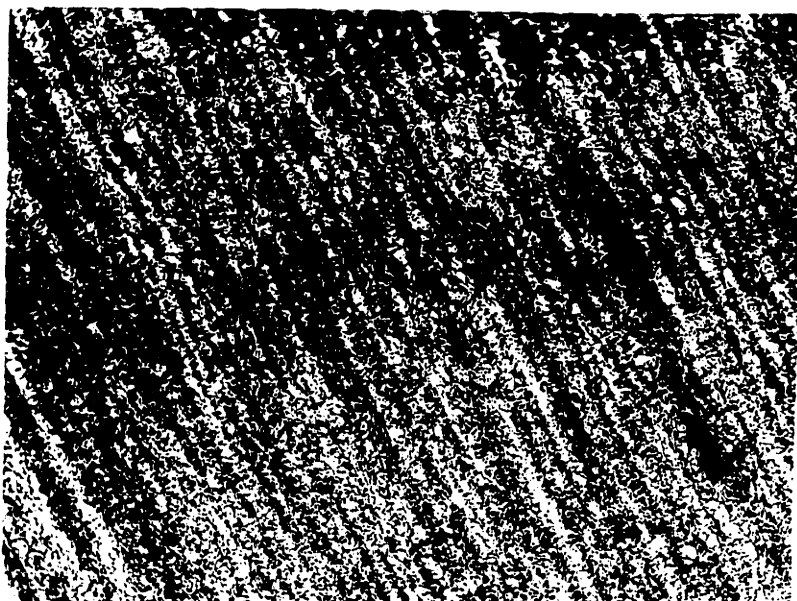


Figure 31. Modified H.S. 21. Hot worked at 1150°C , cold rolled to 7.1% RA, heat treated at 1000°C for 10 minutes, air cooled. 5% HCl electrolytic etch. 158X.

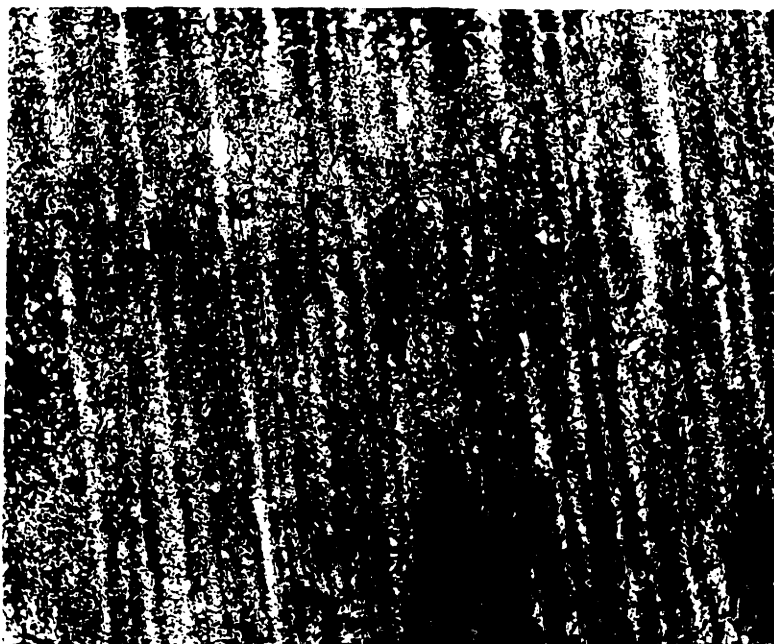


Figure 32. Modified H.S. 21. Hot worked at 1150°C , cold rolled to 7.1% RA, heat treated at 1000°C for 60 minutes, air cooled. 5% HCl electrolytic etch. 158X.

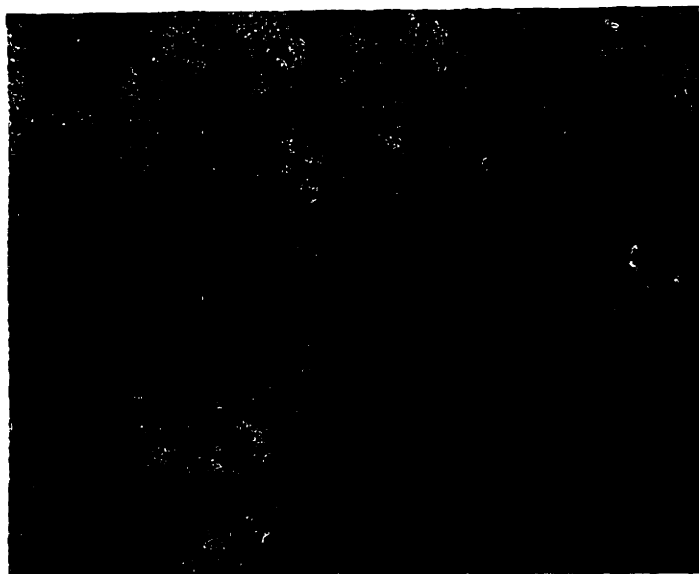


Figure 33. Modified H.S. 21. Hot worked at 1150°C, cold rolled to 7.1% RA, heat treated at 1000°C for 10 minutes, air cooled. 5% HCl electrolytic etch. 679X.

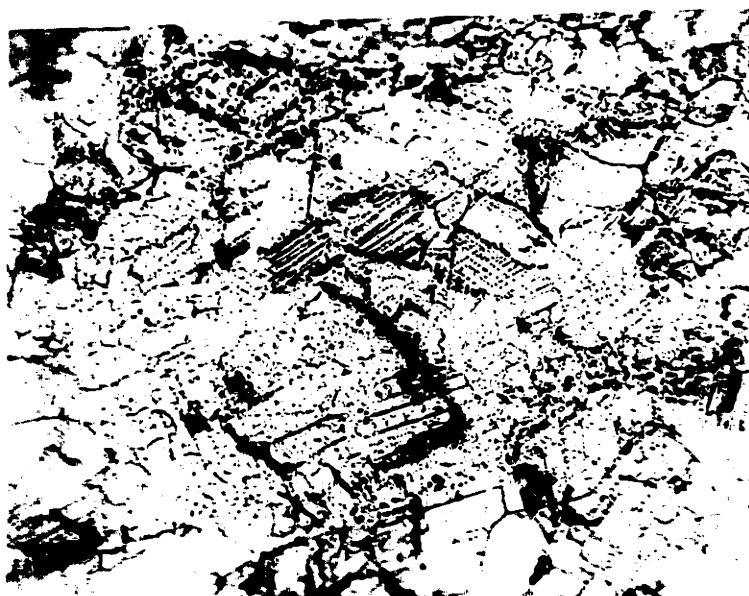


Figure 34. Modified H.S. 21. Hot worked at 1150°C, cold rolled to 7.1% RA, heat treated at 1000°C for 60 minutes, air cooled. 5% HCl electrolytic etch. 679X.

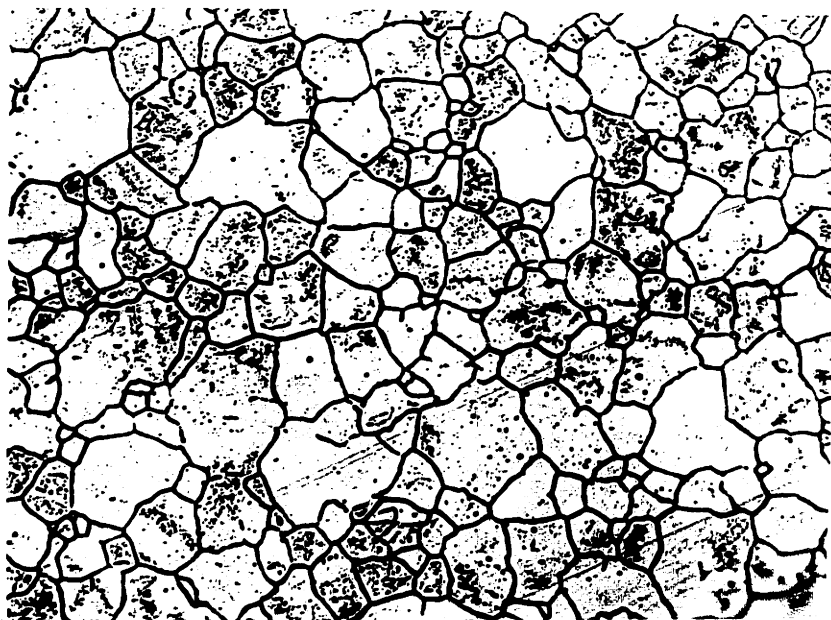


Figure 35. Modified H.S. 21. Hot worked at 1150°C , cold rolled to 7.1% RA, heat treated at 1100°C for 10 minutes, air cooled. 5% HCl electrolytic etch. 158X.

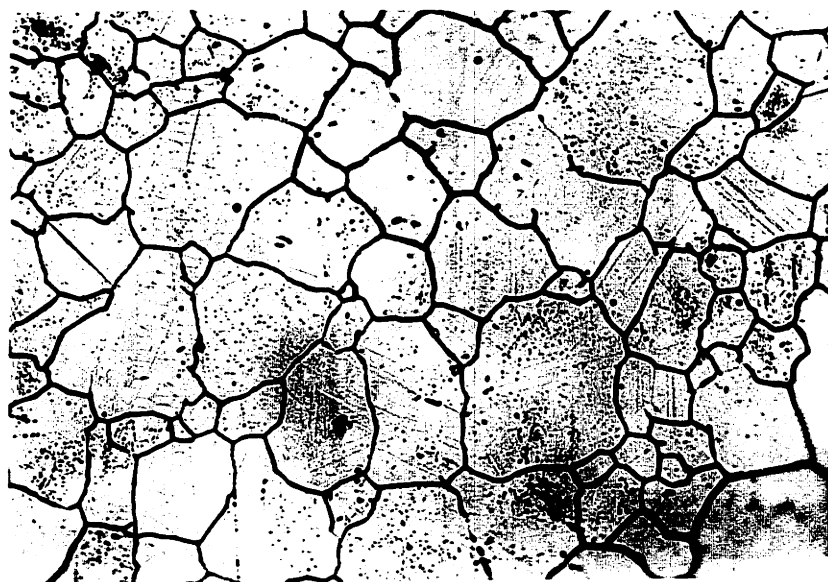


Figure 36. Modified H.S. 21. Hot worked at 1150°C , cold rolled to 7.1% RA, heat treated at 1100°C for 60 minutes, air cooled. 5% HCl electrolytic etch. 158X.

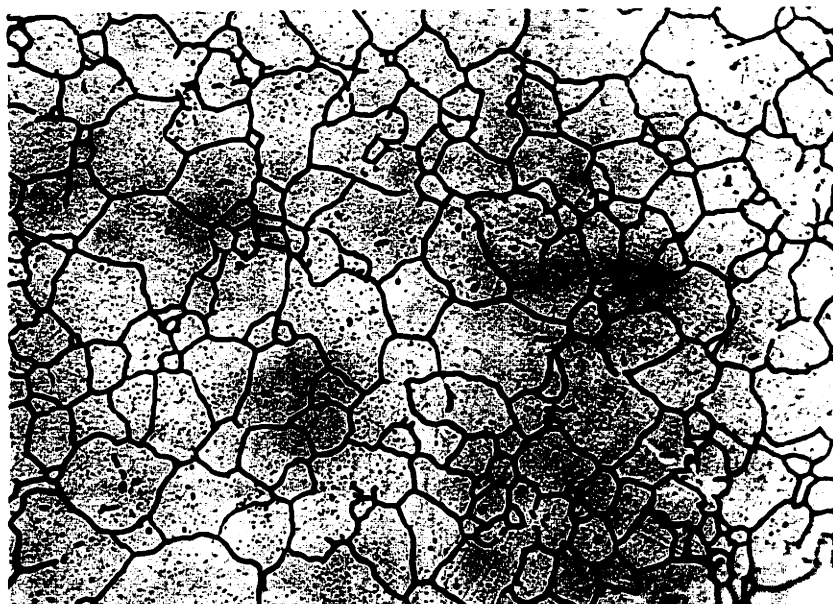


Figure 37. Modified H.S. 21. Hot worked at 1150°C, cold rolled to 7.1% RA, heat treated at 1200°C for 10 minutes, air cooled. 5% HCl electrolytic etch. 158X.

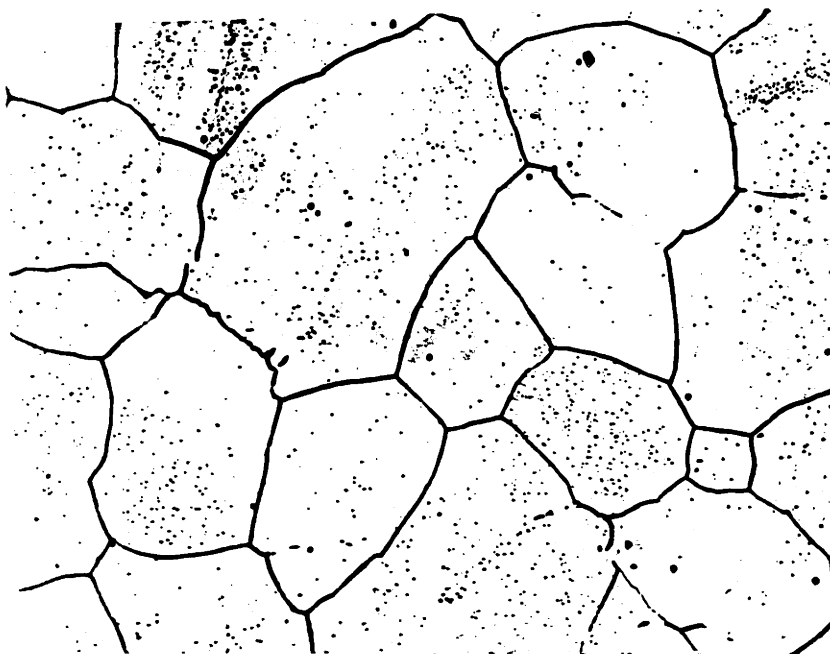
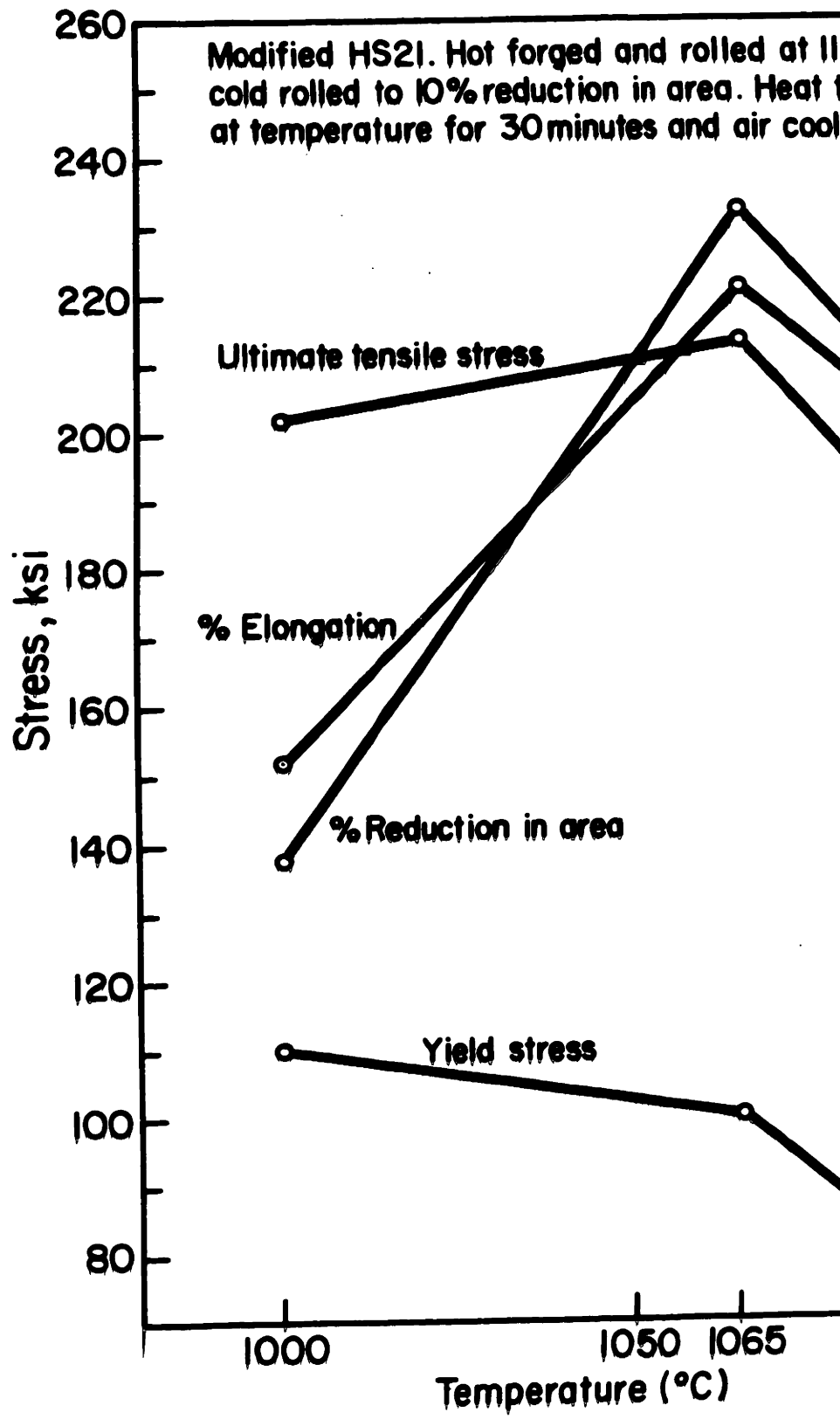


Figure 38. Modified H.S. 21. Hot worked at 1150°C, cold rolled to 7.1% RA, heat treated at 1200°C for 60 minutes, air cooled. 5% HCl electrolytic etch. 158X.

Figure 39. Tensile properties of 10% cold worked modified H.S. 21 heat treated at 1000°C, 1065°C, and 1100°C for 30 minutes and air cooled.



Percent



Figure 40. Modified H.S. 21. Hot worked at to 9.9% RA, heat treated at 1000 air cooled. 5% HCl electrolytic



Figure 41. Modified H.S. 21. Hot worked at to 9.9% RA, heat treated at 1065 air cooled. 5% HCl electrolytic

cold rolled
0 minutes,
158X.

cold rolled
minutes,
58X.

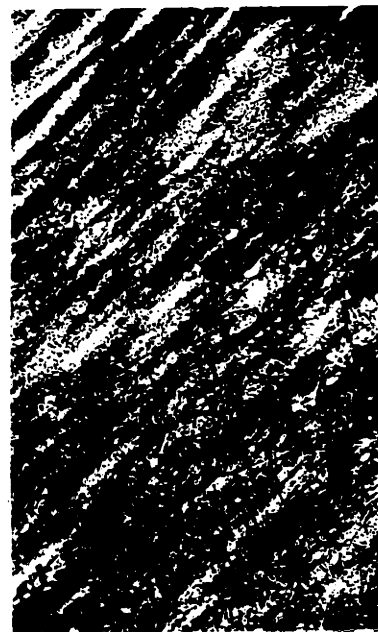


Figure 42. Modified H.S. 21.
to 9.9% RA, heat
air cooled. 5% H

°C, cold rolled
for 30 minutes,
m. 158X.



Figure 43. Effect of prior co
anneal at 1065°C o

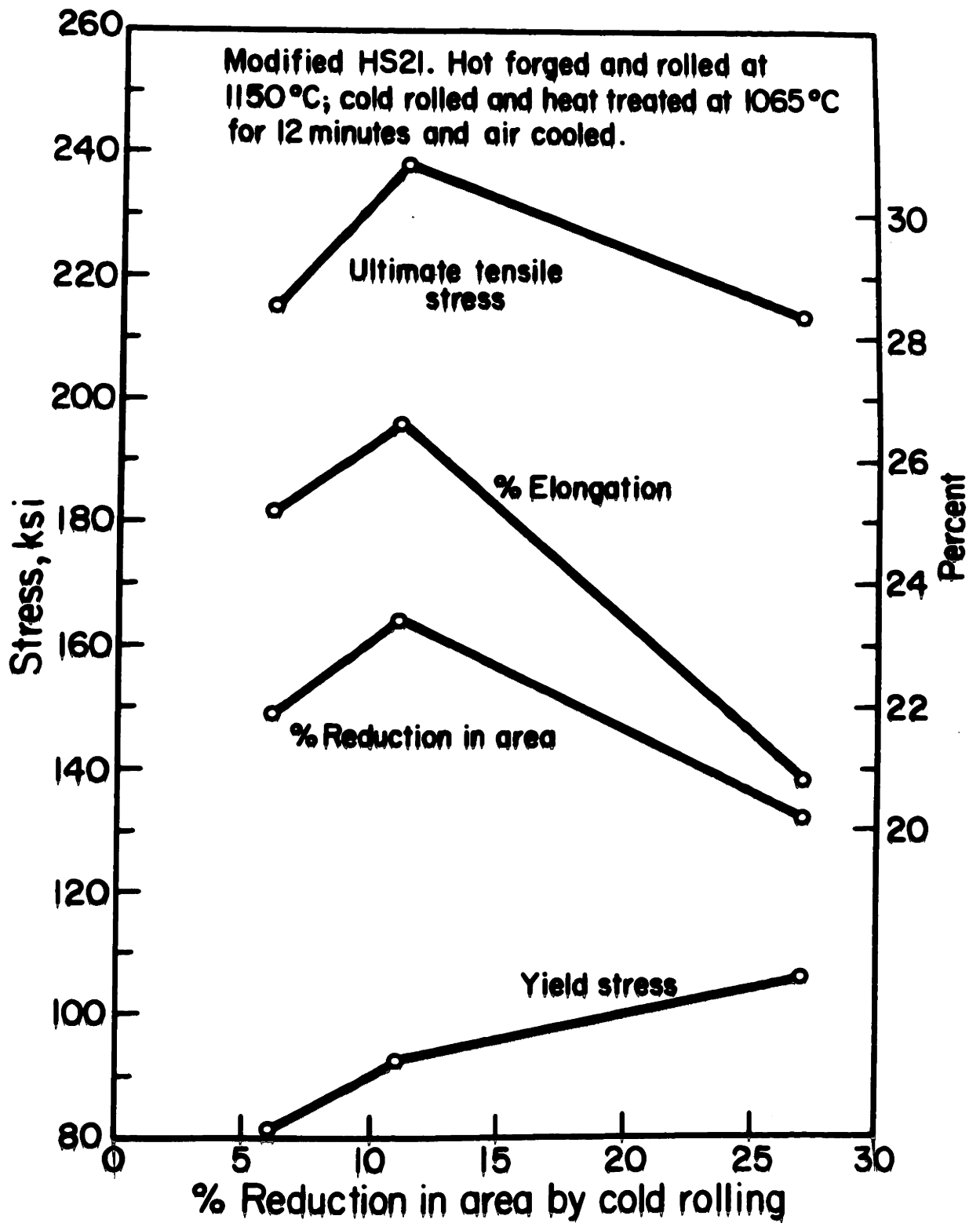


Figure 44. Effect of prior cold rolling subsequent to a 30 minute anneal at 1065°C on modified H.S. 21.

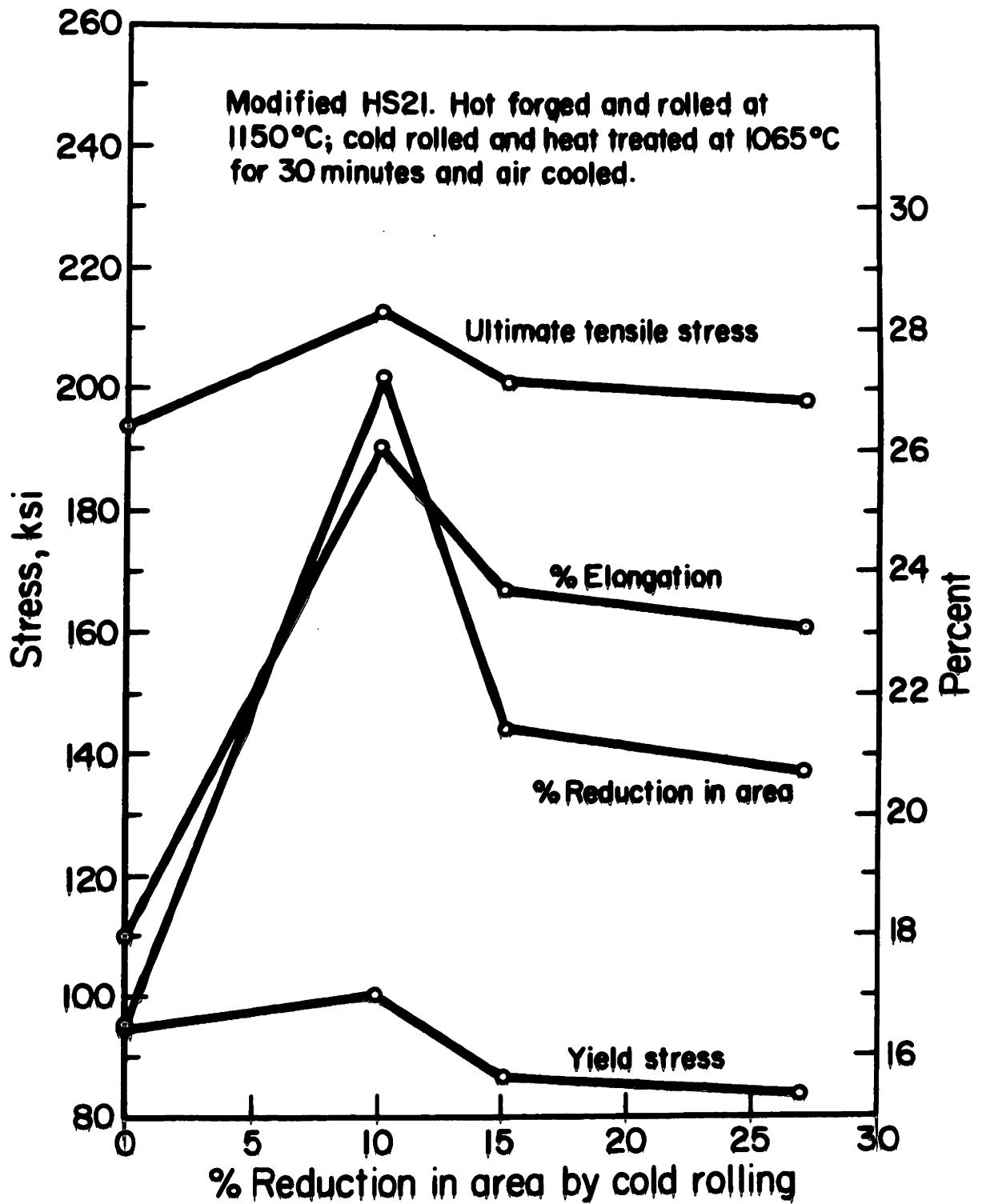
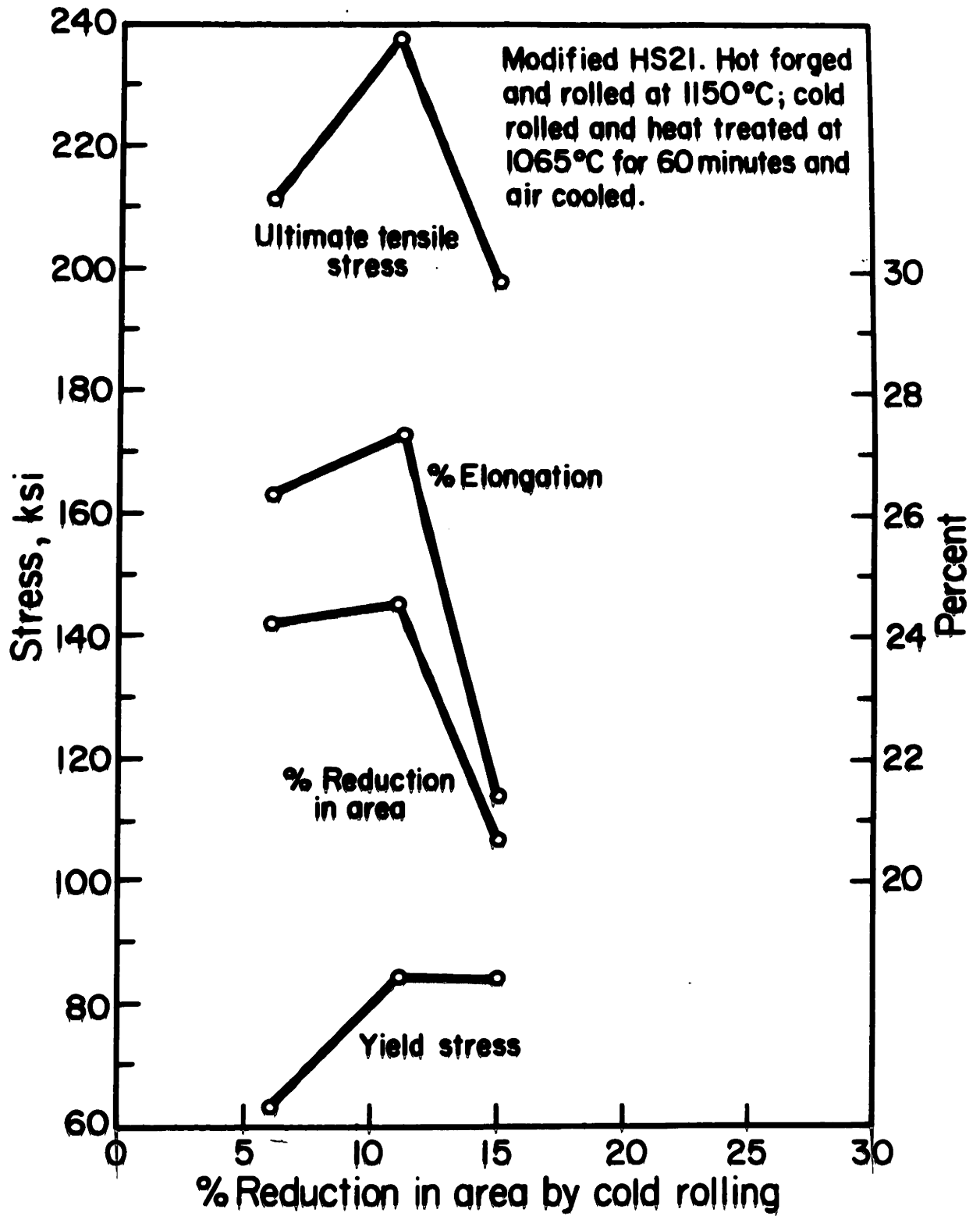


Figure 45. Effect of prior cold rolling subsequent to a 60 minute anneal at 1065°C on modified H.S. 21.



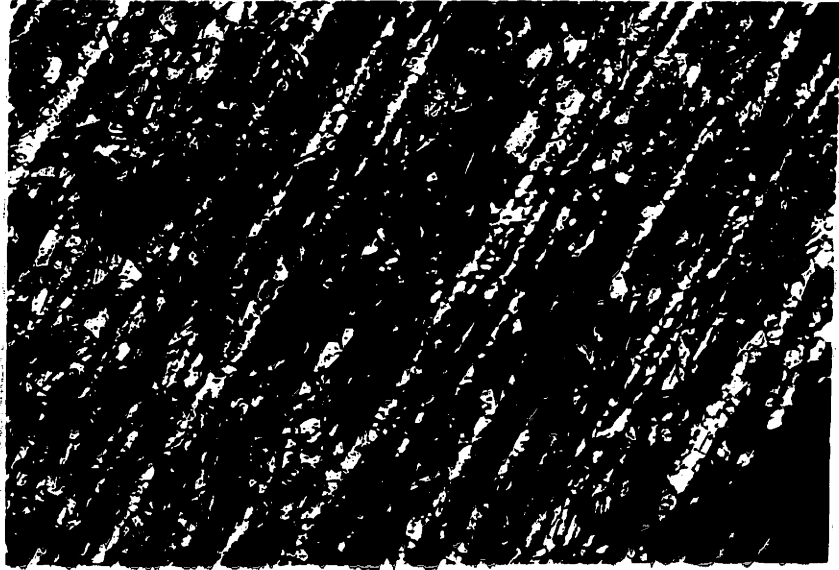


Figure 46. Modified H.S. 21. Hot worked at 1150°C , cold rolled to 6% RA, heat treated at 1065°C for 12 minutes, air cooled. 5% HCl electrolytic etch. 158X.



Figure 47. Modified H.S. 21. Hot worked at 1150°C , cold rolled to 11.1% RA, heat treated at 1065°C for 12 minutes, air cooled. 5% HCl electrolytic etch. 158X.

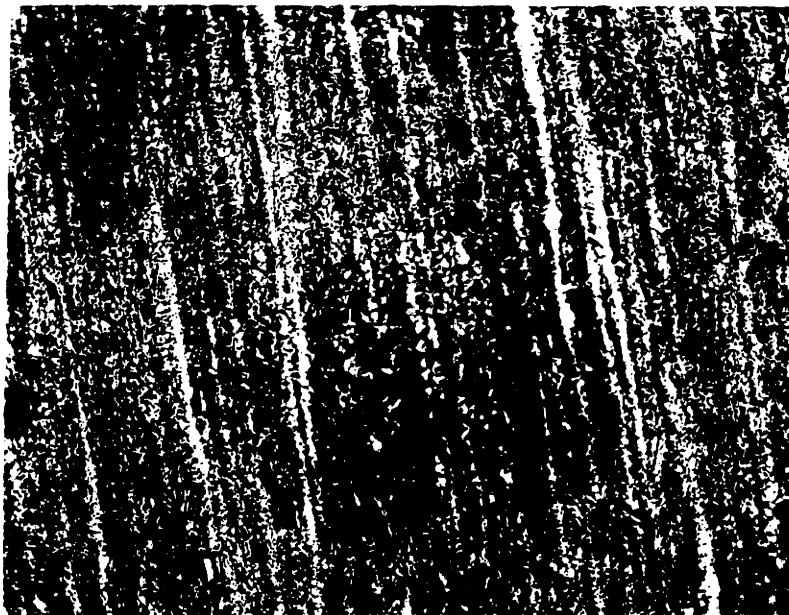


Figure 48. Modified H.S. 21. Hot worked at 1150°C , cold rolled to 27.0% RA, heat treated at 1065°C for 12 minutes, air cooled. 5% HCl electrolytic etch. 158X.

Figure 49. Rotating bending fatigue tests of alloys listed in Table 3.

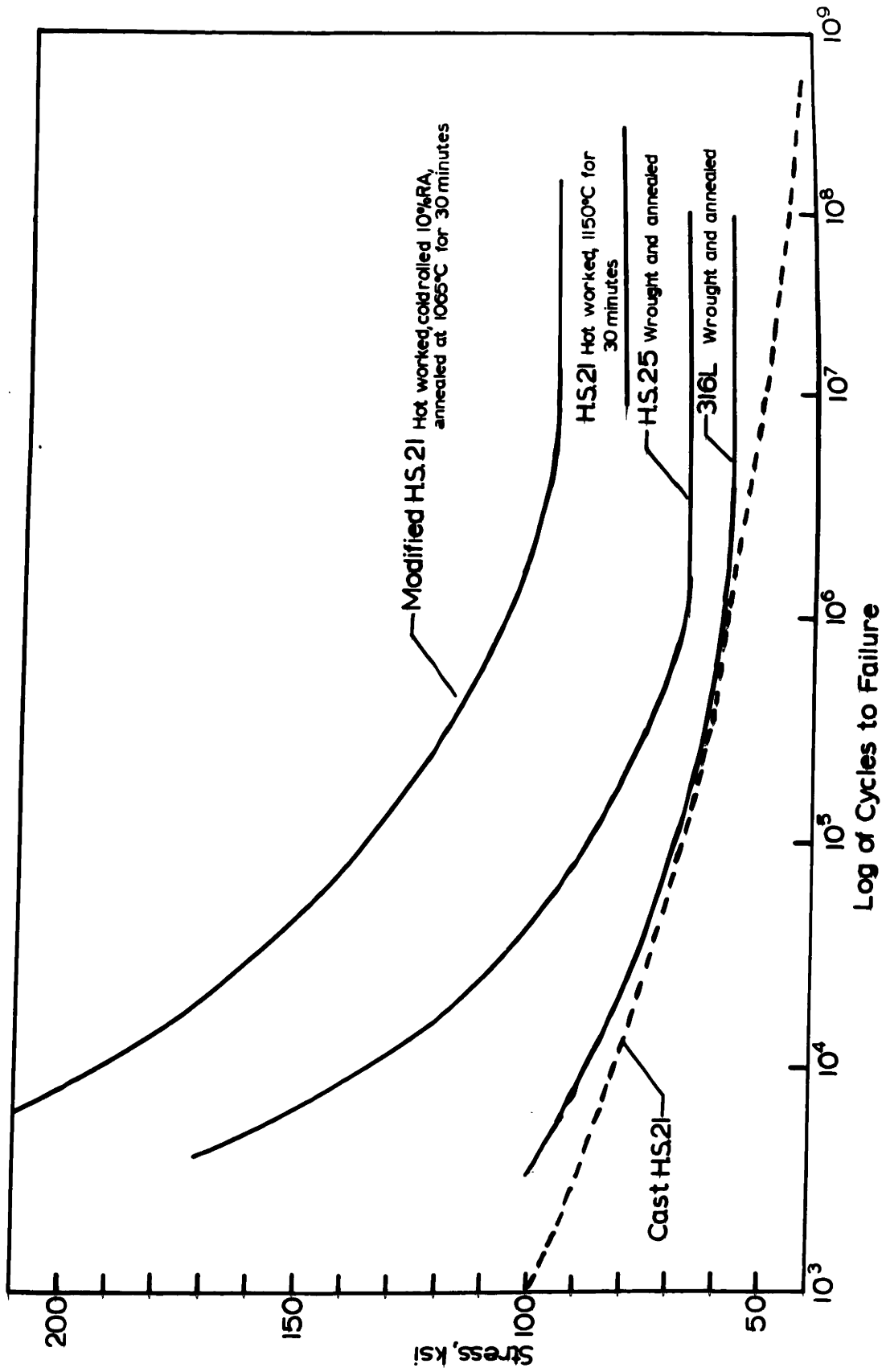


Figure 50. Potential variation with time of creviced samples of several alloys immersed in oxygenated 10% HCl + 1% FeCl₃ at 37°C.

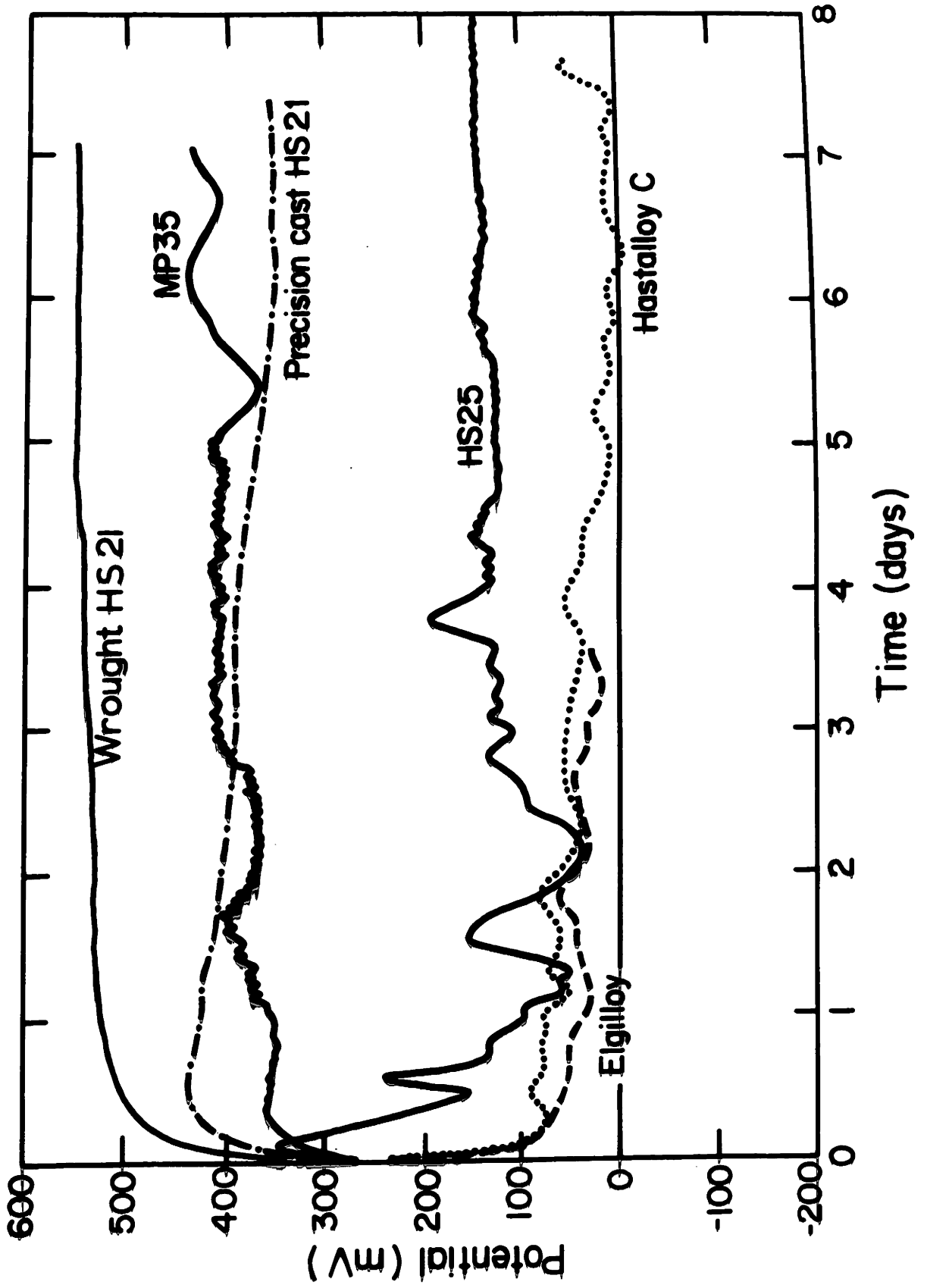
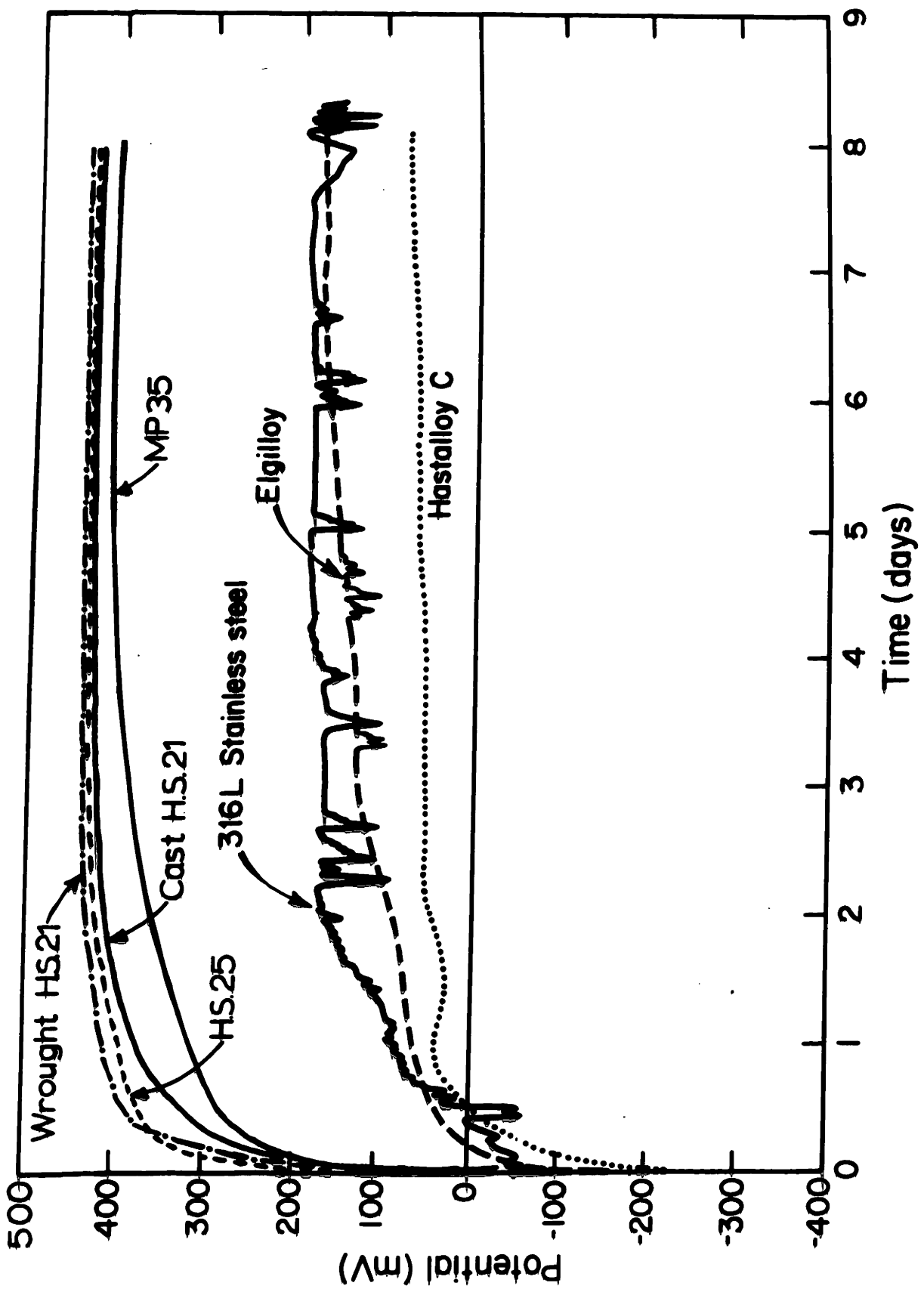


Figure 51. Potential variation with time of creviced samples of several alloys immersed in oxygenated 0.9% NaCl at 37°C.



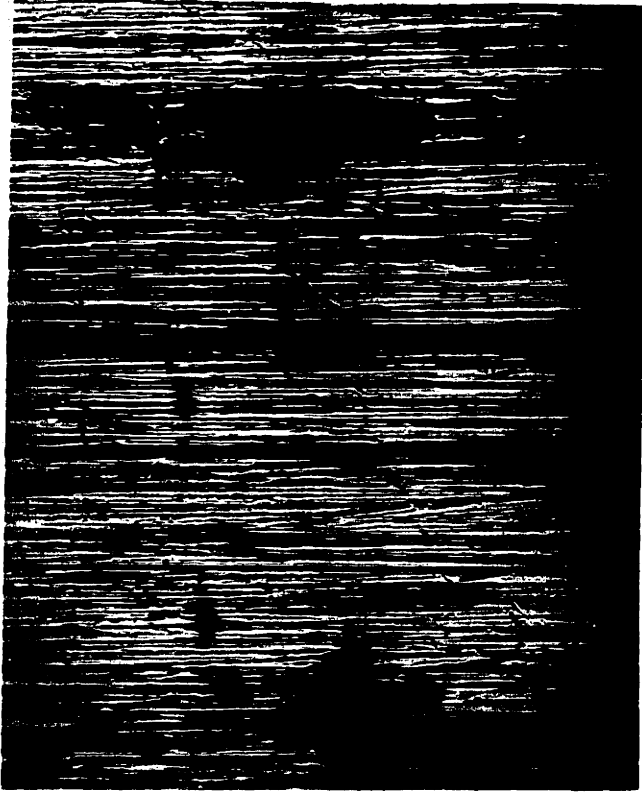
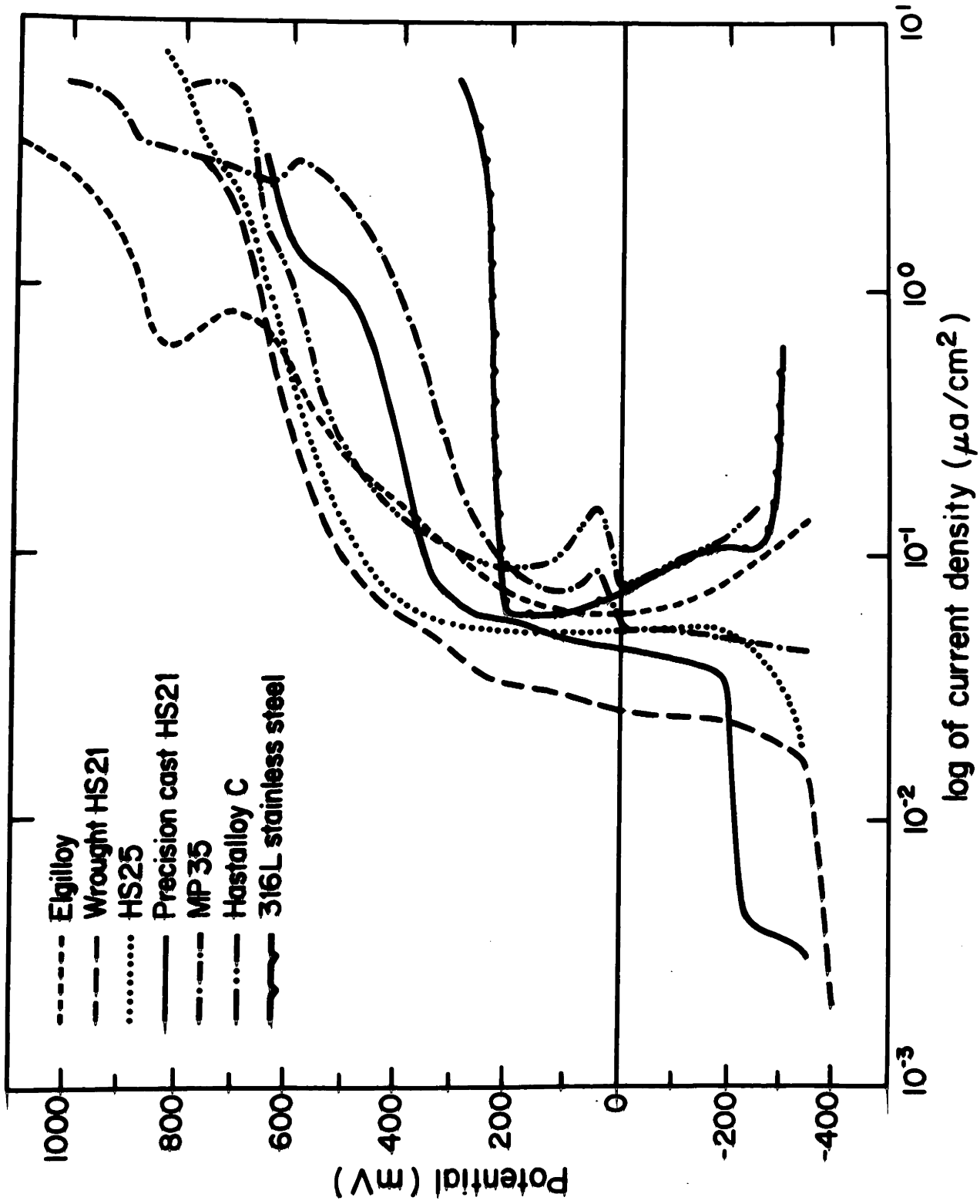


Figure 52. Creviced sample of 316L stainless steel following 9 days of immersion in 0.9% NaCl.

The following pages are missing from the original

#125

Figure 53. Anodic polarization curves of several alloys in deaerated 10% HCl + 1% FeCl₃ at 37°C.



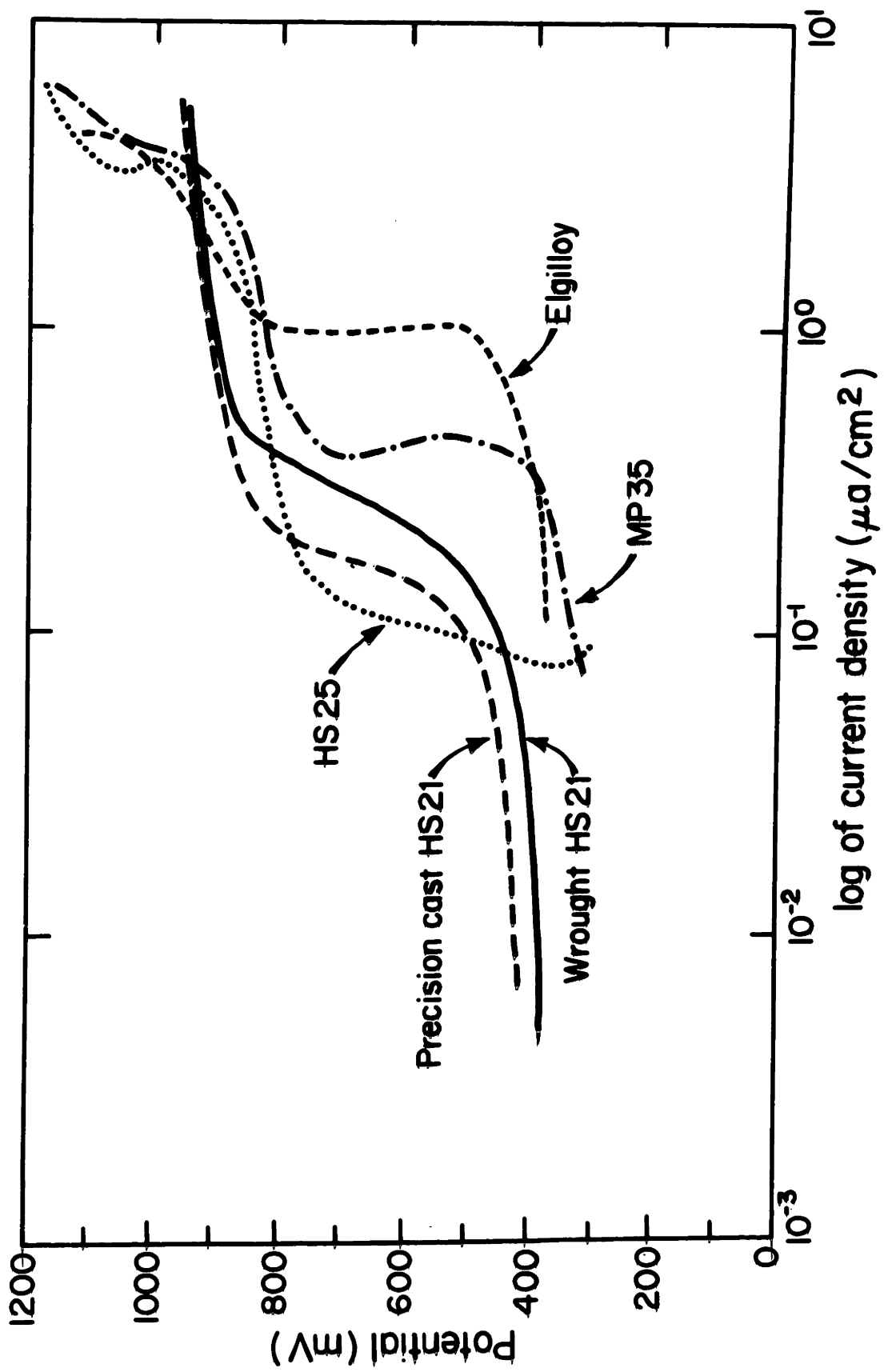


Figure 54. Cyclic anodic polarization of Elgilloy in deaerated 10% HCl + 1% FeCl₃ at 37°C.

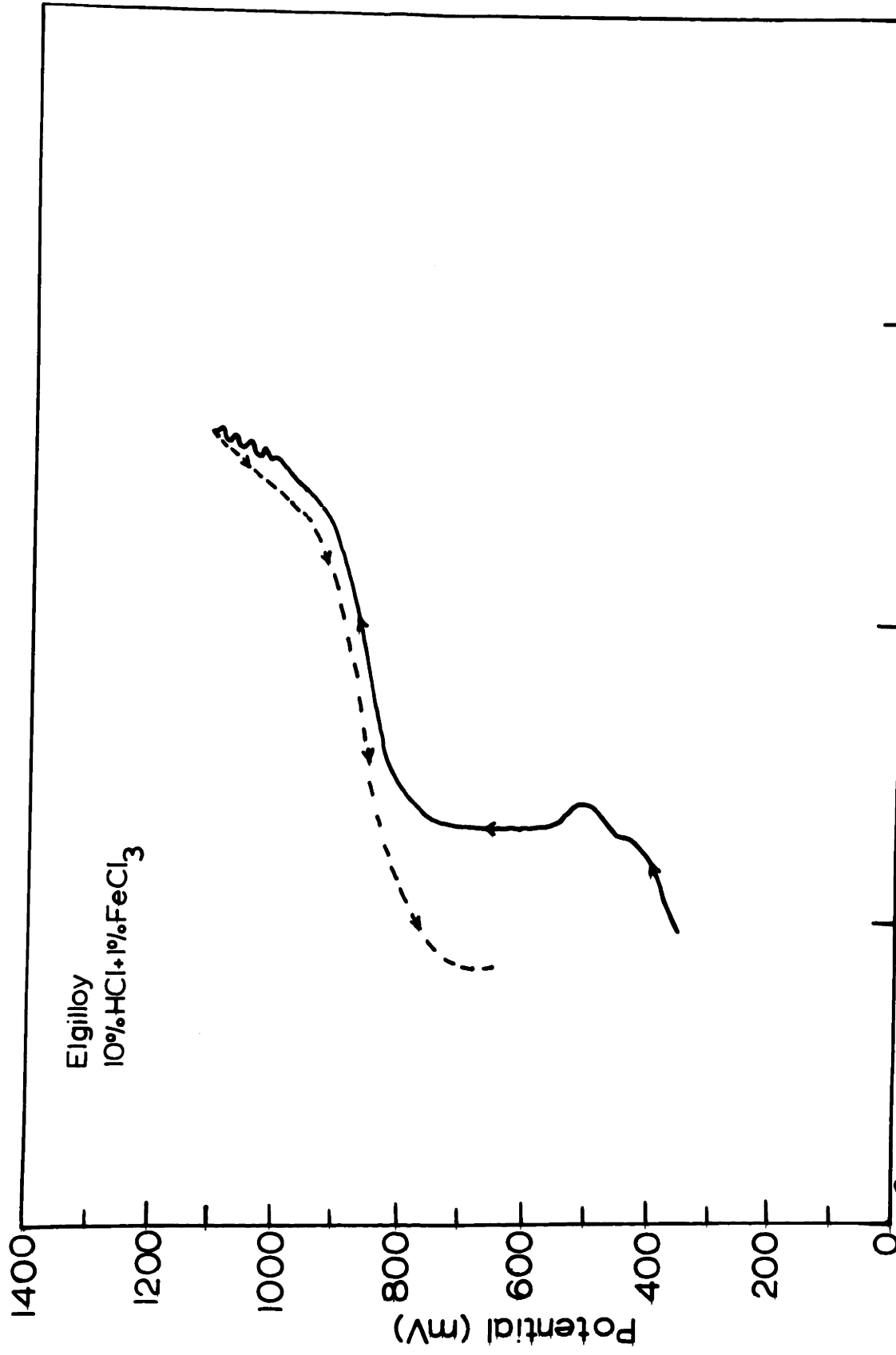


Figure 55. Cyclic anodic polarization of Hastalloy C in deaerated 10% HCl + 1% FeCl₃ at 37°C.

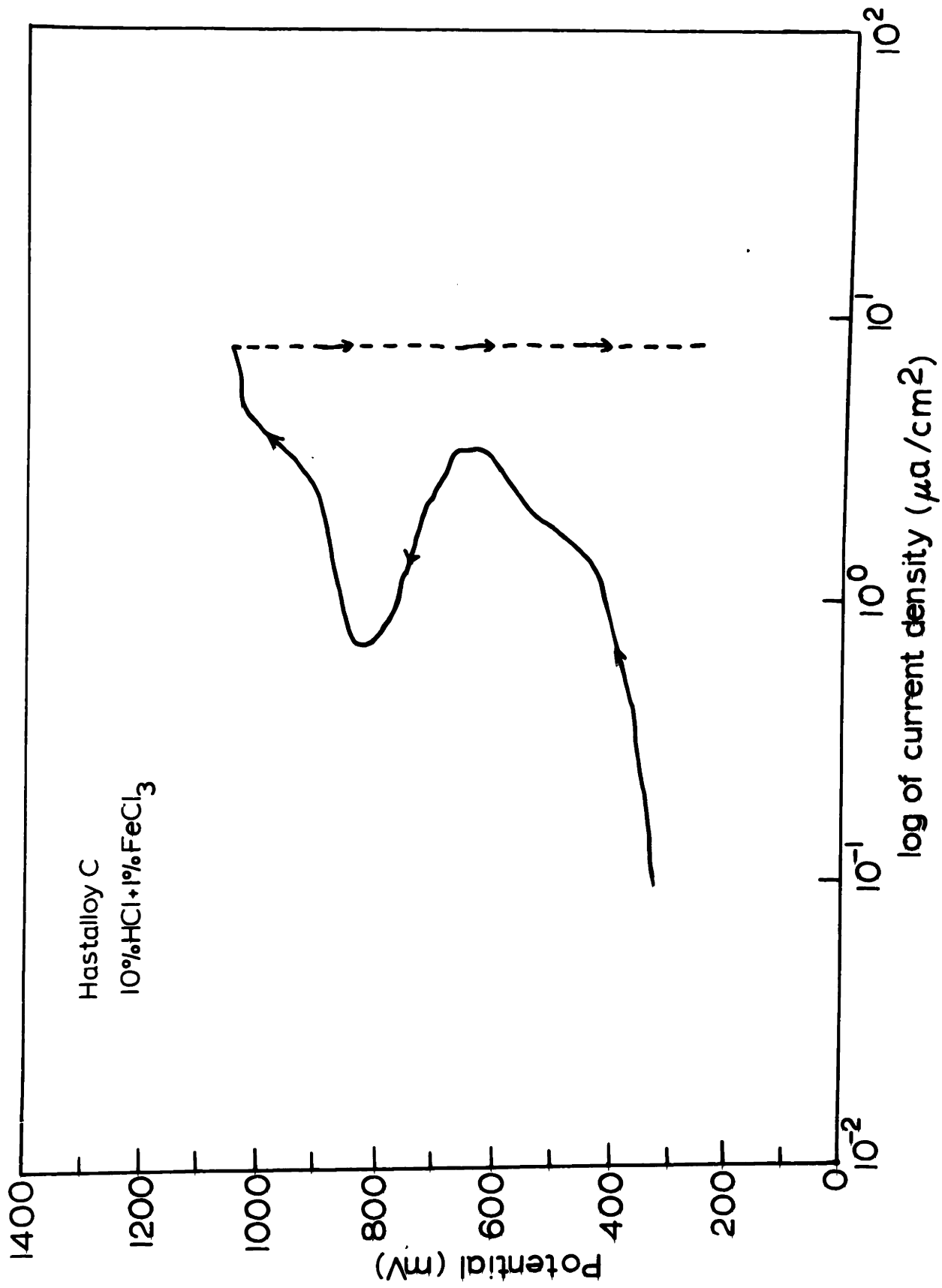


Figure 56. Cyclic anodic polarization of MP35N in deaerated 10% HCl + 1% FeCl₃ at 37°C.

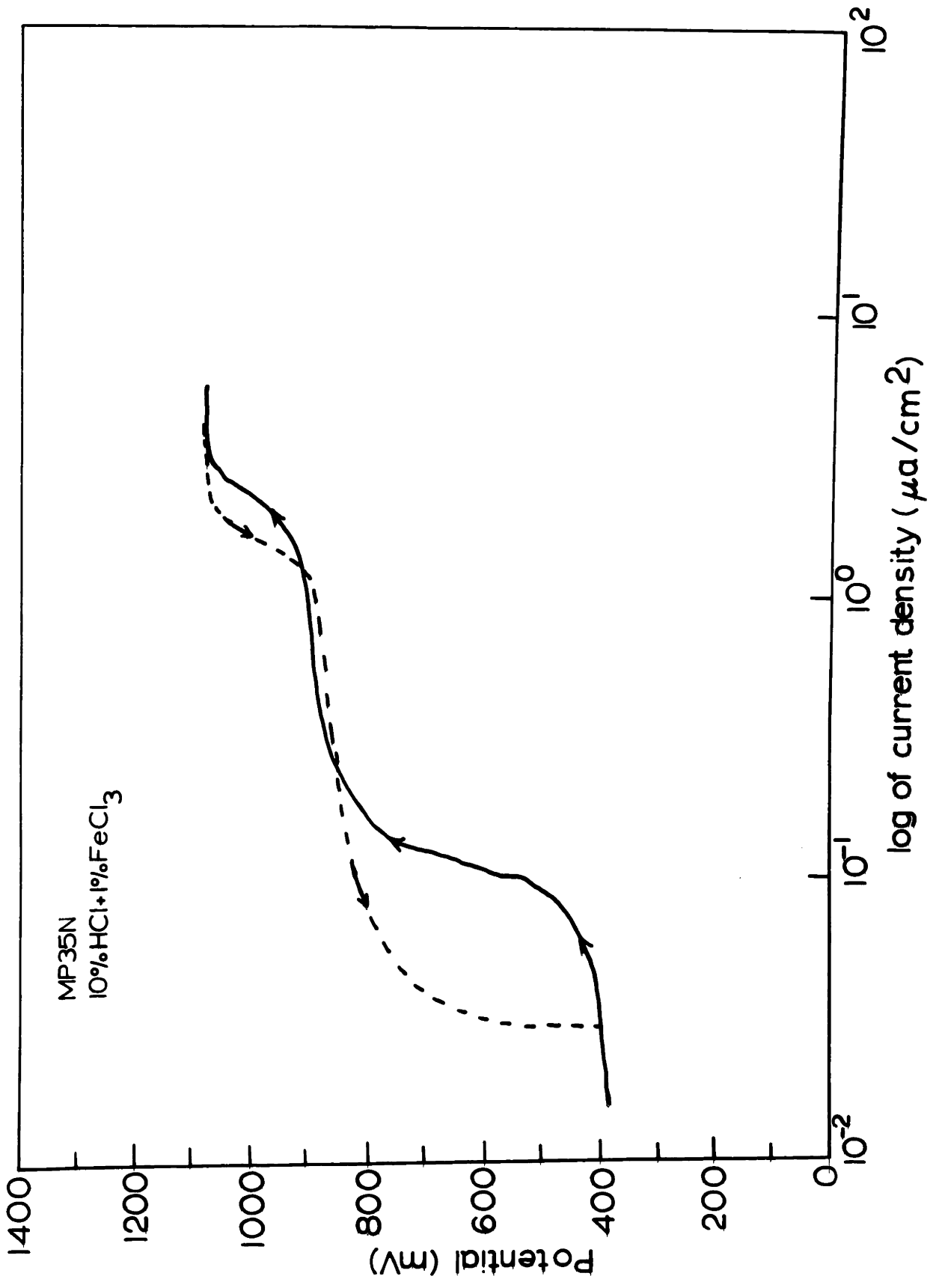


Figure 57. Cyclic anodic polarization of H.S. 25 in deaerated 10% HCl + 1% FeCl₃ at 37°C.

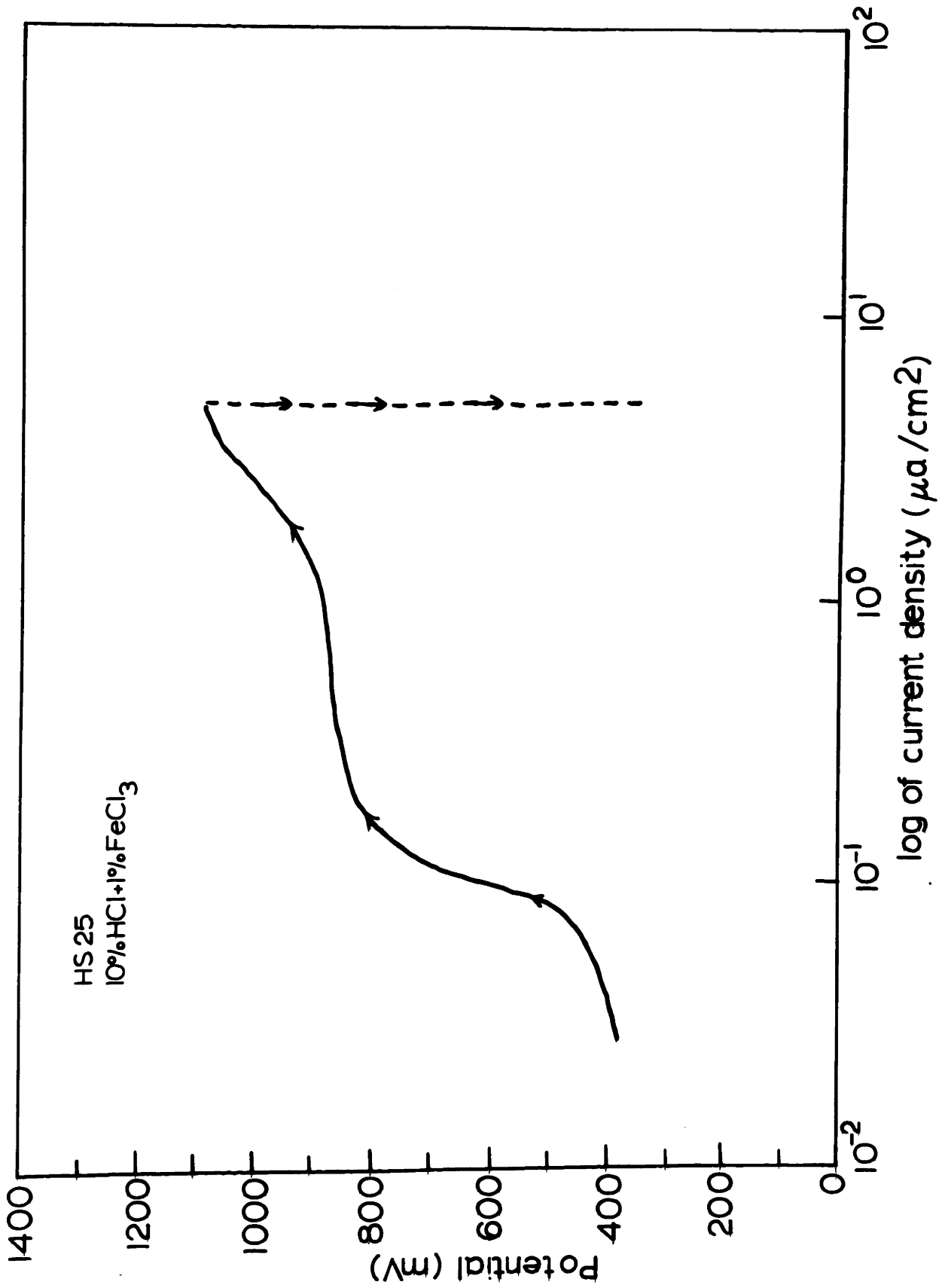


Figure 58. Cyclic anodic polarization of precision cast H.S. 21 in deaerated 10% HCl + 1% FeCl₃ at 37°C.

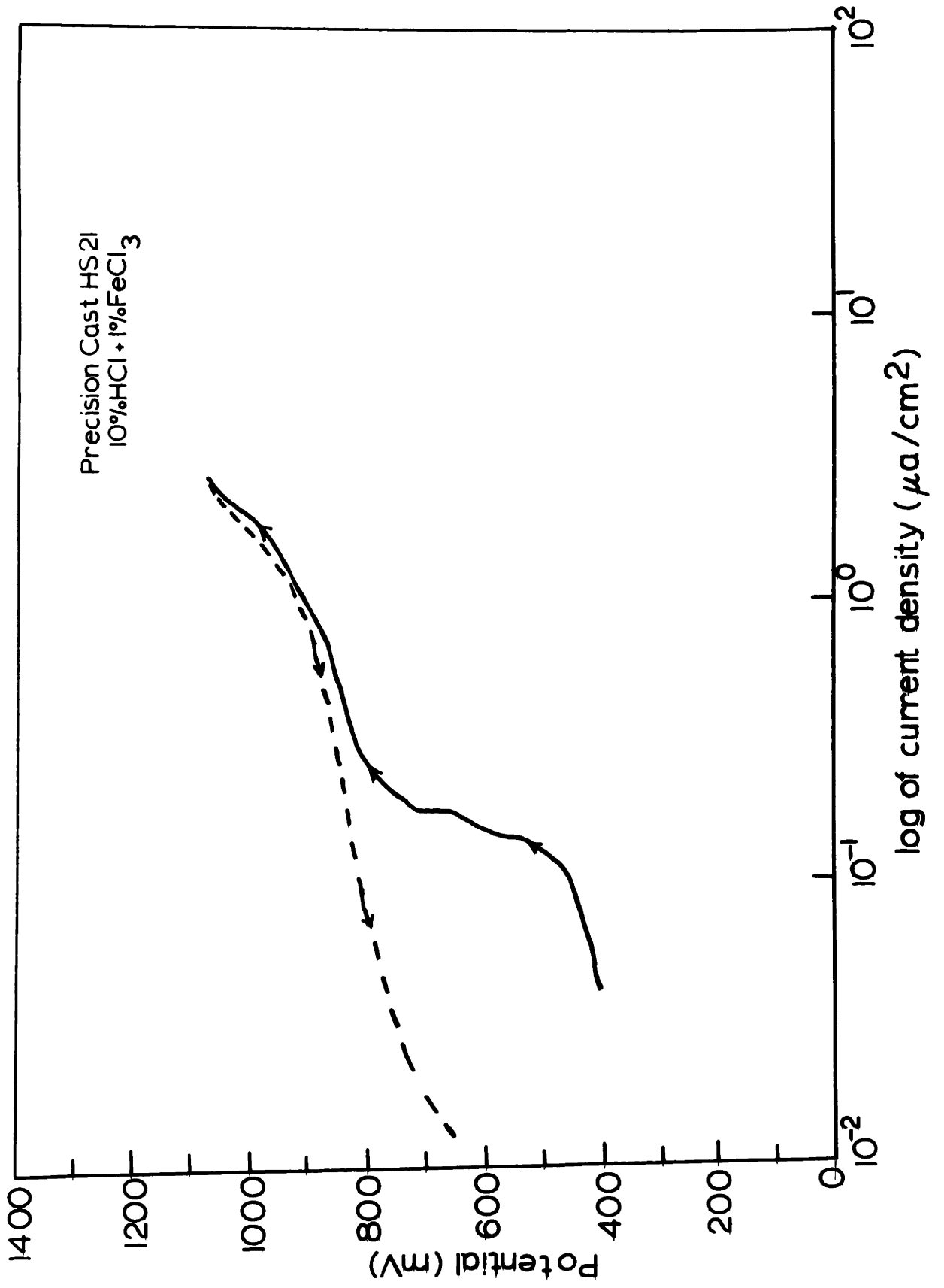


Figure 59. Cyclic anodic polarization of wrought H.S. 21 in deaerated 10% HCl + 1% FeCl₃ at 37°C.

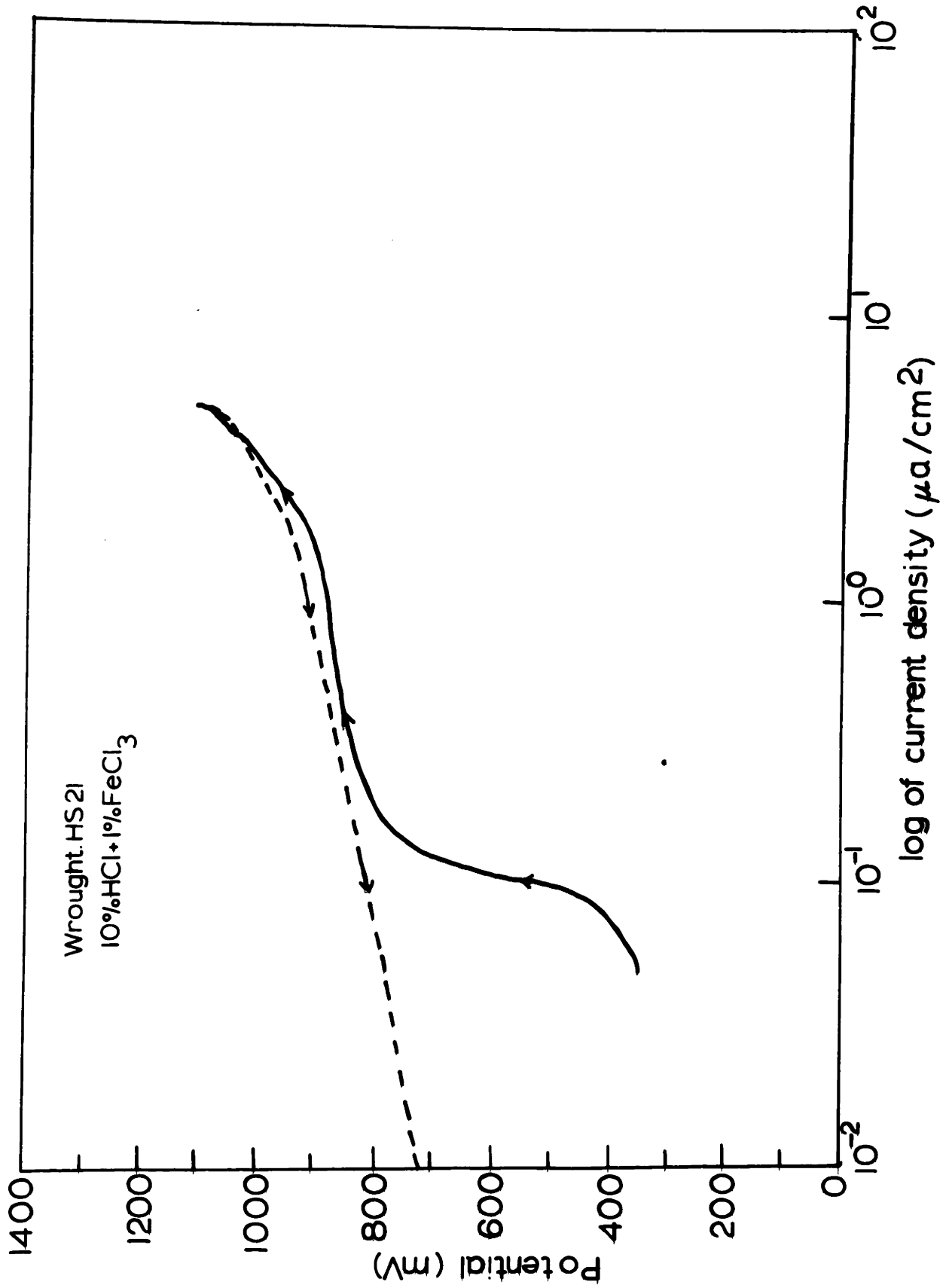


Figure 60. Cyclic anodic polarization of 316L stainless steel in deaerated 0.9% NaCl at 37°C.

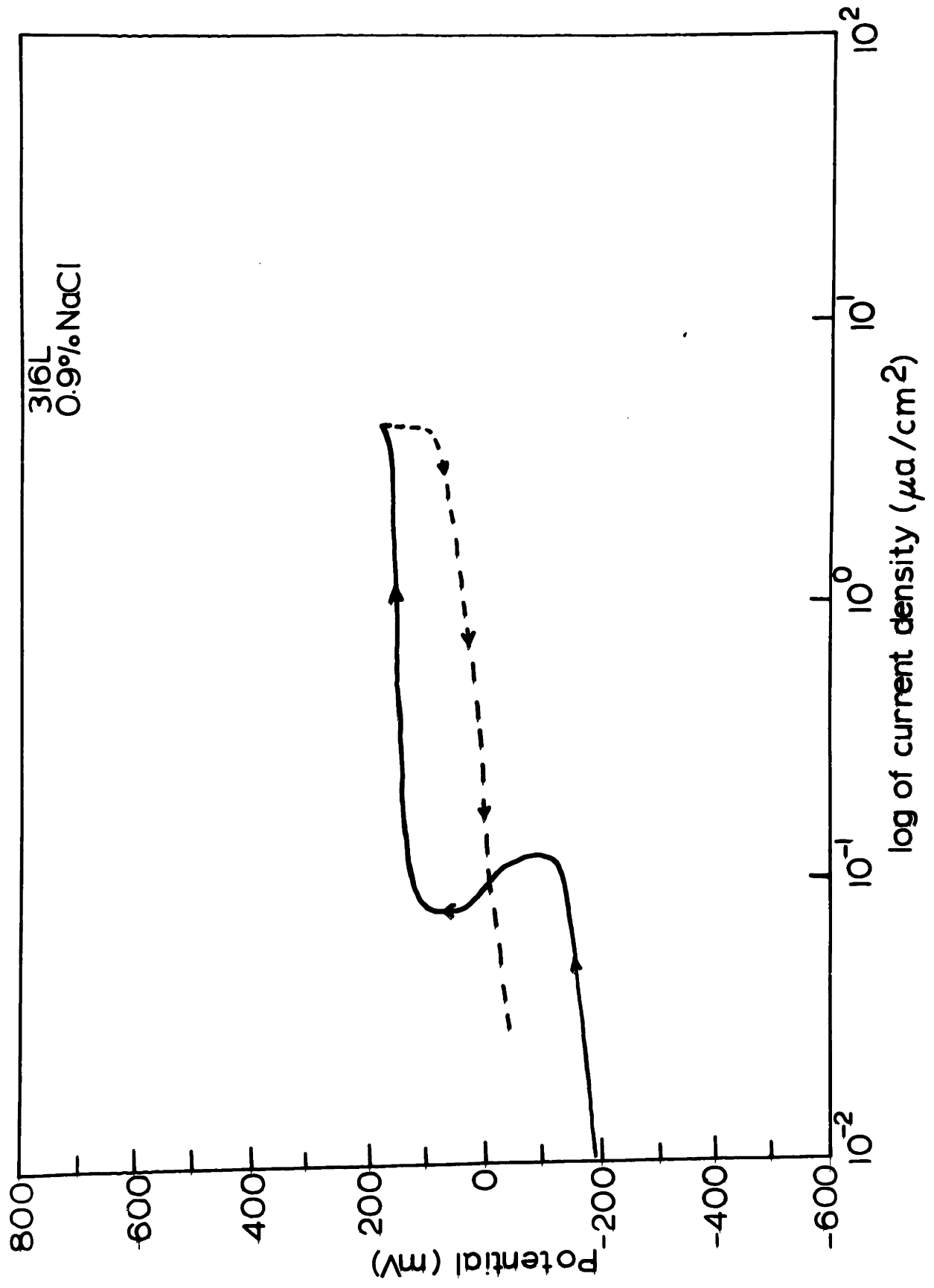


Figure 61. Cyclic anodic polarization of Elgilloy in deaerated 0.9% NaCl at 37°C.

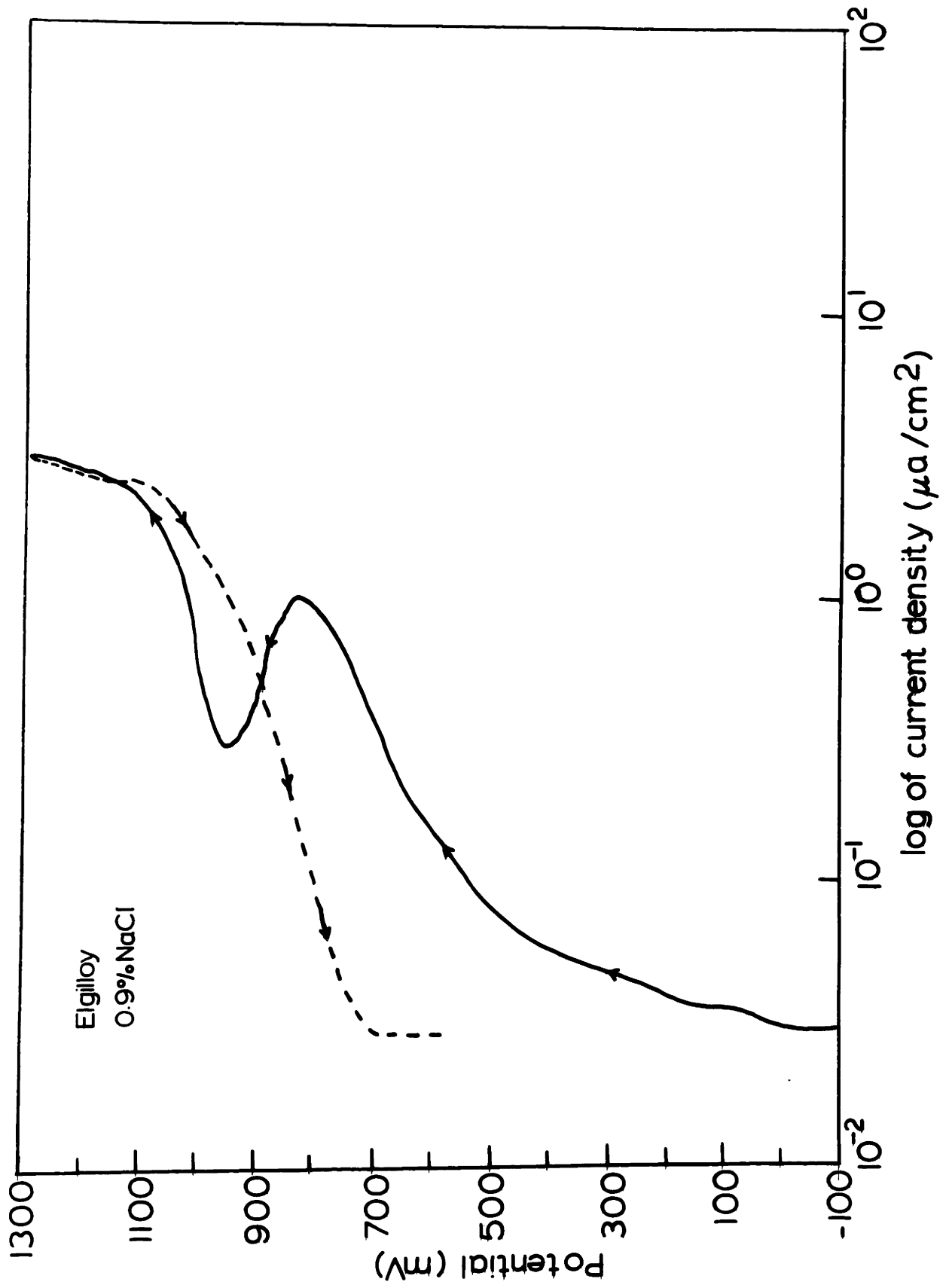


Figure 62. Cyclic anodic polarization of Hastalloy C in deaerated 0.9% NaCl at 37°C.

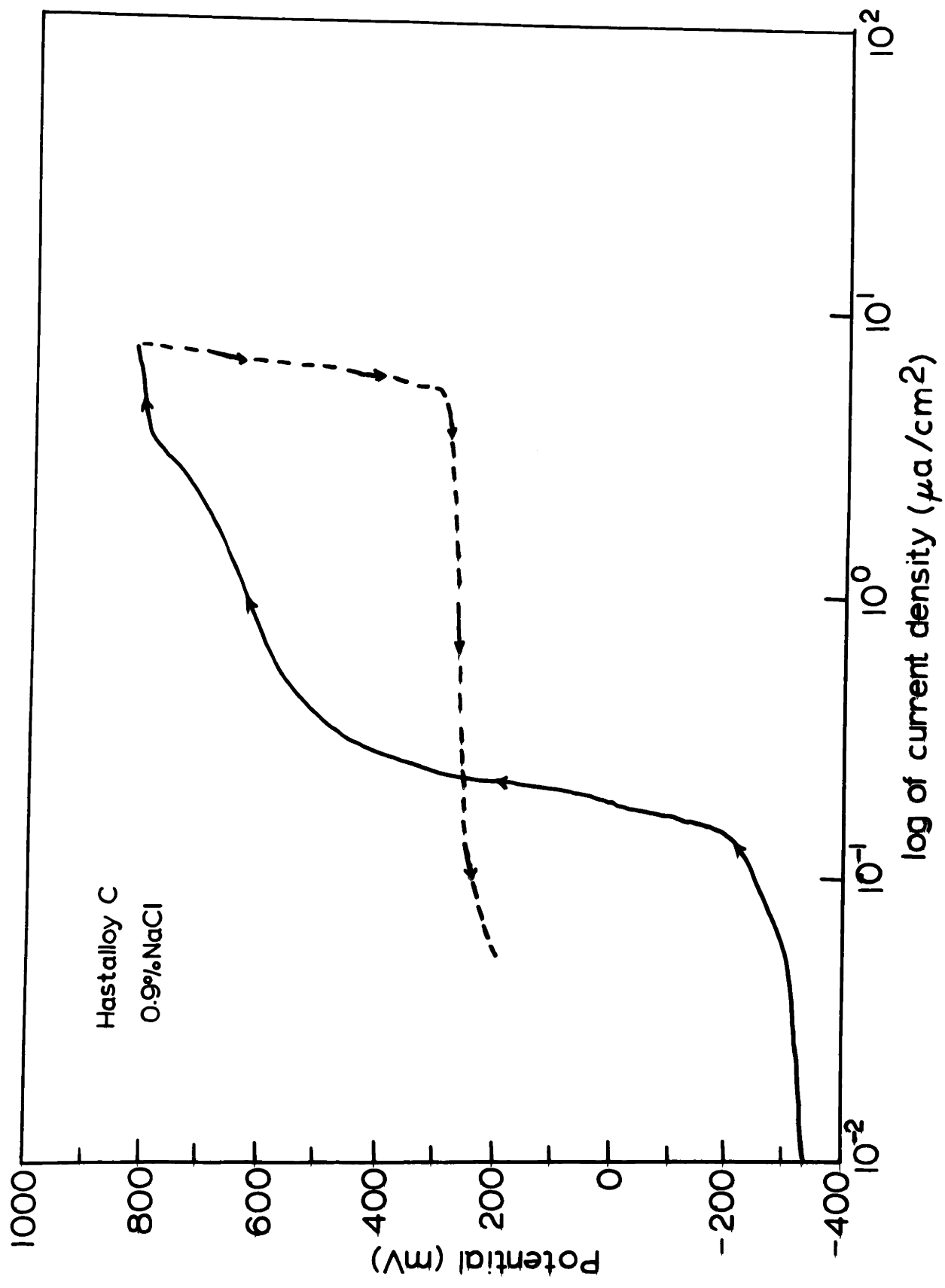


Figure 63. Cyclic anodic polarization of MP35 in deaerated 0.9% NaCl at 37°C.

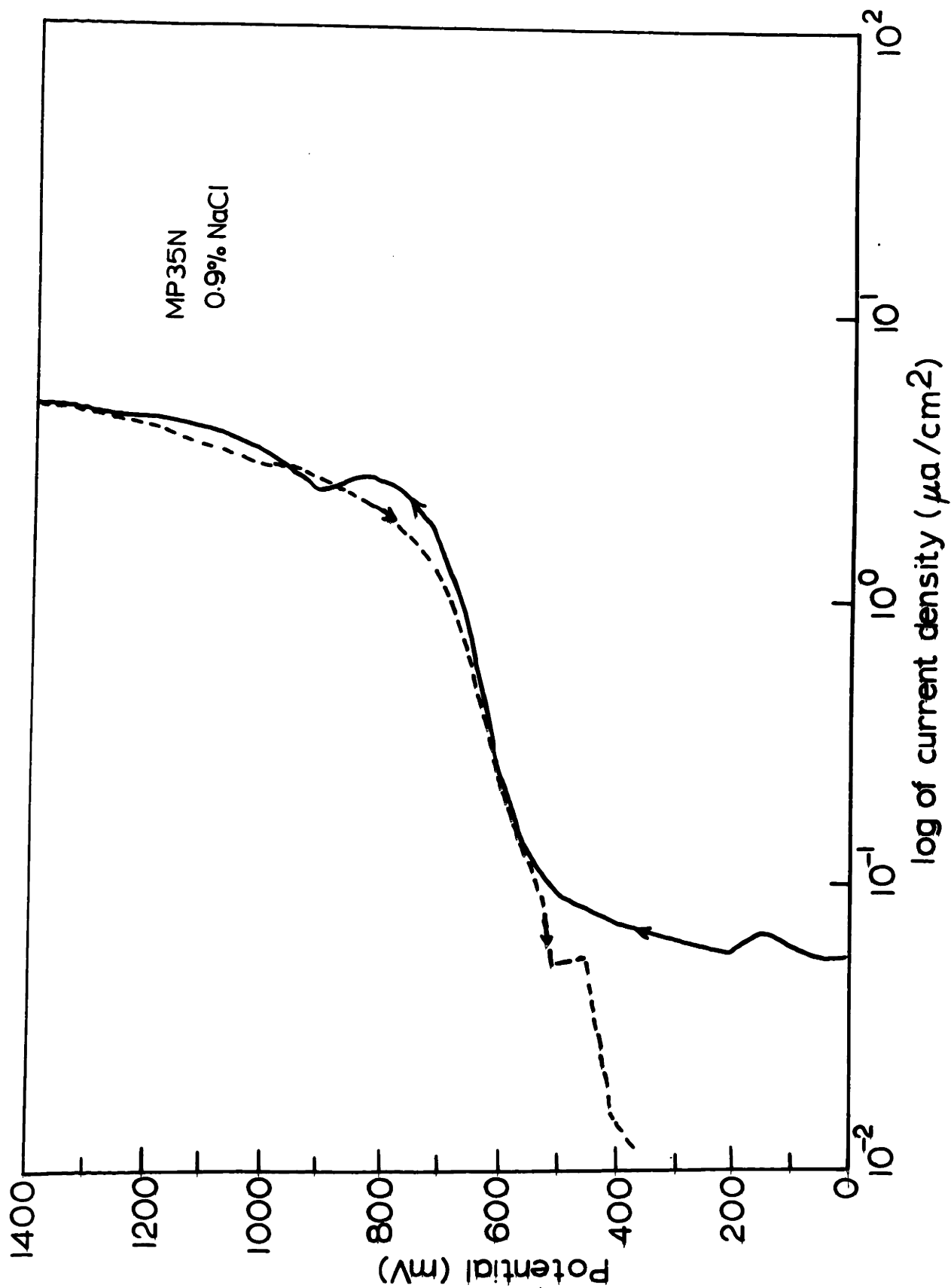


Figure 64. Cyclic anodic polarization of H.S. 25 in deaerated 0.9% NaCl at 37°C.

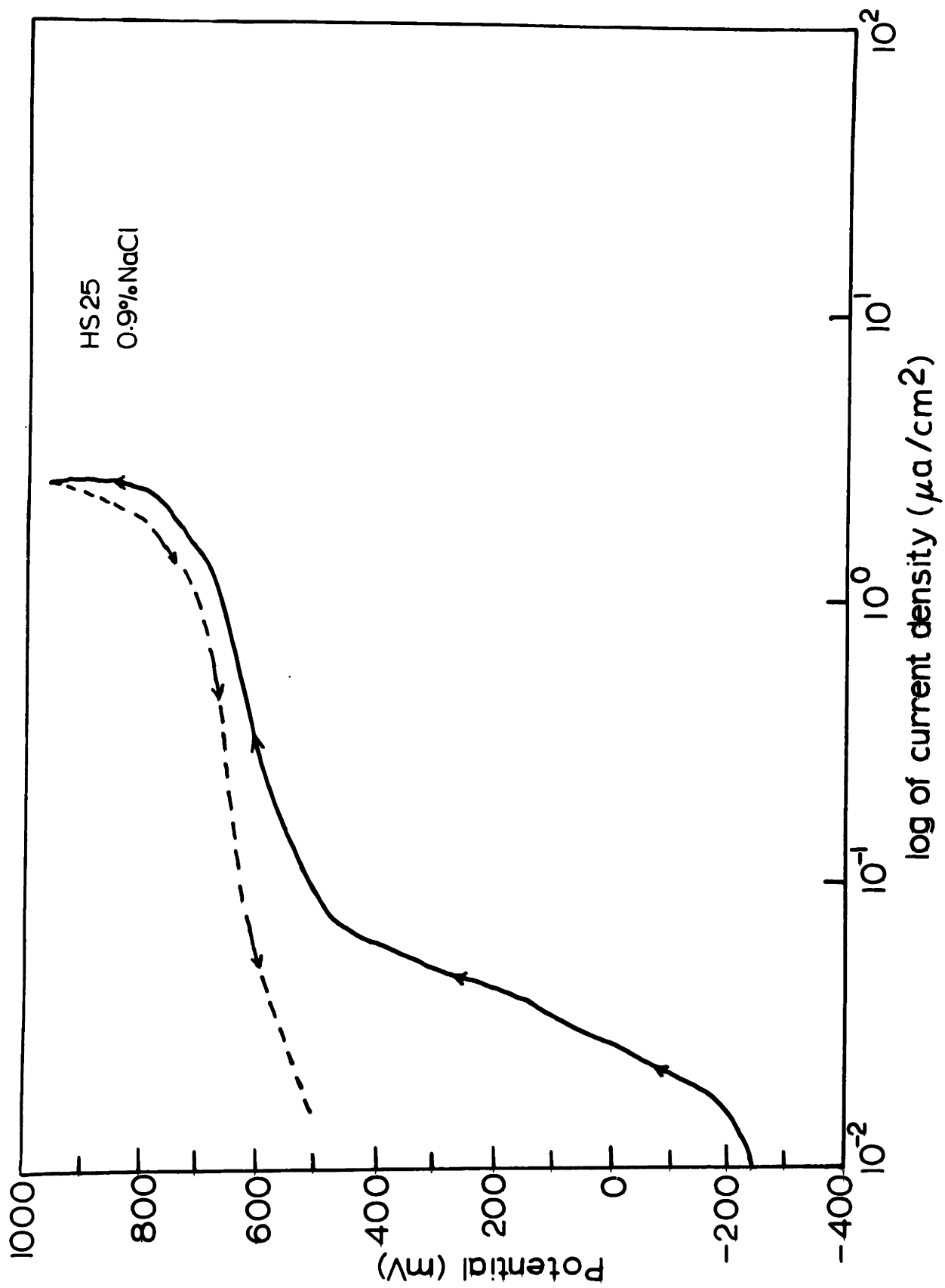


Figure 65. Cyclic anodic polarization of precision cast H.S. 21 in deaerated 0.9% NaCl at 37°C.

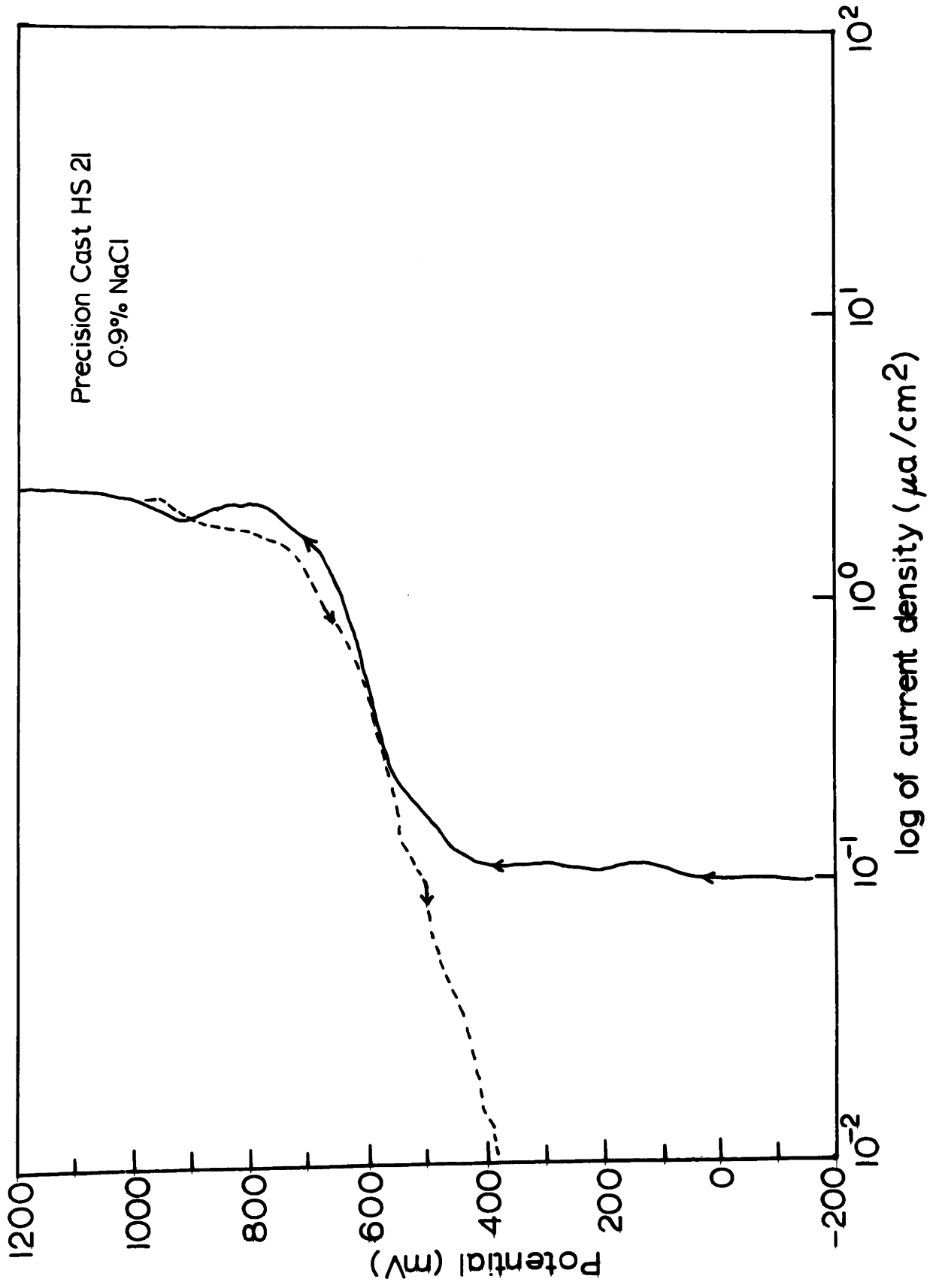


Figure 66. Cyclic anodic polarization of wrought H.S. 21 in deaerated 0.9% NaCl at 37°C.

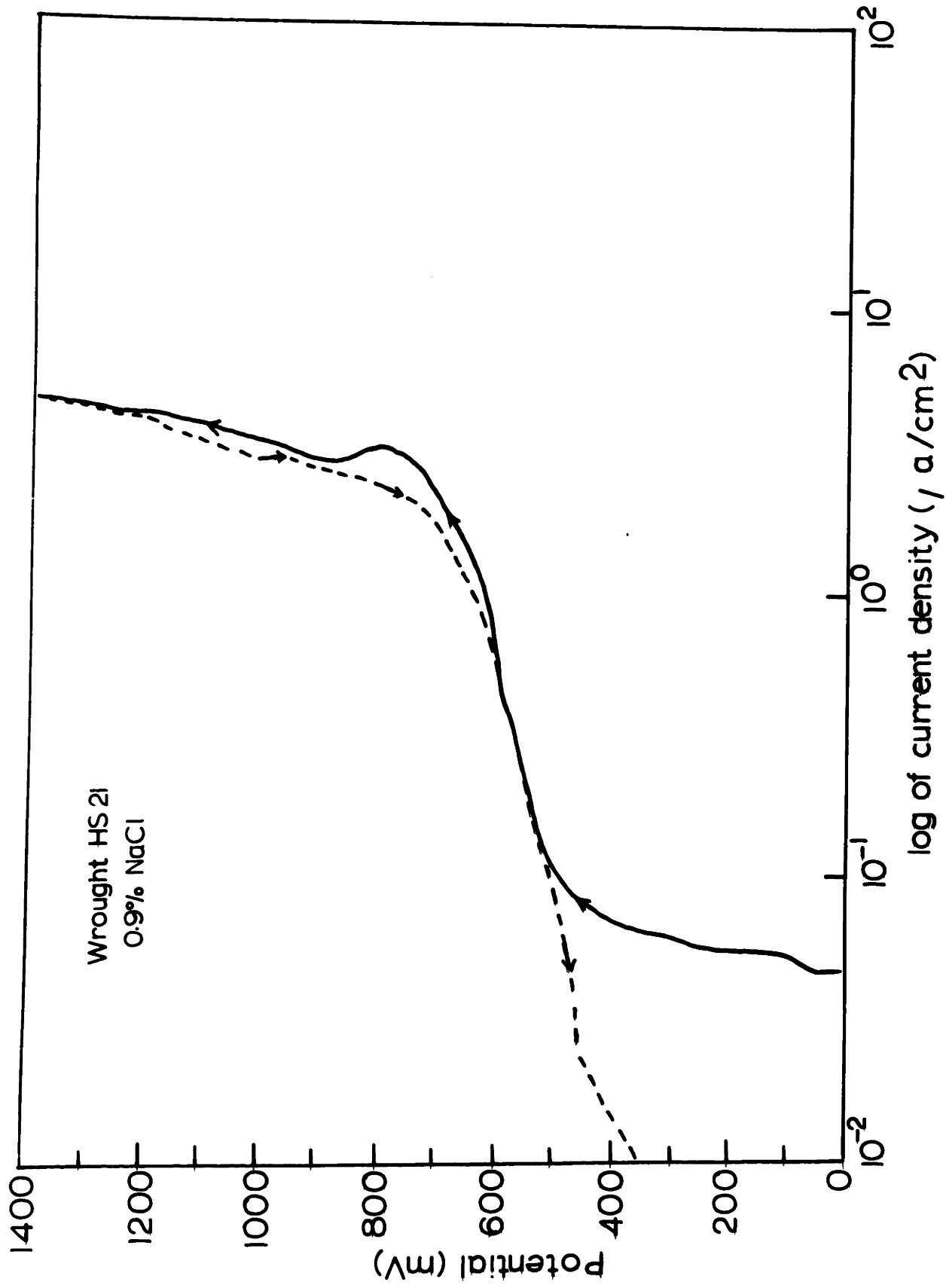


Figure 67 Corrosion current density variation with time of creviced samples of 316L stainless steel at various applied potentials in deaerated 10% HCl + 1% FeCl₃ at 37°C.

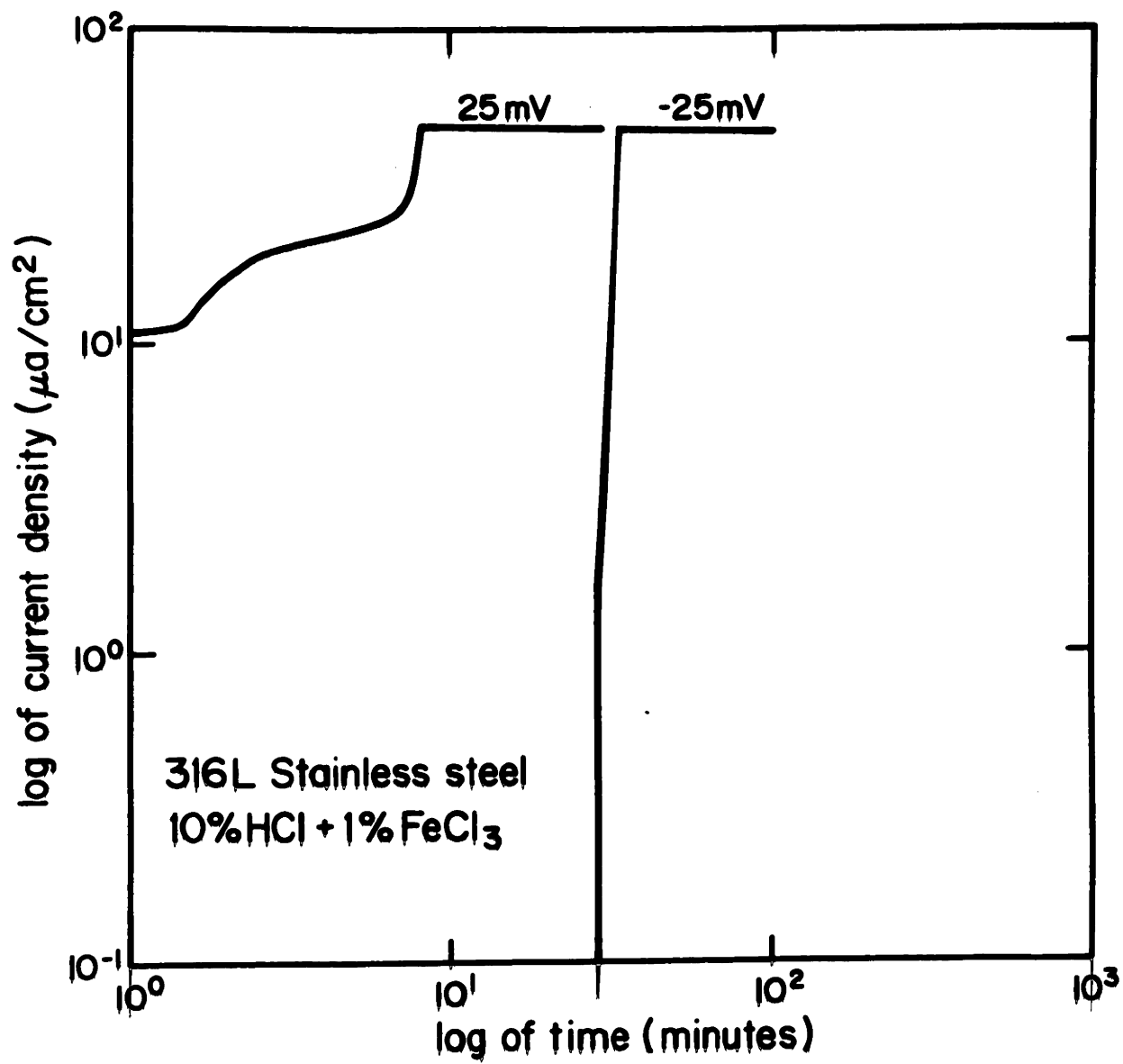


Figure 67. Corrosion current density variation with time of creviced samples of Elgilloy at various applied potentials in deaerated 10% HCl + 1% FeCl₃ at 37°C.

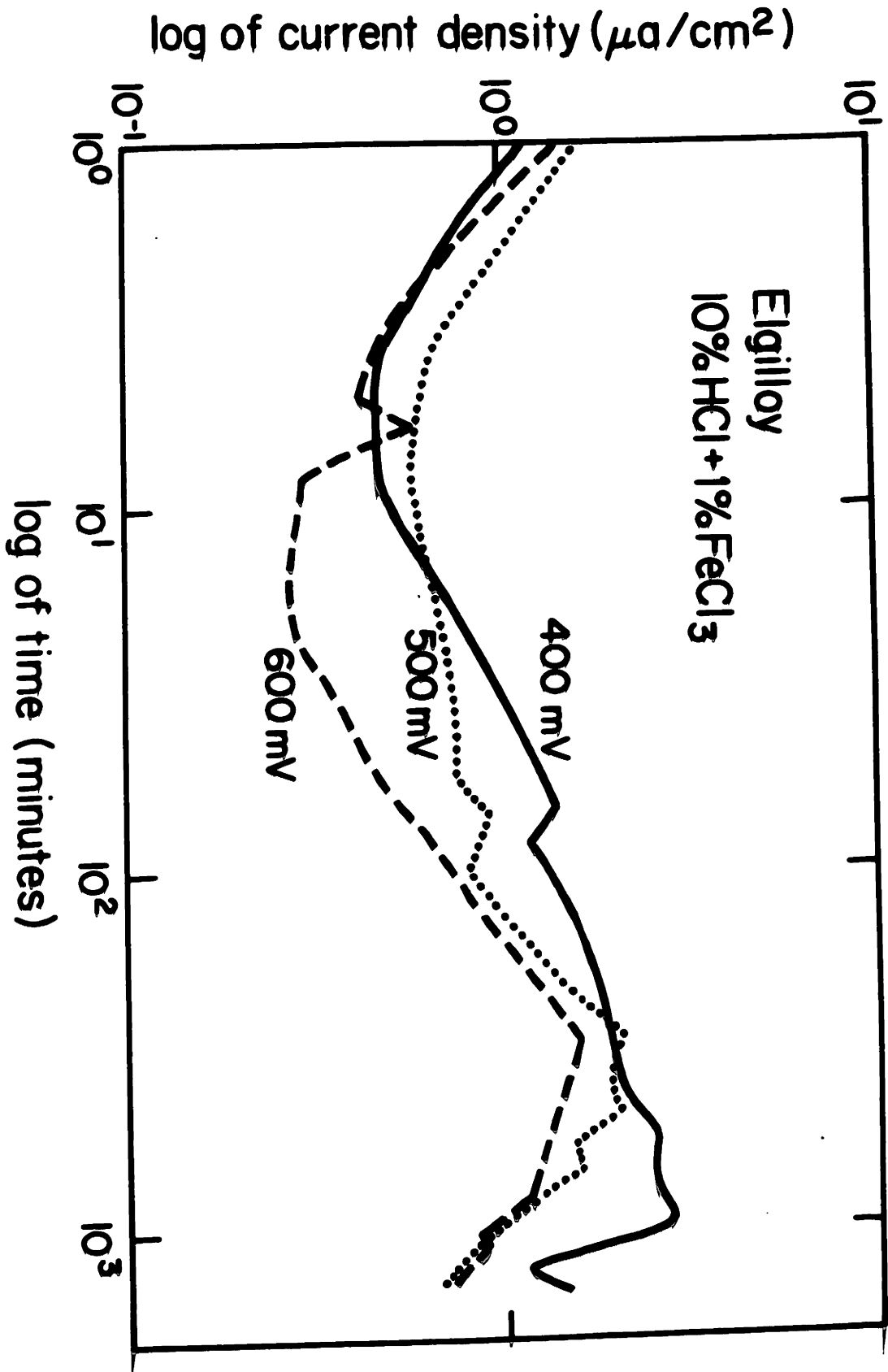


Figure 68. Corrosion current density variation with time of creviced samples of Hastalloy C at various applied potentials in deaerated 10% HCl + 1% FeCl₃ at 37°C.

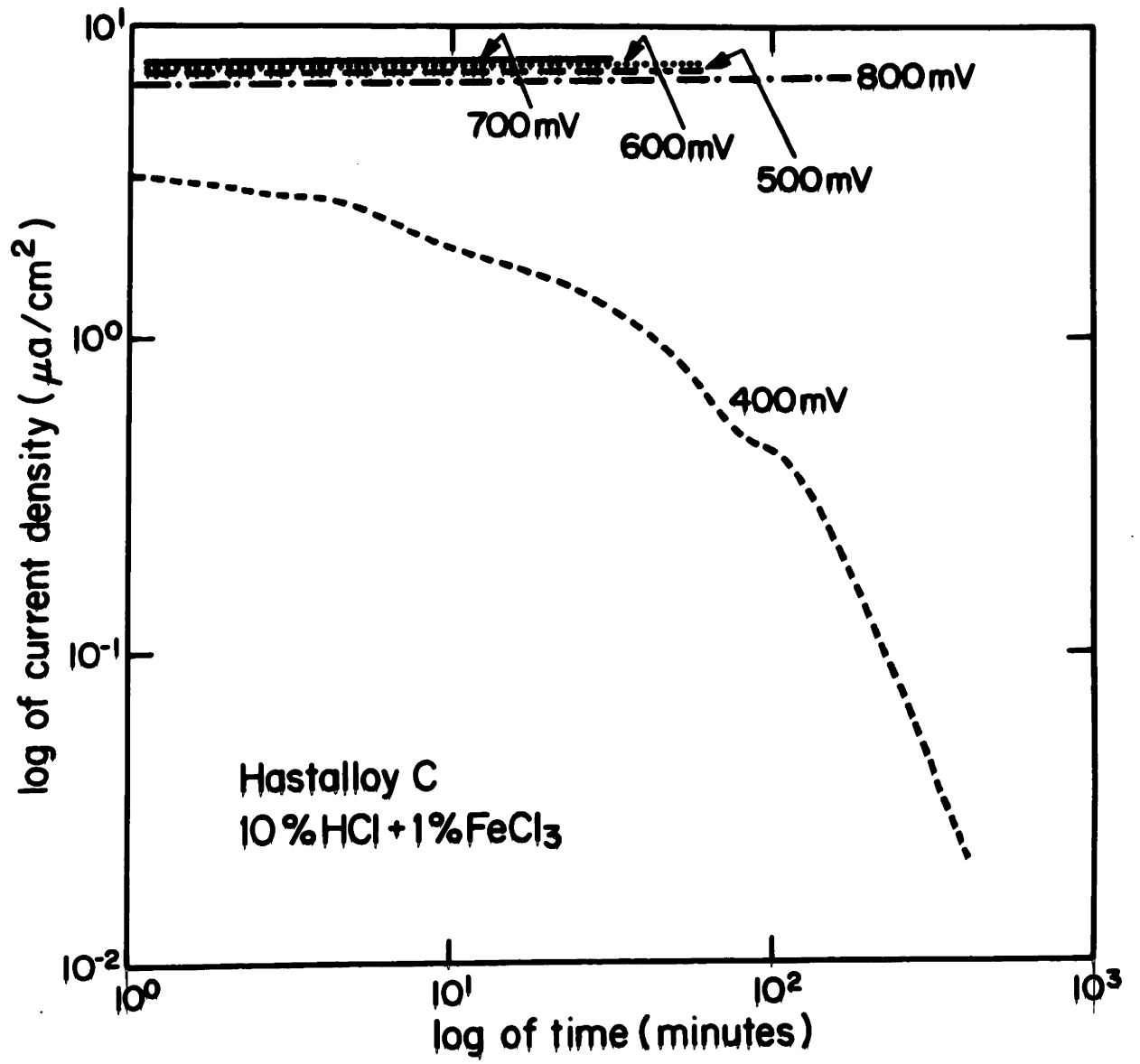


Figure 69. Corrosion current density variation with creviced samples of MP35 at various appl. in deaerated 10% HCl + 1% FeCl₃ at 37°C.

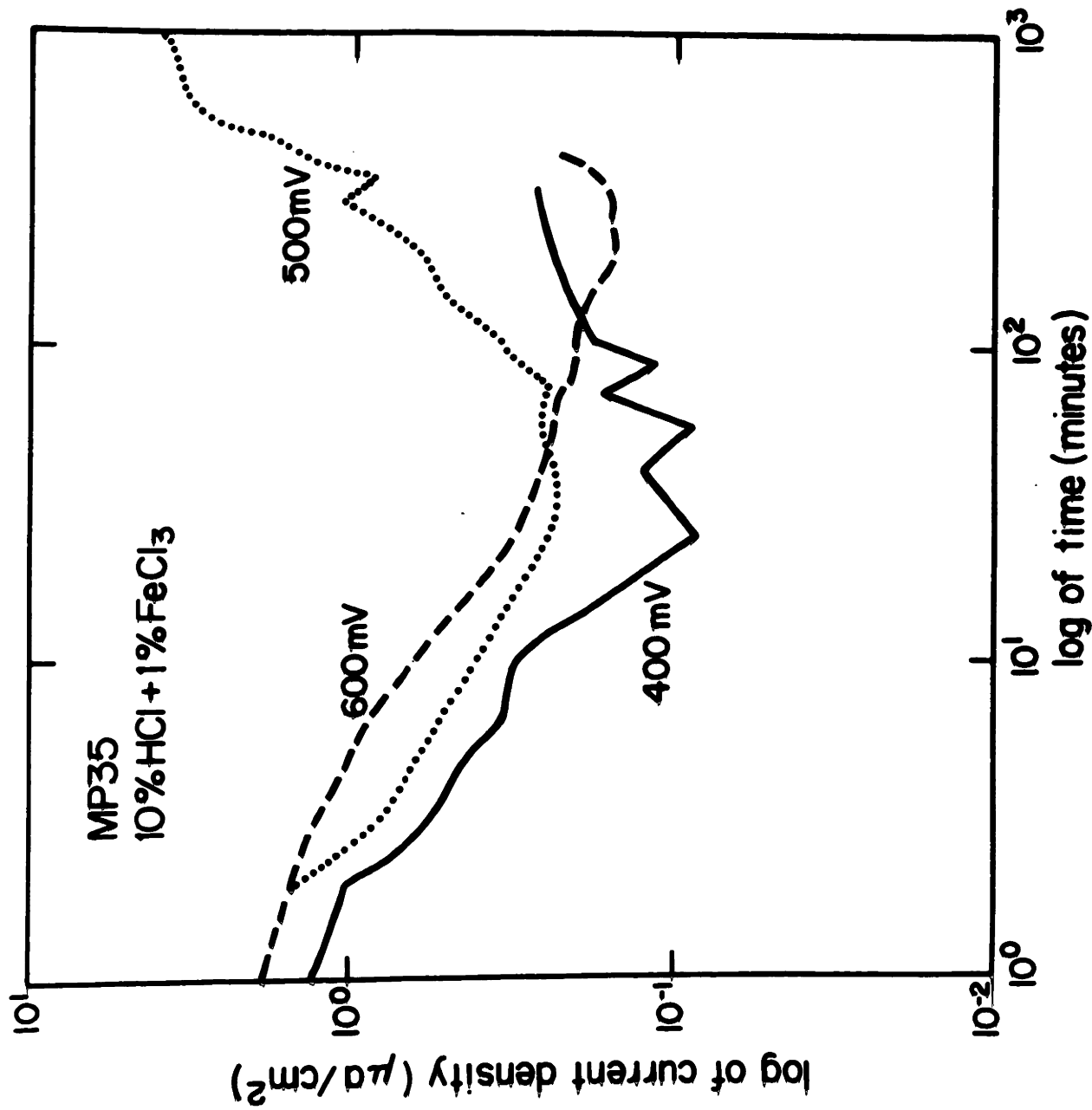


Figure 70. Corrosion current density variation with time of creviced samples of H.S. 25 at various applied potentials in deaerated 10% HCl + 1% FeCl₃ at 37°C.

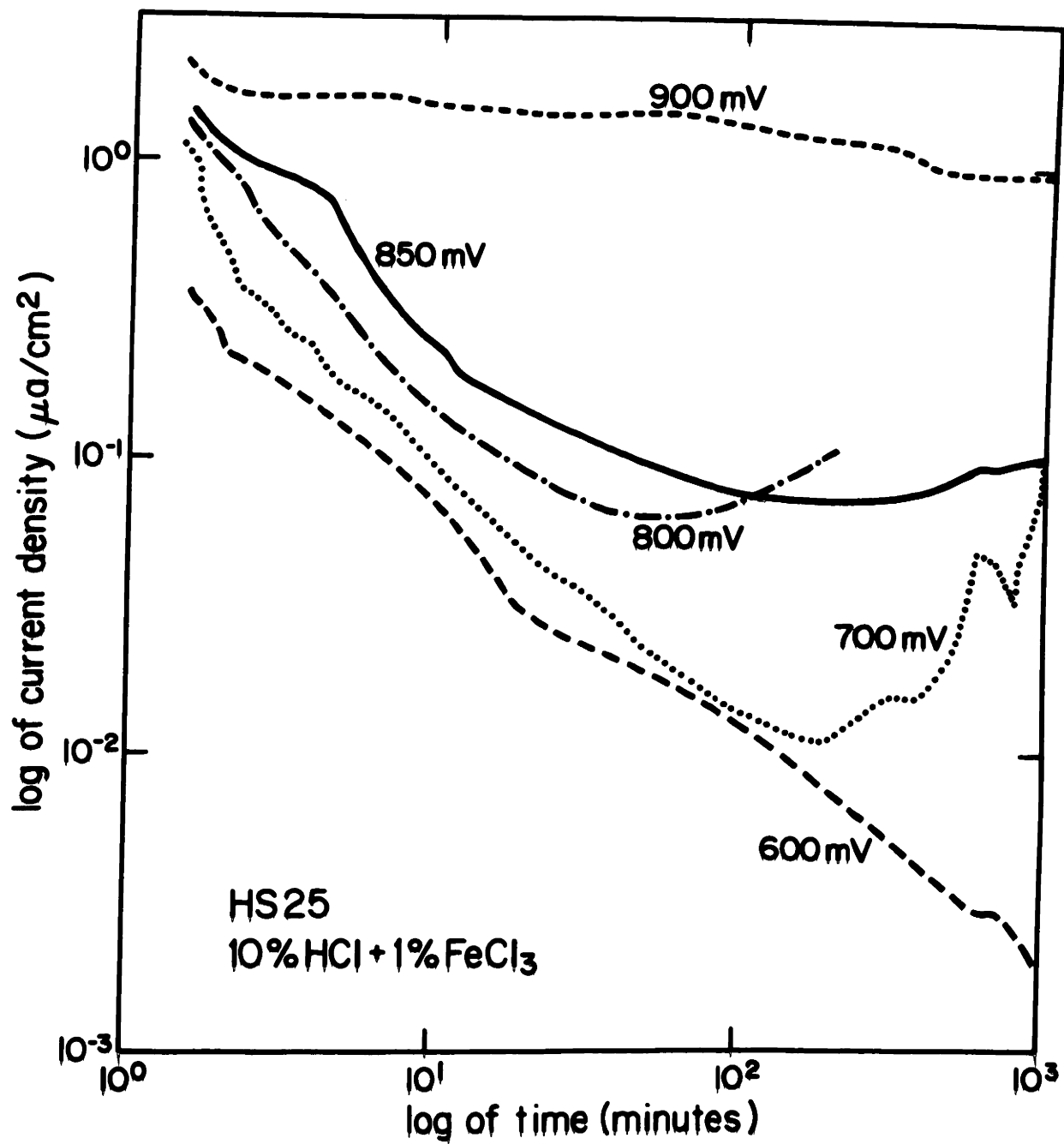


Figure 71. Corrosion current density variation with time of creviced samples of wrought H.S. 21 at various potentials in deaerated 10% HCl + 1% FeCl₃ at 37°C.

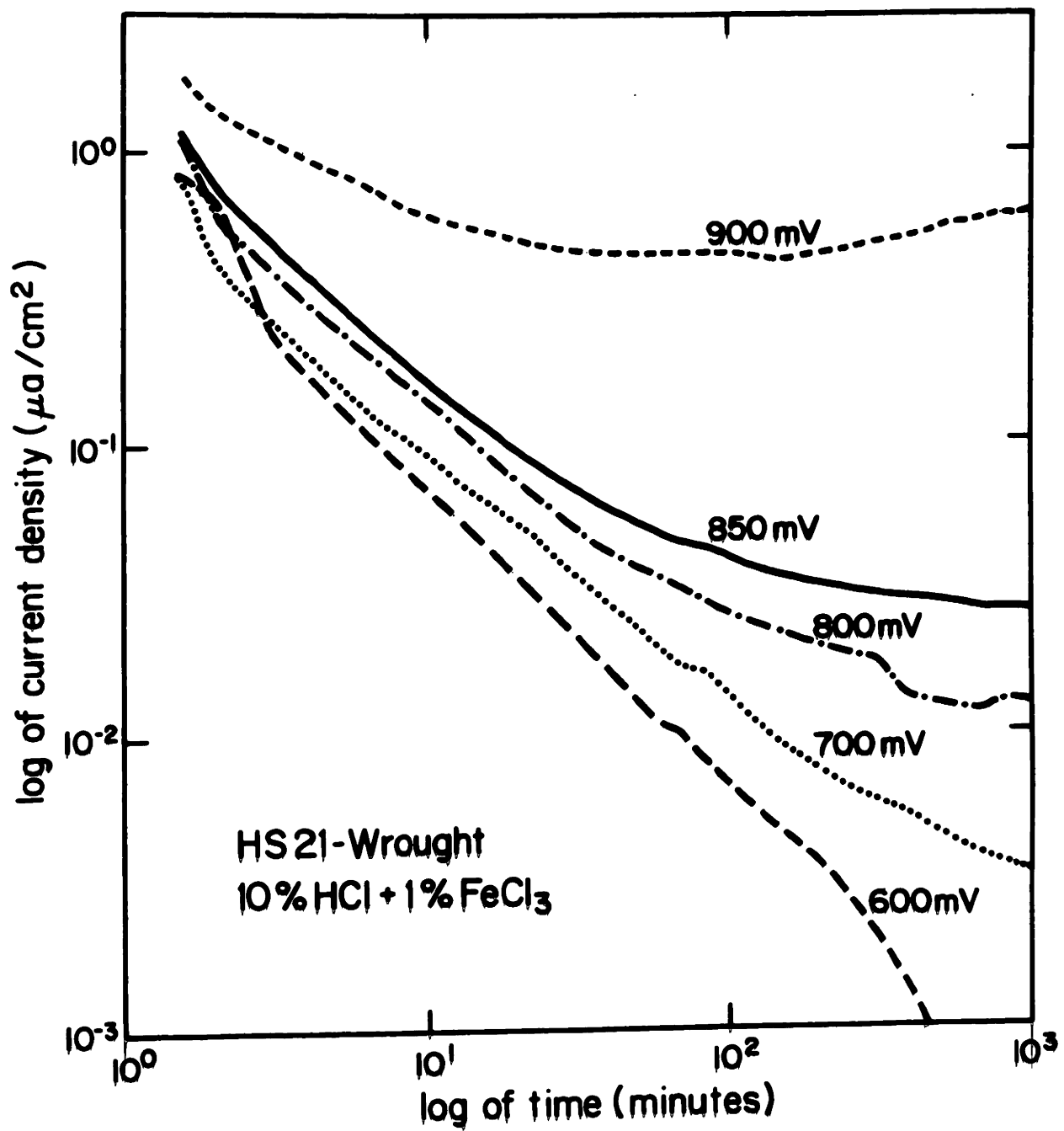


Figure 72. Corrosion current density variation with time of creviced samples of cast H.S. 21 at various applied potentials in deaerated 10% HCl + 1% FeCl₃ at 37°C.

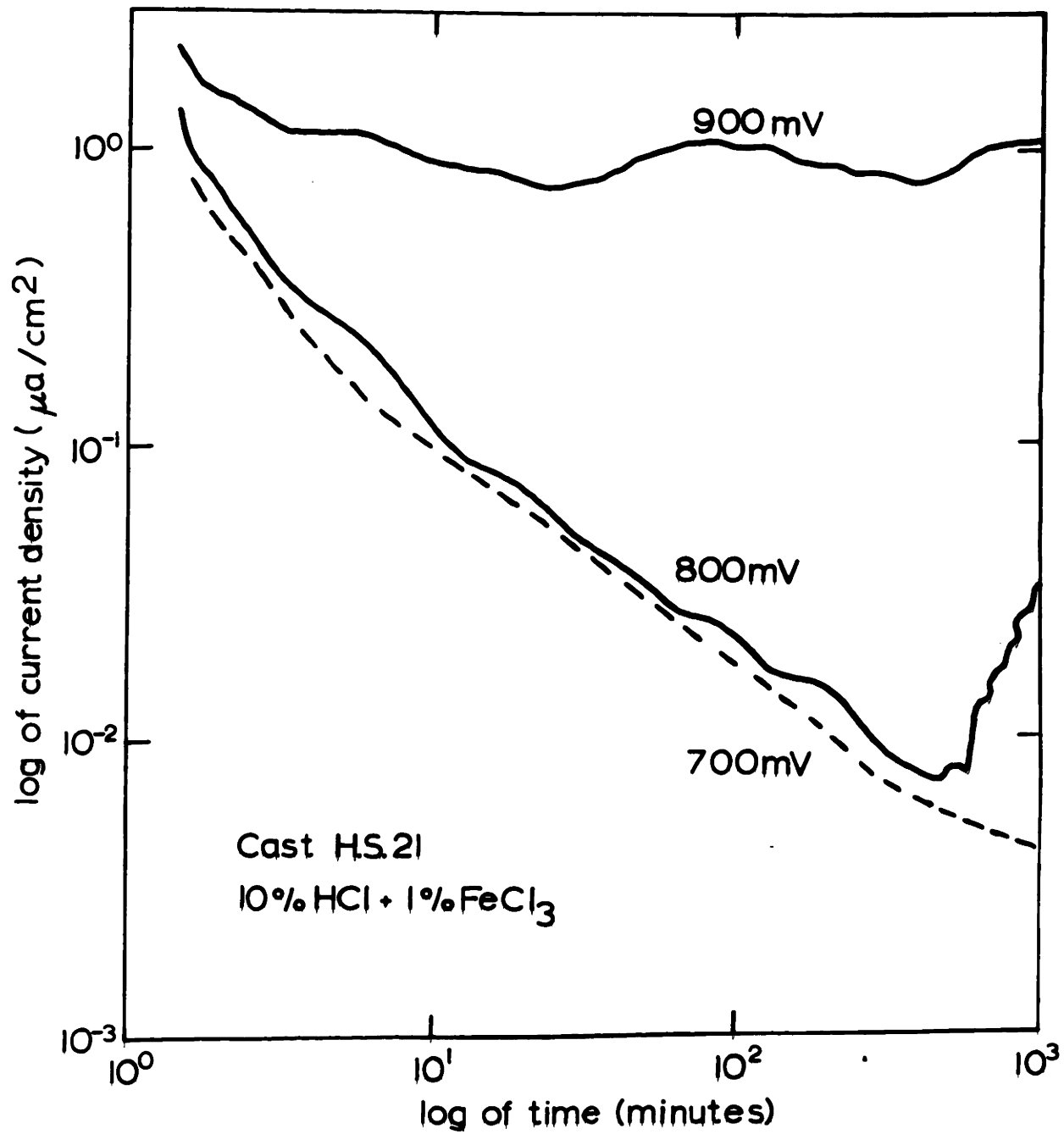


Figure 73. Corrosion current density variation with time of creviced samples of 316L stainless steel at various applied potentials in deaerated 0.9% NaCl at 37°C.

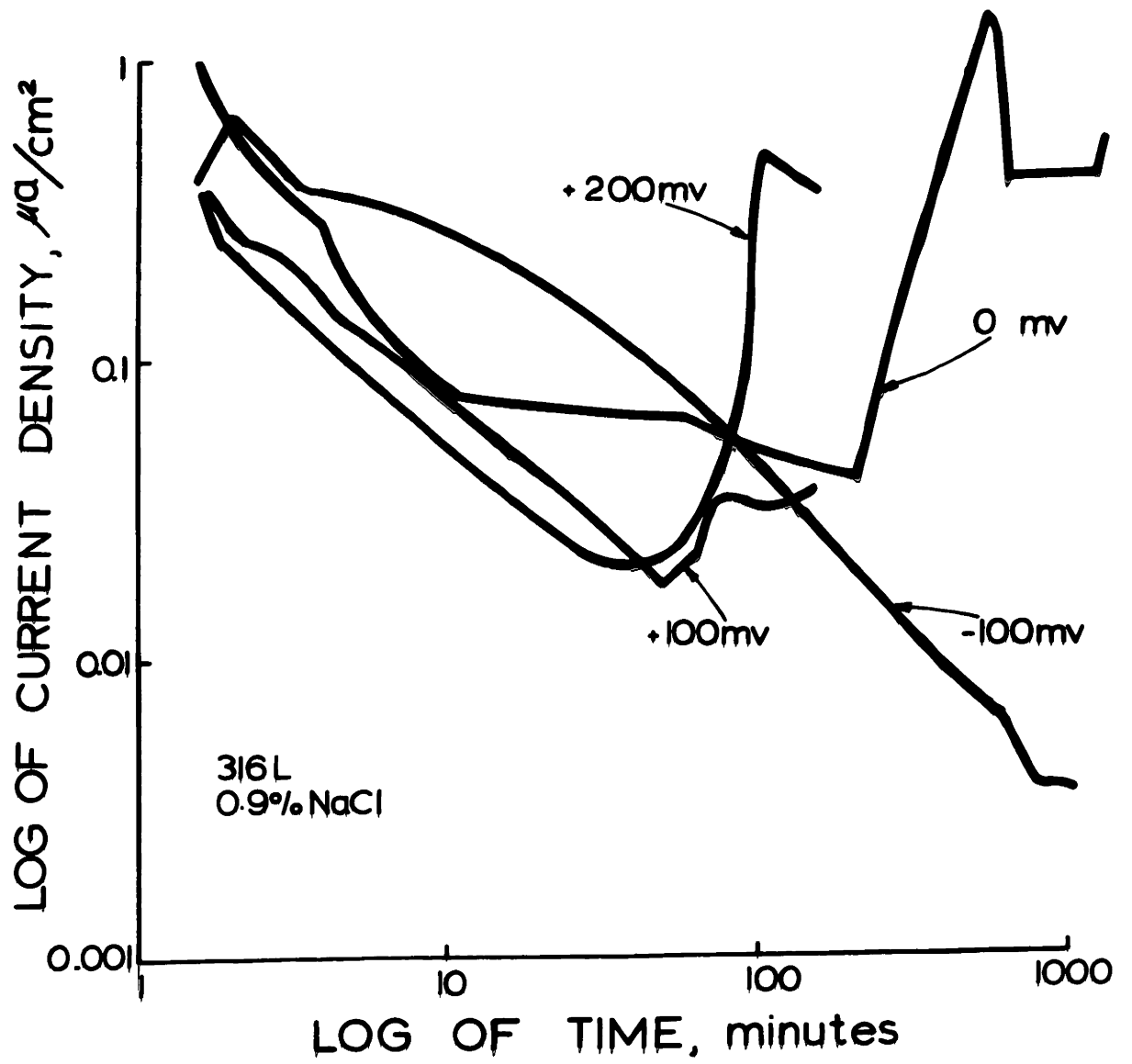


Figure 74. Corrosion current density variation with time of creviced samples of Elgilloy at various applied potentials in deaerated 0.9% NaCl at 37°C.

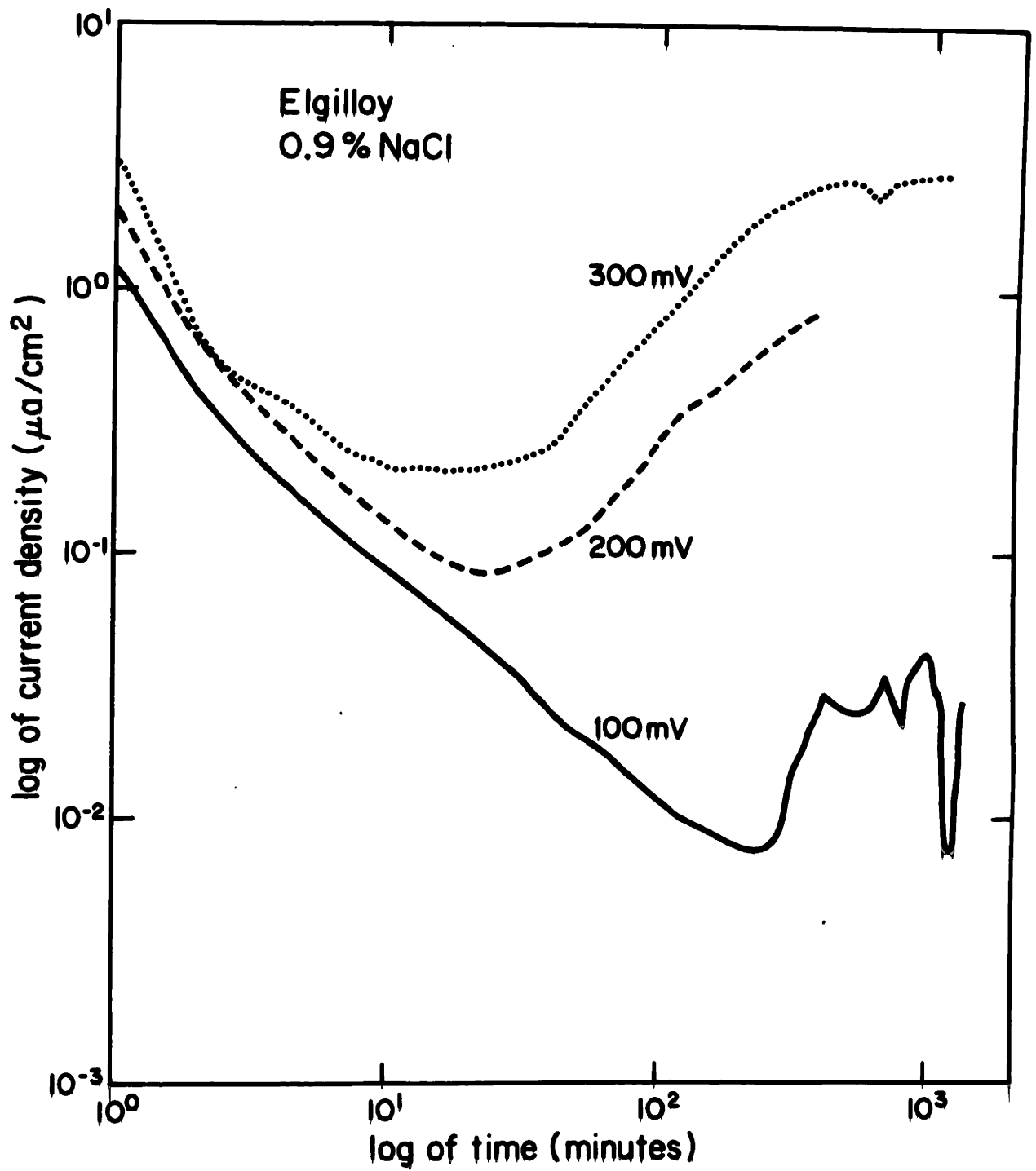


Figure 75. Corrosion current density variation with time of creviced samples of Hastalloy C at various applied potentials in deaerated 0.9% NaCl at 37°C.

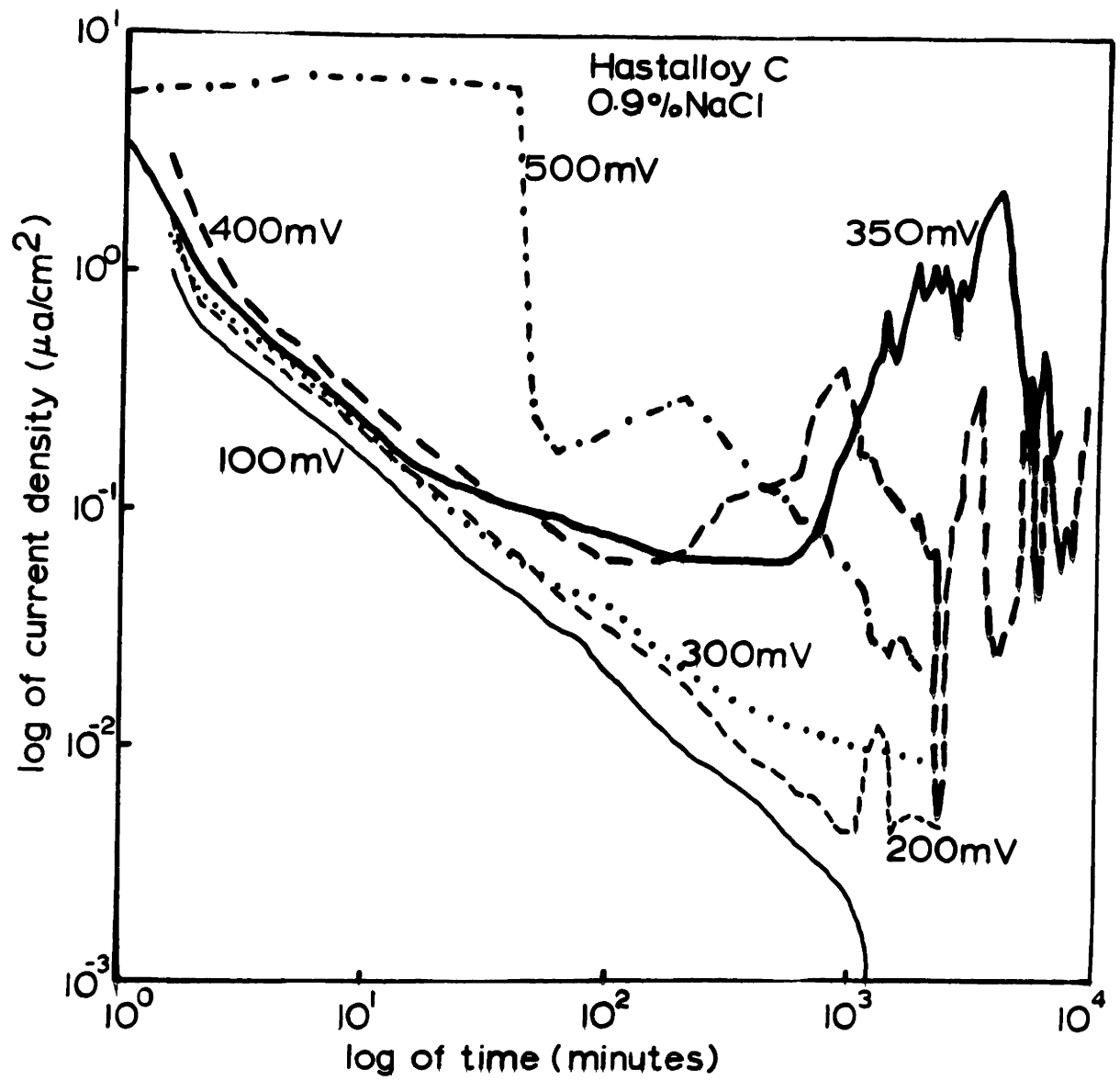


Figure 76. Corrosion current density variation with time of creviced samples of MP35 \bar{F} at various applied potentials in deaerated 0.9% NaCl at 37°C.

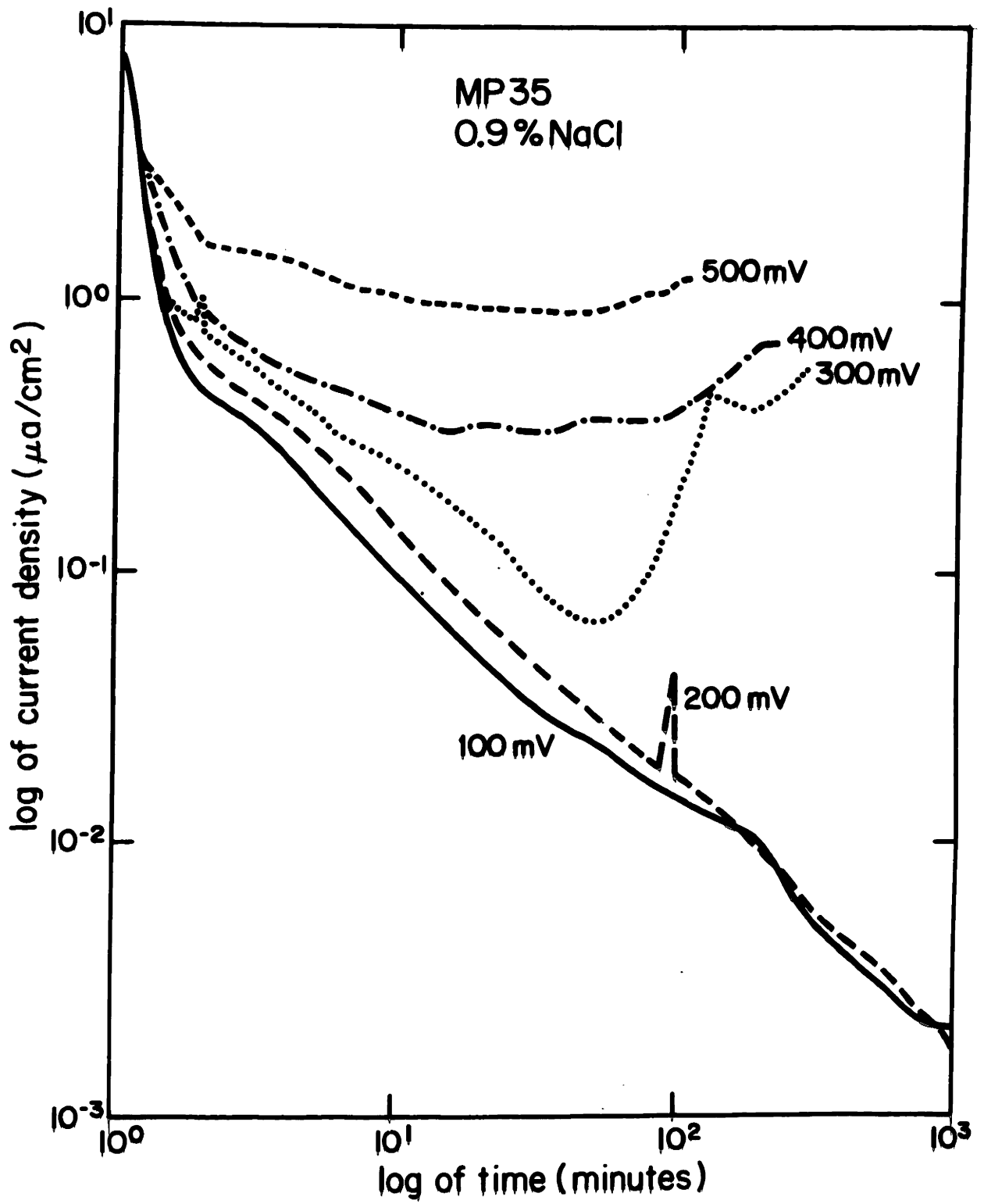


Figure 77. Corrosion current density variation with time of creviced samples of H.S. 25 at various applied potentials in deaerated 0.9% NaCl at 37°C.

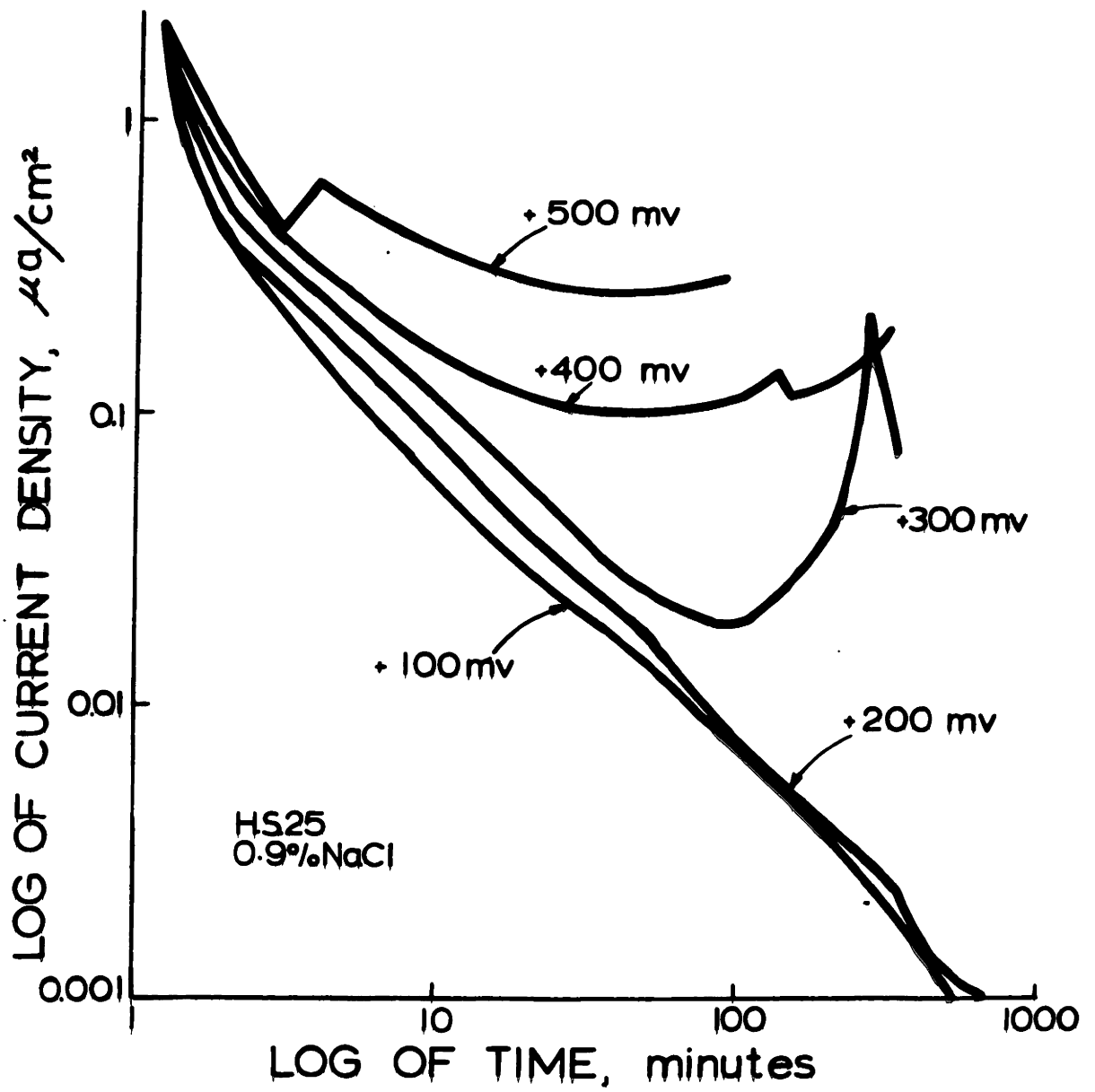


Figure 78. Corrosion current density variation with time of creviced samples of precision cast H.S. 21 at various applied potentials in deaerated 0.9% NaCl at 37°C.

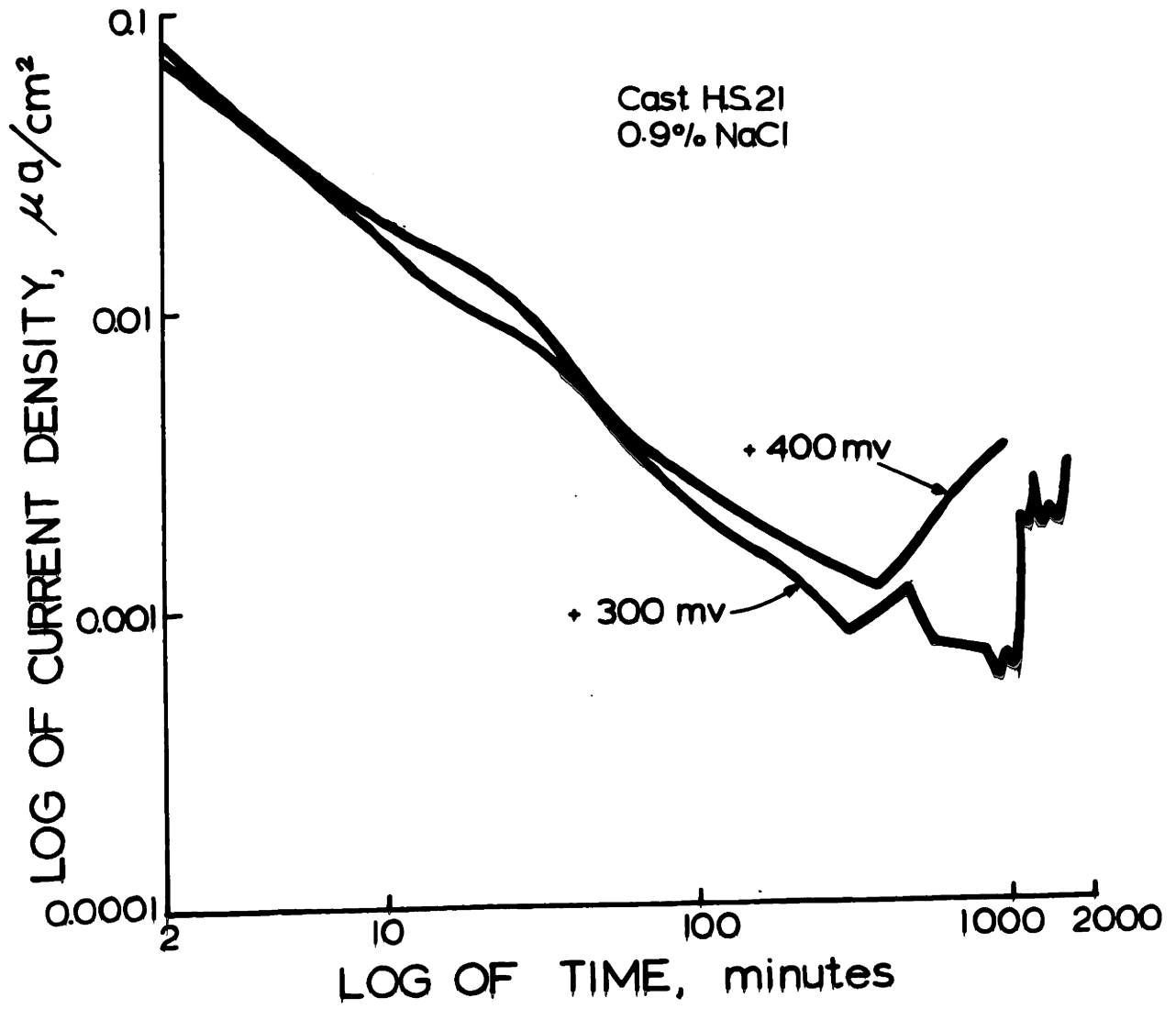


Figure 79. Corrosion current density variation with time of creviced samples of wrought H.S. 21 at various applied potentials in deaerated 0.9% NaCl at 37°C.

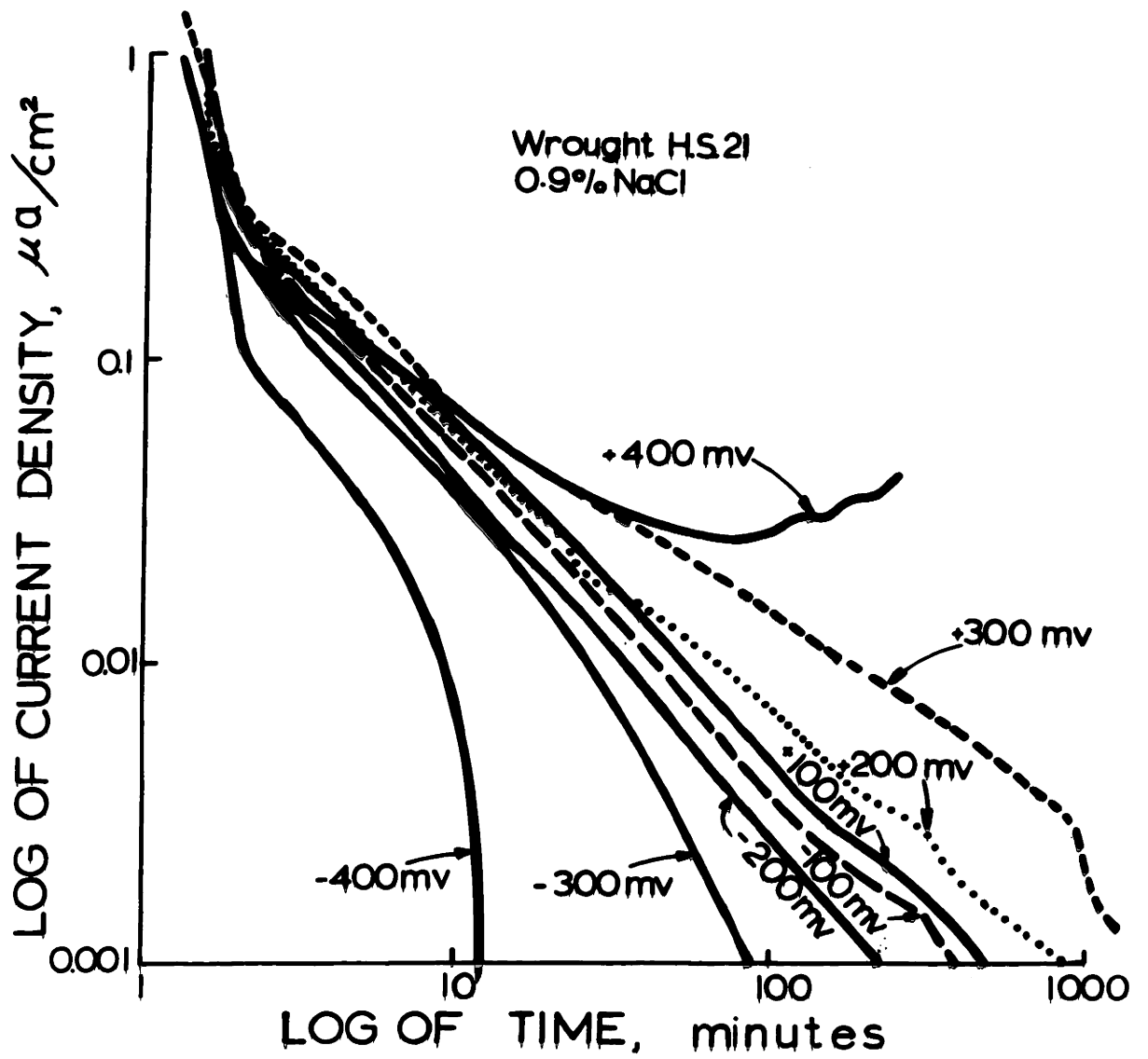


TABLE 1

Summary of Statistics Compiled by J. T. Scales

Percentage of Corroded Implants Among 667 Removed

	<u>S. S.</u>	<u>Co-Cr-Mo</u>	<u>Titanium</u>
Number and percent of total number of implants	478 (71.6%)	83 (12.4%)	106 (15.8%)
Percentage corrosion and/or fretting	62.6	21.7	22.6

313 Multipiece Implants = 1,759 Components Used in Weight-Bearing Alloys

	<u>S. S.</u>	<u>Co-Cr-Mo</u>	<u>Titanium</u>
Percentage with contact crevice corrosion and/or fretting	87	59.3	65.4
Percentage with fatigue or torsion failure	0.5	6.5	4.8

1,232 Screws Used with Intertrochanteric and Bone Plates in Weight-Bearing Bone

	<u>S. S.</u>	<u>Co-Cr-Mo</u>	<u>Titanium</u>
Percentage with contact crevice corrosion and/or fretting	55	41.9	43.2
Percentage with fatigue or torsion failure	0.2	8.03	4.2

TABLE 2

The Effect of Thermomechanical Processing and Heat Treatment on the

Tensile Properties of a 20 Wt. % Chromium-10 Wt. % Molybdenum Balance Cobalt Alloy

<u>Treatment</u>	<u>Yield Strength (psi)</u>	<u>Ultimate Tensile Strength (psi)</u>	<u>% Elongation</u>	<u>% Reduction in Area</u>	<u>Rockwell C Hardness</u>
As Precision Cast	45,000	53,000	20.0	22.2	18
3"X8" ingot. Vacuum melted in graphite mold. Press forged to 1" square cross section at 1175°C. Hot rolled to 0.187" plate. Annealed at 1175°C for 1 hour. Cold rolled to 16% RA.	142,860	177,400	8.0	8.6	40
3"X8" ingot. Vacuum melted in graphite mold. Press forged to 1" square cross section at 1175°C. Hot rolled to 0.187" plate. Annealed at 1175°C for 1 hour. Cold rolled to 16% RA.	75,000	141,300	22.0	25.0	30

<u>Treatment</u>	<u>Yield Strength (psi)</u>	<u>Ultimate Tensile Strength (psi)</u>	<u>% Elongation</u>	<u>% Reduction in Area</u>	<u>Rockwell C Hardness</u>
3"X8" ingot. Vacuum melted in graphite mold. Press forged to 1" square cross section at 1175°C. Hot rolled to 0.187" plate. Annealed at 1175°C for 1 hour. Cold rolled to 26% RA. Heat treat at 1050°C for 30 minutes, air cool.	125,000	206,000	26.0	27.0	34

TABLE 3

Nominal Compositions of Some Commercially
Available Corrosion Resistant Alloys

<u>Alloy</u>	<u>Cr</u>	<u>Mo</u>	<u>W</u>	<u>Ni</u>	<u>C</u>	<u>Fe</u>	<u>Co</u>
316L	17-20	2-4	--	10-14	0.03	Bal	--
Elgilloy	20	7	--	15	0.15	Bal	40
MP35N	20	10	--	35	--	--	35
H.S. 25	19-21	--	14-16	9-11	0.15	3	Bal
Hastalloy C	13-17.5	16-18	3.7-5.3	Bal	--	4.5-7.0	--
H.S. 21	27.5	5.5	--	2.5	0.35	2.0	Bal
M.I.T. Experimental	20	10	--	--	0.10	--	Bal
Modified H.S. 21	26.70	5.46	--	.01	0.145	0.10	Bal

TABLE 4

The Effect of Thermomechanical Processing and Heat Treatment
on the Mechanical Properties of H.S. 21

<u>Treatment</u>	<u>Yield Strength (psi)</u>	<u>Ultimate Tensile Strength (psi)</u>	<u>% Elongation</u>	<u>% Reduction in Area</u>	<u>Rockwell C Hardness</u>
As Precision Cast	80	101	8	9	30
3"X8" vacuum melted ingot. Press forged to 1" square cross section at 1175°C. Hot rolled to 0.125" plate.	173,000	194,900	11	13	48
3"X8" vacuum melted ingot. Press forged to 1" square cross section at 1175°C. Heat treated at 1050°C for 2 hours, water quench.	106,300	151,600	15	16	33
3"X8" vacuum melted ingot. Press forged to 1" square cross section at 1175°C. Cold rolled to % RA. Heat treat at 1050°C for 40 minutes, air cool.	127,000	196,500	19	21	40

<u>Treatment</u>	<u>Yield Strength (psi)</u>	<u>Ultimate Tensile Strength (psi)</u>	<u>% Elongation</u>	<u>% Reduction in Area</u>	<u>Rockwell C Hardness</u>
1" diameter vacuum melted ingot. Extruded at 1205°C to 80% RA. Heat treated at 1200°C for 4 hours, quench in water.	81,250	114,600	17.5	14.7	22
1" diameter vacuum melted ingot. Extruded at 1205°C to 80% RA. Heat treated at 1100°C for 1 hour, air cool. Cold swaged to 35% RA and heat treated at 1100°C for 2 hours, then quenched in water.	105,700	137,400	16.5	11.8	26
1" diameter vacuum melted ingot. Extruded at 1150°C to 80% RA. Heat treated at 1200°C for 4 hours, quenched in water.	84,740	140,000	17.0	13.7	22
1" diameter vacuum melted ingot. Extruded at 1150°C to 80% RA. Heat treated at 1100°C for 1 hour, air cooled. Cold swaged to 35% RA, heat treated at 1100°C for 2 hours, water quenched.	104,000	146,500	22.5	17.9	28

<u>Treatment</u>	<u>Yield Strength (psi)</u>	<u>Ultimate Tensile Strength (psi)</u>	<u>% Elongation</u>	<u>% Reduction in Area</u>	<u>Rockwell C Hardness</u>
1" diameter vacuum melted ingot. Extruded at 1094°C to 80% RA. Heat treated at 1200°C for 4 hours, quenched in water.	79,000	140,800	17.0	20.0	21
1" diameter vacuum melted ingot. Extruded at 1094°C to 80% RA. Heat treated at 1100°C for 1 hour, cooled in air. Cold swaged to 35% RA, heat treated at 1100°C for 2 hours, quenched in water.	110,000	142,500	18.0	20.5	29

TABLE 5

Mechanical Properties of As-Hot Worked Modified H.S. 21

<u>Treatment</u>	<u>Yield Strength (psi)</u>	<u>UTS (psi)</u>	<u>% Elongation</u>	<u>% Reduction in Area</u>	<u>Rockwell C Hardness</u>
300 lb. vacuum melted and electroslag remelted ingot. Forged and rolled at 1150°C	107,000	180	10	11	37.5

TABLE 6

The Effect of 30 Minute Heat Treatments on the
Mechanical Properties of Hot and Cold Worked, Modified H.S. 21

<u>Treatment</u>	<u>Yield Strength (psi)</u>	<u>Ultimate Tensile Strength (psi)</u>	<u>% Elongation</u>	<u>% Reduction in Area</u>	<u>Rockwell C Hardness</u>
300 lb. vacuum melted and electroslag re-melted ingot. Forged and rolled at 1150°C. Cold rolled to 9.94% RA and heat treated at 1100°C for 30 minutes, air cooled.	71,000	174,000	23.2	23.2	30
300 lb. vacuum melted and electroslag re-melted ingot. Forged and rolled at 1150°C. Cold rolled to 9.94% RA and heat treated at 1065°C for 30 minutes, air cooled.	100,000	235,000	26.1	27.2	35
300 lb. vacuum melted and electroslag re-melted ingot. Forged and rolled at 1150°C. Cold rolled to 9.53% RA and heat treated at 1000°C for 30 minutes, air cooled.	110,000	202,000	19.2	17.8	38

TABLE 7

The Effect of Prior Cold Working Subsequent to a 12 Minute Anneal
at 1065°C on the Mechanical Properties of Modified H.S. 21

<u>Treatment</u>	<u>Yield Strength (psi)</u>	<u>Ultimate Tensile Strength (psi)</u>	<u>% Elongation</u>	<u>% Reduction in Area</u>	<u>Rockwell C Hardness</u>
300 lb. ingot vacuum melted and electroslag remelted. Forged and rolled at 1150°C. Cold rolled to 6% RA. Heat treated at 1065°C for 12 minutes and air cooled.	81,500	215,000	25.2	21.9	32
300 lb. ingot vacuum melted and electroslag remelted. Forged and rolled at 1150°C. Cold rolled to 11.1% RA. Heat treated at 1065°C for 12 minutes and air cooled.	92,600	238,000	26.6	23.4	34
300 lb. ingot vacuum melted and electroslag remelted. Forged and rolled at 1150°C. Cold rolled to 27% RA. Heat treated at 1065°C for 12 minutes and air cooled.	106,200	213,400	20.8	20.2	36

TABLE 8

The Effect of Prior Cold Working Subsequent to a 30 Minute Anneal

at 1065°C on the Mechanical Properties of Modified H.S. 21

<u>Treatment</u>	<u>Yield Strength (psi)</u>	<u>Ultimate Tensile Strength (psi)</u>	<u>% Elongation</u>	<u>% Reduction in Area</u>	<u>Rockwell C Hardness</u>
300 lb. ingot vacuum melted and electroslag remelted. Forged and rolled at 1150°C. Heat treated at 1065°C for 30 minutes, air cooled.	96,000	194,000	18.0	16.6	34
300 lb. ingot vacuum melted and electroslag remelted. Forged and rolled at 1150°C. Cold rolled to 9.94% RA. Heat treated at 1065°C for 30 minutes, air cooled.	100,000	235,000	26.1	27.2	35
300 lb. ingot vacuum melted and electroslag remelted. Forged and rolled at 1150°C. Cold rolled to 15.1% RA. Heat treated at 1065°C for 30 minutes, air cooled.	86,500	201,400	23.7	21.4	35

<u>Treatment</u>	<u>Yield Strength (psi)</u>	<u>Ultimate Tensile Strength (psi)</u>	<u>% Elongation</u>	<u>% Reduction in Area</u>	<u>Rockwell C Hardness</u>
------------------	-----------------------------	--	---------------------	----------------------------	----------------------------

300 lb. ingot vacuum melted and electroslag remelted. Forged and rolled at 1150°C. Cold rolled to 27% RA. Heat treated at 1065°C for 30 minutes, air cooled.

83,700	198,200	23.1	20.7	34
--------	---------	------	------	----

TABLE 9

The Effect of Prior Cold Working Subsequent to a 60 Minute Anneal
at 1065°C on the Mechanical Properties of Modified H.S. 21

<u>Treatment</u>	<u>Yield Strength (psi)</u>	<u>Ultimate Tensile Strength (psi)</u>	<u>% Elongation</u>	<u>% Reduction in Area</u>	<u>Rockwell C Hardness</u>
300 lb. ingot vacuum melted and electroslag remelted. Forged and rolled at 1150°C. Cold rolled to 6% RA. Heat treated at 1065°C for 60 minutes, air cooled.	63,200	211,300	26.3	24.2	32
300 lb. ingot vacuum melted and electroslag remelted. Forged and rolled at 1150°C. Cold rolled to 11.1% RA. Heat treated at 1065°C for 60 minutes, air cooled.	84,500	237,400	27.3	24.5	34
300 lb. ingot vacuum melted and electroslag remelted. Forged and rolled at 1150°C. Cold rolled to 15.1% RA. Heat treated at 1065°C for 60 minutes, air cooled.	84,100	197,900	21.4	20.7	33

TABLE 10

Corrosivity of Some Corrosion Resistant Alloys

in 10% HCl + 1% FeCl₃ Solution at 37°C

<u>Alloy</u>	<u>Condition</u>	<u>Average Weight Loss in gms./day of Bare Samples</u>	<u>Average Weight Loss in gms./day of Crevice Samples</u>	<u>Remarks</u>
316L	Wrought and annealed	0.0204	0.0210	All samples severely pitted in two hours.
Elgilloy	Wrought and annealed	0.0064	0.0086	Four samples crevice corroded in 2 days and six in 3 days.
MP35N	Wrought and annealed	0.0030	0.0045	Four samples crevice corroded in 3 days and 6 in four days.
Hastalloy C	Wrought and annealed	0.0005	0.0050	Four samples crevice corroded in 4 days and six in 6 days.
H.S. 25	Wrought and annealed	0.0002	0.0020	Four samples crevice corroded in 4 days and 6 in 6 days.
H.S. 21	As Precision cast	0.0000	0.0005	Four samples crevice corroded in 14 days and six in 21 days.

<u>Alloy</u>	<u>Condition</u>	Average Weight Loss in gms./day of Bare Samples	Average Weight Loss in gms./day of Creviced Samples	<u>Remarks</u>
H.S. 21	Factory Cast, hot extruded and annealed	0.00000	0.00001	No visible sign of crevice corrosion or etching in 4 weeks.
M.I.T. Experimental	Factory cast, hot forged and rolled and annealed	0.00000	0.00000	No visible sign of crevice corrosion or etching in 4 weeks.

TABLE 11

Times to Initiate Marked Serrations in Potential vs Time
Plot of Creviced Samples Immersed in Oxygenated
10% HCl + 1% FeCl₃

<u>Alloy</u>	<u>Time</u>
316L	Active
Elgilloy	15 minutes
Hastalloy C	35 minutes
H.S. 25	10 hours
MP35N	1 day
H.S. 21 (Precision Cast)	8 days
H.S. 21 (Wrought)	8 days

TABLE 12

Times to Initiate Marked Serrations in Potential vs Time
Plot of Creviced Samples Immersed in Oxygenated
0.9% NaCl

<u>Alloy</u>	<u>Time</u>
316L	180 hours
Elgilloy	192 hours
MP35N	192 hours
Hastalloy C	192 hours
H.S. 25	192 hours
H.S. 21 (Precision Cast)	192 hours
H.S. 21 (Wrought)	192 hours

TABLE 13

Crevice Corrosion Behavior of Some Corrosion
Resistant Alloys in 0.9% NaCl Solution at 37°C

<u>Alloy</u>	<u>Condition</u>	<u>Appearance After 60 day Immersion in 0.9% NaCl</u>	<u>Reference to In Vivo Corrosivity</u>
316L	Wrought and annealed	All four samples crevice corroded.	1-6, 15
Elgilloy	Wrought and annealed	Two samples exhibited isolated pits under gaskets; one sample crevice corroded.	
MP35N	Wrought and annealed	Two samples crevice corroded.	
Hastalloy C	Wrought and annealed	One sample crevice corroded.	
H.S. 25	Wrought and annealed	One sample crevice corroded.	48, 49
H.S. 21	Precision cast and annealed	No crevice corrosion.	6, 15
H.S. 21	Wrought and annealed	No crevice corrosion	

Pitting Potentials of Alloys in
Deaerated 10% HCl + 1% FeCl₃

<u>Alloy</u>	<u>ϕ_p</u>
316L	Active
Elgilloy	+ 800 mV
Hastalloy C	+ 820 mV
MP35N	+ 750 mV
H.S. 25	+ 760 mV
H.S. 21 (Precision Cast)	+ 830 mV
H.S. 21 (wrought)	+ 860 mV

TABLE 15

Protective Potential in 10% HCl + 1% FeCl₃

<u>Alloy</u>	<u>$\phi_{\text{protective}}$</u>
Elgilloy	--
MP35N	+ 850
Hastalloy C	--
H.S. 25	--
H.S. 21 (Precision Cast)	--
H.S. 21 (Wrought)	--

Protective Potential in 0.9% NaCl

<u>Alloy</u>	<u>$\phi_{\text{protective}}$</u>
316 _L	
Elgilloy	+880
MP35N	
Hastalloy C	+255
H.S. 25	
H.S. 21 (Precision Cast)	
H.S. 21 (wrought)	

TABLE 17

Lowest Applied Potential at Which Crevice
Corrosion Occurs in Deaerated 10% HCl + 1% FeCl₃

<u>Alloy</u>	<u>Crevice Corrosion Potential</u>	<u>Time to Initiate Crevice Corrosion at Crevice Corrosion Potential</u>
316L	Active	
Elgilloy	+ 400 mV	7 minutes
MP35N	+ 400 mV	350 minutes
Hastalloy C	+ 500 mV	Immediately
H.S. 25	+ 700 mV	200 minutes
H.S. 21 (Precision Cast)	+ 800 mV	850 minutes
H.S. 21 (Wrought)	No evidence of crevice corrosion	

TABLE 18

Lowest Applied Potential at Which Crevice
Corrosion Occurs in Deaerated 0.9% NaCl

<u>Alloy</u>	<u>Crevice Corrosion= Potential</u>	<u>Time to Initiate Crevice Corrosion at Crevice Corrosion Potential</u>
316L	+ 100 mV	50 minutes
Elgilloy	+ 100 mV	200 minutes
MP35N	+ 200 mV	200 minutes
H.S. 25	+ 300 mV	100 minutes
Hastalloy C	+ 350 mV	200 minutes
H.S. 21 (Precision Cast)	+ 400 mV	400 minutes
H.S. 21 (Wrought)	No evidence of crevice corrosion	

AUTOBIOGRAPHICAL SKETCH

I, Thomas Maurice Devine, Jr., was born in Boston, Massachusetts, on August 4, 1948. I received my diploma from St. Dominic Savio High School in East Boston, Massachusetts, in May of 1966. In the fall of 1966, I began my studies at the Massachusetts Institute of Technology and was awarded the Bachelor of Science and Master of Science degrees in Metallurgy and Materials Science on June 6, 1971. On June 7, 1970, I was married to the former Ms. Patricia Marie Howard of Boston, Massachusetts, and on August 3, 1973, our first son Patrick Thomas was born. During the summer vacation periods of 1969 and 1970, I worked as a metallurgist at the Paul D. Merica Research Laboratory of the International Nickel Company. Since September of 1966, I have throughout each academic term worked on a research project concerned with surgical implant alloys under the supervision of Professor John Wulff and the sponsorship of the National Science Foundation.